Fall 2009

Ambient measurements of chemical and physical properties of organic aerosols: Insights into formation, growth, and heterogeneous chemistry

Luke D. Ziemba
University of New Hampshire, Durham

AMBIENT MEASUREMENTS OF CHEMICAL AND PHYSICAL PROPERTIES OF ORGANIC AEROSOLS: INSIGHTS INTO FORMATION, GROWTH, AND HETEROGENEOUS CHEMISTRY

BY

LUKE D. ZIEMBA

B.S., Rochester Institute of Technology, 2002

M.S., University of New Hampshire, 2005

DISSERTATION

Submitted to the University of New Hampshire

In Partial Fulfillment of

The Requirements for the Degree of

Doctor of Philosophy

In

Earth and Environmental Science

September, 2009

This dissertation has been examined and approved.

Dissertation Director, Dr. Robert J. Griffin
Associate Professor of Civil and Environmental Engineering, Rice University

Dr. Jack E. Dibb
Research Associate Professor of Earth Sciences

Dr. Kevin H. Gardner
Associate Professor of Civil Engineering

Dr. Alexander A. Pszenny
Research Associate Professor of Earth Sciences

Dr. Ruth K. Varner
Research Assistant Professor of Earth Sciences

16-June-2009
Date

ACKNOWLEDGEMENTS

Financial support for this work was provided by the Office of Oceanic and Atmospheric Research of the National Oceanic and Atmospheric Administration under AIRMAP grant #NA06OAR4600189 to UNH and is much appreciated. I would also like to acknowledge CH2M HILL Polar Services, the New York Air National Guard 109th Airlift Wing, the staff and scientists at Summit Camp, the University of Houston, the staff at the Shoals Marine Laboratory, and especially the staff at UNH for logistical assistance.

I would like to personally thank my committee members, Rob Griffin, Jack Dibb, Ruth Varner, Kevin Gardner, and Alex Pszenny, for guidance throughout my Ph.D experience. I would like to recognize my collegues for their direct contributions to this work, especially Pieter Beckman, Laura Cottrell, Carolyn Jordan, Casey Anderson, Chelsea Corr, Pat Wilkinson, Mel Knorr, Barry Lefer, Greg Huey, Qi Zhang, Eric Scheuer, and Sallie Whitlow. I would like to thank Jack for providing me the opportunity to visit and work in the most unique laboratory on Earth. I would especially like to thank Rob for being a wonderful advisor, scientist, rebounder, and friend over the past six years. I am forever grateful to you both for your help and encouragement.

Lastly, I would like to thank my family for all of their support through the years. I truly have the perfect wife and son, and equally great parents, grandparents, and siblings. This is dedicated to my grandmother who has always been, and will continue to be an inspiration to me and my family.

TABLE OF CONTENTS

CHAPTER PAGE

CHAPTER PAGE

LIST OF TABLES

LIST OF FIGURES

ABSTRACT

AMBIENT MEASUREMENTS OF CHEMICAL AND PHYSICAL PROPERTIES OF ORGANIC AEROSOL:

INSIGHTS INTO FORMATION, GROWTH, AND HETEROGENENEOUS CHEMISTRY

by

Luke D. Ziemba

University of New Hampshire, September, 2009

Organic aerosols are a ubiquitous component of the troposphere, from heavily polluted cities to the remote Arctic. In Chapters II, III, and V of this dissertation, the formation of organic aerosol through observations of ambient size distributions is addressed. Chapter IV presents a new pathway for the formation of nitrous acid (HONO) in the urban atmosphere.

In Chapter II, the size-resolved chemical composition of sub-micron aerosol was measured at a suburban forested site in North Carolina. Two events were identified in which particle growth, presumably by gas-to-particle conversion, was dominated by accumulation of organic aerosol mass. Growth rates between 1.2 nm hr^{-1} and 4.9 nm hr^{-1} were observed. Using a mass-spectral deconvolution method coupled with linear regression analysis, the sub-micron organic aerosol mass observed during the campaign, and during events, was determined to have been influenced by both local and regional secondary processes with only a minor influence from combustion sources.

In Chapter III, the chemical characteristics of sub-10-micron aerosol were explored as a function of ambient particle size at a coastal and inland site in New

England. Average organic carbon (OC) concentrations of 4.9 μg C m^{-3} and 3.4 μg C m^{-3} were observed at the coastal site at the Isles of Shoals (IOS) and at the slightly inland site at Thompson Farm (TF), respectively. An average of 84 and 72% of OC was found to be water-soluble at IOS and TF, respectively. Size distributions indicate that the formation of dicarboxylic acids, especially oxalic acid, is driven by aqueous-phase reactions. A chemical fingerprint analysis suggests that all water-soluble OC at IOS resembles secondary organic aerosol (SOA), while WSOC at TF appears to result from mixed sources.

In Chapter IV, a newly identified formation pathway for nitrous acid (HONO) is presented. HONO is an important precursor to hydroxyl radicals in the troposphere and thus contributes to the oxidative capacity of the atmosphere. The proposed pathway is shown to depend on the surface chemical characteristics of primary organic aerosol, and concentrations of HONO are shown to exceed those that can be explained by previously identified formation pathways.

In Chapter V, particle growth events were observed at Summit, Greenland, an extremely remote Arctic site. Particle growth was linked indirectly to condensation of organic compounds because measured concentrations of sulfuric acid could not explain the observed growth rates of up to 0.963 nm hr^{-1}. The snowpack may be the source of condensable organic precursors, and thus organic aerosol, based on prior observations at the site. This pathway represents a source of global SOA currently not taken into account that may have implications for climate regulation.

CHAPTER I

INTRODUCTION

Aerosols are an important component of the atmosphere that influence economic, health, and climate systems that directly shape the sustainability and quality of life on Earth. The most direct consequence of aerosols on living organisms is manifested in degradation of health; ultrafine aerosol (particles having diameters less than 100 nm) is inhaled efficiently, facilitating the incorporation of potentially toxic substances into the bloodstream through the lungs (Oberdoerster et al., 1995; Lightly et al., 2000). Aerosols regulate Earth's climate through direct absorption (Menon et al., 2002) and reflection (Penner et al., 1998) of incoming solar/outgoing longwave planetary radiation, and through control and alteration of cloud formation and evolution (Lohmann and Feichter, 2005). Aerosols are an important component of global cycling of water, carbon, sulfur, and nitrogen, directly influence the oxidative capacity of the troposphere through heterogeneous reactions (Alicke et al., 2003; Zhou et al., 2001), and contribute to the long-range transport of pollution to remote areas of the globe (Jaffrezo et al., 1998).

Without exception, the effects of aerosols on health, climate, visibility, and chemistry depend fundamentally on aerosol size and chemical composition, which are functions of formation mechanisms and subsequent secondary transformations. Aerosols enter the atmosphere by two pathways: 1.) direct emission in the condensed phase (primary); and 2.) gas-to-particle conversion of semi- or non-volatile species formed by chemical reactions in the atmosphere (secondary). The size and chemical composition of

aerosols evolve upon transport, as condensation, evaporation, coagulation, and heterogeneous chemical reactions continually alter the size distribution and composition of aerosol populations.

Thus, to elucidate the sources and effects of aerosols on a global scale, an unambiguous understanding of how aerosol size and chemical composition vary with geographic location is necessary. Processes controlling the physical properties of tropospheric aerosol can be both regionally specific (O'Dowd et al., 2002) and globally ubiquitous (Kulmala et al., 2000), and the chemical composition of aerosols can vary significantly on continental scales (Malm et al., 2004; Zhang et al., 2007).

Organic compounds represent a large fraction of tropospheric aerosol mass globally but are poorly constrained in current models (Heald et al., 2005; Kanakidou et al., 2005). Molecular speciation is useful for source apportionment (Schauer et al., 1996) but is only able to resolve a minor fraction of tropospheric organic aerosol (OA) mass. The effects, though, of organic aerosols on climate are considerable. Unlike aerosols composed of inorganic constituents like ammonium sulfate, particle-phase organic molecules of varying composition both absorb and scatter light efficiently (Ramanathan et al., 2007), and both enhance and inhibit aerosol cloud activation (Yu, 2000; Feingold and Chuang, 2002). Thus, the quantitative climate forcing of OA is not understood clearly, and research is ongoing to further elucidate the chemical composition, size distribution, and tropospheric chemistry of OA.

The current work focuses on this topic through ambient observations in urban, rural, and remote atmospheres. Each of the following four chapters represents an independent document, and together these works explore the properties of tropospheric

OA. The chapters are arranged in chronological order of the time in which observations occurred. Chapter II focuses on measurements in a suburban, forest location in North Carolina using a mass spectrometric technique to link general sources of OA with secondary organic aerosol (SOA) growth. Chapter III explores the mass-based size distribution of OA at a coastal and inland site in New Hampshire to identify formation processes using both molecular speciation and bulk functionality analyses. Chapter IV relates heterogeneous conversion of gas-phase nitric acid (HNO_3) to nitrous acid (HONO) on the surface of urban organic combustion aerosol. Chapter V shows observations of number-based size distributions of ambient aerosol at an extremely remote Arctic site and identifies several growth events potentially related to snowpack emissions of organic compounds. Each of these works is summarized and suggestions for further work are outlined in Chapter VI.

References

Alicke, B., Geyer, A., Hofzumahaus, A., Holland, F., Konrad, S., Patz, H.W., Schafer, J., Stutz, J., Voltz-Thomas, A., and Platt, U., 2003. OH formation by HONO photolysis during the Berlioz experiment. Journal of Geophysical Research-Atmospheres 108, doi:10.1029/2001JD000579.

Feingold, G. and Chuang, P.Y., 2002. Analysis of the influence of film-forming compounds on droplet growth: Implications for cloud microphysical processes and climate. Journal of Atmospheric Sciences 59, 2006-2018.

Heald, C.L., Jacob, D.J., Park, R.J., Russell, L.M., Huebert, B.J., Seinfeld, J.H., Liao, H., and Weber, R.J., 2005. A large organic aerosol source in the free troposphere missing from current models. Geophysical Research Letters 32, doi:10.1029/2005GL02381.

Jaffrezo, J.L., Davidson, C.I., Kuhns, H.D., Bergin, M.H., Hillamo, R., Maenhaut, W., Kahl, J.W., and Harris, J.M., 1998. Biomass burning signatures in the atmosphere of central Greenland, Journal of Geophysical Research 103, 31067-31078.

Kanikidou, M. et al., 2005. Organic aerosol and global climate modeling: a review. Atmospheric Chemistry and Physics 5, 1053-1123.

Kulmala, M., Pirjola, U., and Makela, J.M., 2000. Stable sulphate clusters as a source of new atmospheric particles, Nature 404, 66-69.

Lightly, J.S., Veranth, J.M., and Sarofim, A.F., 2000. Combustion aerosols: Factors governing their size and composition and implications to human health, Journal of Air and Waste Management Association 50, 1565-1618.

Lohmann, U. and Feichter, J., 2005. Global indirect aerosol effects: A review. Atmospheric Chemistry and Physics 5, 715-737.

Malm, W.C., Schichtel, B.A., Pitchford, M.L., Ashbaugh, L.L., and Eldred, R.A., 2004. Spatial trends in speciated fine aerosol concentration in the United States, Journal of Geophysical Research 109, doi:10.1029/2003JD003739.

Menon, S., Hansen, J., Nazarenko, L., and Luo, Y.F.,2002. Climate effects of black carbon aerosols in China and India. Science 297, 2250-2253.

Oberdörster, G., 2000. Toxicology of ultrafine particles: in vivo studies. Philosphical Transactions of the Royal Society of London 358, 2719-2740.

O'Dowd, C.D., Jimenez, J.L., Bahreini, R., Flagan, R.C., Seinfeld, J.H., Hameri, K., Pirjola, L., Kulmala, M., Jennings, S.G., and Hoffmann, T., 2002. Marine aerosol formation from biogenic iodine emissions. Nature 417, 632-636.

Penner, J.E., Chuang, C.C., and Grant, K., 1998. Climate forcing by carbonaceous and sulfate aerosols. Climate Dynamics 14, 839-851.

Ramanathan, V., Li, F., Ramana, M.V., Praveen, P.S., Kim, D., Corrigan, C.E., Nguyen, H., Stone, E.A., Schauer, J.J., Carmichael, G.R., Adhikary, B., and Yoon, S.C., 2007. Atmospheric brown clouds: Hemispheric and regional variations in long-range transport, absorption, and radiative forcing. Journal of Geophysical Research 112, doi:10.1029/2006JD008124.

Schauer, J.J., Rogge, W.F., Hildemann, L.M., Mazurek, M.A., and Cass, G.R., 1996. Source apportionment of airborne particulate matter using organic compounds as tracers. Atmospheric Environment 30, 3837-3855.

Yu, S., 2000. Role of organic acids (formic, acetic, pyruvic, and oxalic) in the formation of cloud condensation nuclei (CCN): A review. Atmospheric Research 53, 185-217.

Zhang, Q. et al., 2007. Ubiquity and dominance of oxygenated species in organic aerosols in anthropogenically-influenced Northern Hemisphere midlatitudes. Geophysical Research Letters 34, doi:10.1029/2007GL029979.

Zhou, X.L., Gao, H.L., He, Y., Huang, G., Bertman, S.B., Civerolo, K., Schwab, J., 2003. Nitric acid photolysis on surfaces in low-NO_X environments: Significant atmospheric implications. Geophysical Research Letters 30, doi:10.1029/2003GL018620.

CHAPTER II

CHARACTERIZATION OF ORGANIC AEROSOL ASSOCIATED WITH SMALL PARTICLE NUMBER CONCENTRATION EVENTS IN A SUBURBAN FORESTED ENVIRONMENT

Abstract

Two elevated particle number/mass growth events associated primarily with Aitken mode particles (diameter greater than 40 nm but smaller than 100 nm) were observed over the course of a sampling campaign (13-29 September 2004) at the Duke University Forest-Atmosphere Carbon Transfer and Storage Free-Air CO_2 Enrichment facility. Aerosol growth rates between 1.2 nm hr^{-1} and 4.9 nm hr^{-1} were observed, resulting in net increases in geometric mean diameter of 21 and 37 nm during events. Growth was dominated by addition of organic compounds that were oxidized, and therefore likely secondary, in nature.

Over the campaign, average aerosol mass concentrations measured by an Aerodyne quadrupole aerosol mass spectrometer (Q-AMS) were 1.9 ± 1.6 (one standard deviation), 1.6 ± 1.9, 0.1 ± 0.1, and 0.4 ± 0.4 μg m^{-3} for organic mass (OM), sulfate, nitrate, and ammonium, respectively. These values represent 47%, 40%, 3%, and 10%, respectively, of the measured sub-micron aerosol mass. Based on Q-AMS spectra, OM was apportioned to hydrocarbon-like organic aerosol (HOA) and two types of oxidized organic aerosol (OOAI and OOAII), which constituted on average, 6%, 58%, and 36%, respectively, of the observed OM. Based on spectral analysis, OOAI appears to represent

aged, regional secondary organic aerosol (SOA), while OOAII likely reflects less aged SOA formed locally.

Organic aerosol characteristics associated with the identified events are compared to those of the campaign average and to each other. Particularly in one event, the contribution of OOAII to overall OM levels was enhanced relative to the campaign average, indicating the likelihood of local biogenic SOA contributing to these events. Statistical analyses investigate the relationship between HOA, OOAI, OOAII, other aerosol concentrations, mixing ratios of gas-phase species, and auxiliary meteorological data during the campaign and individual events. It appears that no single parameter indicates the probability of a particle growth event.

Introduction

Aerosol particles are critically important in the atmosphere due to their ability to act as the nuclei around which liquid and ice clouds form and because of their ability to scatter or absorb light, thereby affecting the radiative balance at the surface of the Earth (Charlson et al., 1992). The capacity of these particles to cause light extinction also leads to visibility degradation in affected areas (Schichtel et al., 2001). In addition, such aerosol particles provide surface area upon which heterogeneous reactions of atmospheric relevance occur (Cwiertny et al., 2008) and have been associated with increased rates of morbidity and mortality among exposed populations (Schwartz et al., 1996). Lastly, deposition to the Earth's surface of particles represents a pathway for inter-phase transport of material within the Earth system (Jordan and Talbot, 2000). It is thus important to increase understanding of the formation, chemistry, and processing of the associated particles.

In recent work, it has been demonstrated that new particle formation occurs frequently throughout the entire troposphere, including the mixed layer closest to the Earth's surface (Kulmala, 2003). These particles grow by coagulation and condensation to sizes large enough to participate in processes affecting human health and climate as described above. Consequently it is important to understand the conditions that favor small particle formation and subsequent growth in a variety of environments such as urban, rural, and marine. Of particular interest is the role that organic components play in this particle formation phenomenon because inorganic species such as sulfate often are not always able theoretically to account completely for particle formation and growth (Smith et al., 2008). Using an Aerodyne quadrupole aerosol mass spectrometer (Q-

AMS), organic compounds were identified as the major constituent of sub-100 nm diameter aerosol following new particle formation events at a forested site in southern Finland (Allan et al., 2006). In a more polluted atmosphere near Pittsburgh, PA, ammonium and sulfate contributed the majority of condensable mass during the early stages of growth events; however, photochemically produced secondary organic aerosol (SOA) contributed significantly to growth during later stages of these events (Zhang et al., 2004; Zhang et al., 2005). In contrast, Hock et al. (2008) observed a growth event in rural southern Germany with significant mass contribution from aerosol nitrate.

Biogenic volatile organic compounds (BVOCs) are emitted to the atmosphere on a global scale at a rate that is an order of magnitude larger than those from anthropogenic sources (Guenther et al., 1995). Many of these BVOCs have been shown to be efficient precursors of SOA; SOA forms from the partitioning to the particulate phase (via condensation, heterogeneous uptake, etc.) of the oxidation products of the primary VOCs (Seinfeld and Pankow, 2003). Despite numerous studies investigating this phenomenon, many uncertainties remain regarding new particle formation, SOA yields, and product identification (Seinfeld and Pankow, 2003). Therefore, continued studies aimed at understanding the role of BVOCs in SOA and new particle formation and growth are warranted; these topics are the focal points of the current manuscript.

Methods

An investigation of BVOC-SOA chemistry was conducted at the Duke University Forest-Atmosphere Carbon Transfer and Storage facility, specifically within the Free-Air CO_2 Enrichment (FACE) section, from 13 to 29 September 2004. The FACE site is

located at 35°58'N and 79°05'W and lies approximately 160 meters above sea level. The area contains three typical types of vegetation: a field of herbaceous vegetation that is mowed annually, a pine plantation planted in 1983 but that currently contains more than 40 woody species, and an oak-hickory forest. The most common species present, and therefore likely to influence BVOC-SOA chemistry, are loblolly pine, shortleaf pine, and Virginia pine. Based on loblolly pine emissions, α-pinene and β-pinene are expected to be the primary monoterpenes affecting SOA formation at the FACE site (Phillips et al., 1999).

Measurements

Aerosol measurements were collected at the base of towers erected inside two of the FACE site tree rings, one with ambient CO_2 and the other with CO_2 enriched (during the daytime) to approximately twice the ambient level. Bulk sample was drawn from a tower at a constant laminar flow rate of 10 L min^{-1} through a 0.5-inch outer diameter length of copper tubing with a University Research Glass (Chapel Hill, NC) 2.5-μm cyclone on the inlet. Aerosol instruments sub-sampled from this flow. Because aerosol measurements were only possible at one location at a time, no contemporaneous comparison between rings is possible, and the data are presented as a single time series with a break in the middle when instrumentation was moved from one ring (ambient) to the other (enriched). Therefore, this study is unable to investigate how changes in BVOC emission as a result of enriched CO_2 (Naik et al., 2004) affect SOA formation. Efforts to sample at two different heights (16 and 20 m above ground) and investigate fluxes using the aerosol equipment showed no statistically significant differences in concentration; therefore, the data were composited into a single time series in this manner as well.

Aerosols were characterized by a Q-AMS (Jayne et al., 2000). The Q-AMS provided size-resolved mass composition data of non-refractory (based on a vaporization temperature of 550°C) aerosol species averaged over ten-minute sampling periods. As in our previous work (Cottrell et al., 2008), it is assumed that the presence of the cyclone did not affect the mass concentrations measured by the Q-AMS, as particles larger than a micron mostly are not transmitted through the aerodynamic focusing lens on the instrument inlet. The Q-AMS sub-sampled isokinetically from the inlet line at approximately 140 mL min^{-1}.

Principles of operation and analyses associated with the Q-AMS have been described in great detail elsewhere (Jayne et al., 2000; Jimenez et al., 2003; Canagaratna et al., 2007). Therefore, only a brief overview is given here. Ambient-pressure sample containing aerosol particles enters the instrument through a 130-μm critical orifice, after which particles are collimated using the aerodynamic focusing lens mentioned above (Liu et al., 1995ab). Because of the transmission efficiency of this lens, the Q-AMS measures particles with vacuum aerodynamic diameters (D_{va}) between 40 nm and one micron; this measurement is typically referred to as sub-micron (Liu et al., 1995ab; Jayne et al., 2000; Allan et al., 2003), although the range of 100% transmission of particles is 60 to 600 nm. The resulting particle beam traverses a vacuum chamber of known dimension; during operation of the Q-AMS in particle-time-of-flight (pTOF) mode, measuring the travel time across this distance allows for calculation of D_{va}. Size calibrations were performed using National Institute of Standards-traceable polystyrene latex spheres before and after the campaign.

At the end of the vacuum chamber, particles are collected and vaporized on a resistively heated surface; vaporized material is ionized under a 70-eV electron impact ionization source. When the Q-AMS was operating in mass spectrum mode (alternating with the pTOF mode), these ions were filtered by their mass-to-charge (m/z) ratio in a Balzers (Balzers, Lichtenstein) QMA 410 quadrupole mass spectrometer and detected with a secondary electron multiplier. The Q-AMS scanned the m/z spectrum from 1 to 300 atomic mass units (amu) at 1 amu ms^{-1}. Mass/ionization efficiency calibrations of the Q-AMS were performed on-site every two to three days during the campaign using monodisperse ammonium nitrate aerosol, as described previously (Cottrell et al., 2008).

The algorithms described in Jimenez et al. (2003) and Allan et al. (2003, 2004) were used to process all data collected during this study. The particle collection efficiency for the Q-AMS in this study appeared to be unity based on a regression (slope = 0.97, R^2 = 0.92) between Q-AMS sulfate (x variable) and sulfate aerosol determined by ion chromatographic analysis of the sub-micron stages of a co-located impactor (y variable). For this study (ten-minute averages), the lower detection limits (LDL) of the Q-AMS were 0.02 $\mu g\ m^{-3}$, 0.11 $\mu g\ m^{-3}$, 0.01 $\mu g\ m^{-3}$, and 0.14 $\mu g\ m^{-3}$ for sulfate, ammonium, nitrate, and organic material, respectively. Based on inter-comparison of several Q-AMS instruments with other co-located instruments, an uncertainty of ±25% likely is applicable to the Q-AMS data presented here (Canagaratna et al., 2007).

Additional spectral analyses were performed in order to provide insight into the nature of the organic aerosol measured with the Q-AMS during the campaign. A deconvolution technique was also performed to apportion Q-AMS measured organic aerosol to hydrocarbon-like organic aerosol (HOA, thought to represent primary organic

aerosol (POA) from combustion (motor vehicles, biomass burning), industry, etc.) and two types of oxygenated organic aerosol (OOA, thought to represent SOA in various states of aging) (Zhang et al., 2007). In addition, a delta analysis (McLafferty and Turecek, 1993; Drewnick et al., 2004) was conducted in which the predominance of different m/z signals is used to indicate the probable lability, size, and functionality of detected fragments. Intensities from positive delta values indicate more oxygenated species, while negative delta values result from cyclic, unsaturated, and aromatic compounds.

Additional aerosol measurements performed during this campaign included those of black carbon (BC, for evidence of combustion) using a Magee Scientific (Berkeley, CA) aethalometer (based on an optical measurement) and 24-hour-resolution 8-stage (plus back-up filter) impactor samples. Impactor samples were extracted and analyzed off-line using an ion chromatograph (for ions including ammonium, potassium, magnesium, chloride, nitrate, and sulfate). Ion chromatographic extraction and analysis methods are described by DeBell et al. (2004). These data were used for calculation of the Q-AMS collection efficiency (described above) and to identify potential periods of atypical contributions from biomass burning, sea salt, or soil dust.

For quantification of mixing ratios of VOCs, hourly samples were collected from two inlet heights on the tower (16 and 20 m) using evacuated, polished stainless steel canisters. The gas collected in these canisters was analyzed off-line using the gas chromatographic system with several columns and detectors described by Sive et al. (2005), allowing for accurate quantification of over one hundred different VOC compounds. Specifically, α-pinene and isoprene are used as indicators of BVOC

precursors to SOA (Hoffmann et al., 1997; Kroll et al., 2006), toluene is used as an indicator of a mixed biogenic-anthropogenic (White et al., 2008) primary aromatic precursor to SOA (Odum et al., 1997), and isopropyl nitrate is used as an additional indicator of secondary processing of anthropogenic emissions (deGouw et al., 2005).

Additional gases were measured from the base of the towers. Ozone (O_3) was measured using a miniature O_3 detector that operated on the principle of light absorption (Mao et al., 2006); like isopropyl nitrate, O_3 is used as a tracer of photochemical activity but without insight into relative contributions of biogenic and anthropogenic precursors. When enhanced, nitric oxide (NO) measured using a chemiluminescent technique (Thermo Environmental Instruments (TEI, Woburn, MA) Model 42C-TL) also provides an indication of local combustion activities.

Meteorological parameters collected routinely at the FACE sites are used to characterize overall atmospheric conditions at the times of data collection. These include temperature, wind speed, wind direction, and the flux of photosynthetically active radiation (PAR). PAR is used in this study as a surrogate for total solar radiation and strength of photochemical activity.

Event Definition

Events characterized by enhanced contribution of small particles to aerosol mass were identified in the following manner. Without a measurement of aerosol particle number concentration, values ($N(D_{va})$, cm^{-3}) were calculated for each D_{va} from the Q-AMS data, assuming the diameter of a spherical particle (D_P) is equal to D_{va} divided by the aerosol density (ρ), by

$$N(D_{va}) = 10^9 \frac{6M_{D_{va}}\rho^2}{D_{va}^3 \pi} \qquad (1)$$

where $M_{D_{va}}$ is the total Q-AMS mass concentration (μg m^{-3}) of aerosol (consisting of sulfate, ammonium, nitrate, and organic material) associated with size D_{va} (nm). A unit density correct factor is not shown. Values for ρ were estimated based on a weighted-average calculation using mass concentrations measured by the Q-AMS (Zhang et al., 2005) by

$$\rho = \rho_{org}\left(\frac{M_{org}}{M_{org}+M_{sulf}+M_{nitr}+M_{amm}}\right)+\rho_{inorg}\left(\frac{M_{sulf}+M_{nitr}+M_{amm}}{M_{org}+M_{sulf}+M_{nitr}+M_{amm}}\right) \qquad (2)$$

where ρ_{org} is the density of pure organic aerosol (assumed to be 1.2E-15 μg nm^{-3}), ρ_{inorg} is the density of pure inorganic aerosol (assumed to be 1.77E-15 μg nm^{-3}), and M_{org}, M_{sulf}, M_{nitr}, and M_{amm} are mass concentrations of organics compounds, sulfate, nitrate, and ammonium, respectively. An average ρ of 1.47E-15 μg nm^{-3} (1.47 g cm^{-3}) was calculated for the campaign. Spherical aerosol particles are assumed, and this analysis ignores the contribution of liquid water content. From $N(D_{va})$, a total number concentration ($N_{Q\text{-}AMS}$) at each time was calculated by integrating over the Q-AMS-detectable particle size space. The decreasing sampling efficiency of the Q-AMS for particles at the upper and lower bounds of detectable D_{va} was not accounted for in this analysis and therefore calculated $N_{Q\text{-}AMS}$ values represent a lower limit to actual number concentrations. An event was selected based on $N_{Q\text{-}AMS}$ and the mass concentration of the smallest detectable aerosol ($M_{40\text{-}60}$) using the Q-AMS (D_{va} larger than 40 nm and smaller than 60 nm). An event was defined as having concentrations that exceeded the campaign average 95th-percentile for both $M_{40\text{-}60}$ and $N_{Q\text{-}AMS}$ for a duration of more than two hours. The event day was defined as the 24 hours (1200 to 1200 local time) during which the event occurred. $N_{Q\text{-}AMS}$, $M_{40\text{-}}$

$_{60}$, total aerosol mass concentrations, and the two selected events (henceforth referred to as E1 and E2, respectively) are shown in Figure II.1.

Particle growth is observed as a linear increase in the geometric mean diameter (GMD) of a lognormally distributed aerosol population, typically using a number-based size distribution measured by differential mobility analysis, as in Held et al. (2004). Here, number-based aerosol size distributions are calculated using equation (1). The $N(D_{va})$ values during events were estimated from one-hour averaged Q-AMS data for organics, sulfate, and nitrate separately, resulting in a number-size distribution for each chemical component.

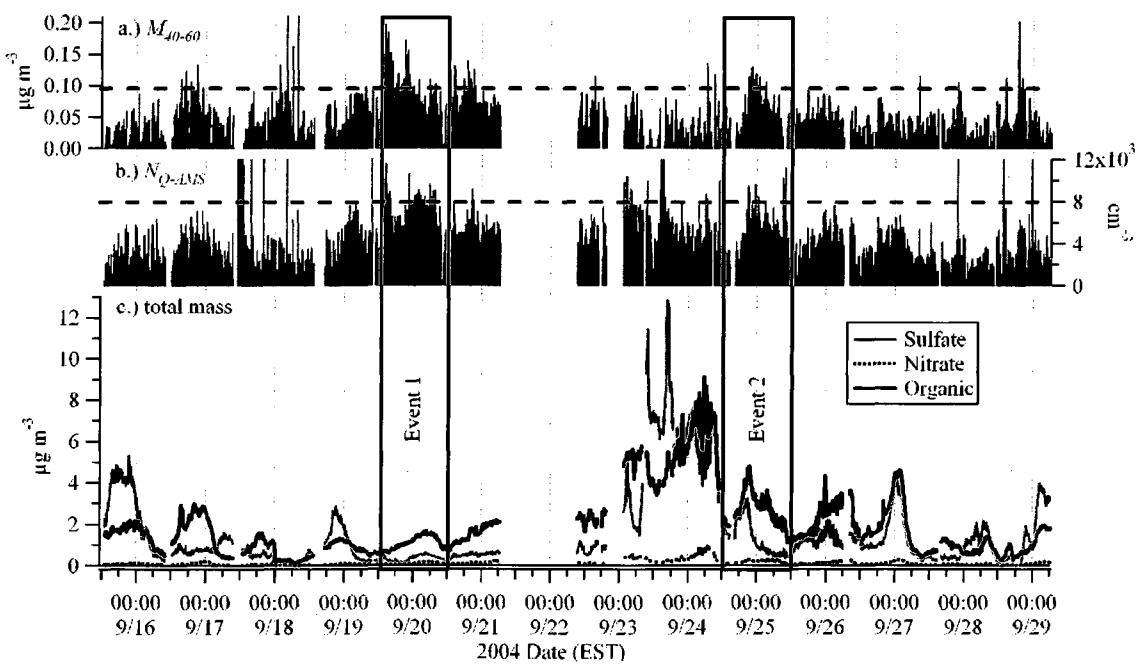

Figure II.1. Time series of a.) M_{40-60}, b.) N_{Q-AMS}, and c.) Q-AMS measured aerosol mass concentrations over the course of the campaign. Events as described in the text are highlighted by boxes around the 24-hour event day. Dotted lines represent threshold 95th-percentile values of a.) 0.0947 μg m^{-3} and b.) 7930 cm^{-3}.

Backward Trajectory Analysis

In order to consider bulk airmass motion affecting the Duke FACE site during each of the particle number events, backward trajectories were calculated for the event days. The Hybrid Single-Particle Lagrangian Integrated Trajectory (HYSPLIT) model (Draxler and Rolph, 2003) was used to calculate 72-hour backward trajectories originating at 1000 m above ground level directly over the FACE site; this height was used for consistency for all simulations given that data for boundary layer height were unavailable. Choice of this height also avoided air masses reaching the surface prematurely. For each event day, backward trajectories were calculated for airmasses arriving at the site at 1200, 1600, 2000, 0000, 0400, and 0800 local (EDT) time. HYSPLIT was run using the archived 40-km Eta Data Assimilation System grid for meteorological input and assuming isobaric vertical motion.

Results

Campaign Overview

An overview of Q-AMS measurements during the campaign is provided in Figure II.1, which shows the time series of the major measured non-refractory components of the sub-micron aerosol. As shown in Figure II.1, aerosol mass loadings were highly variable. Mass concentrations over the entire campaign averaged 1.9 ± 1.6 (one standard deviation; median of 1.5, range of below LDL to 8.2), 1.6 ± 1.9 (median of 0.8, range of 0.02 to 12.5), 0.1 ± 0.1 (median of 0.1, range of 0.01 to 0.9), and 0.4 ± 0.4 (median of 0.2, range of below LDL to 2.9) $\mu g\ m^{-3}$ for organic material, sulfate, nitrate, and ammonium (not shown in Figure II.1), respectively. These lead to an overall average

composition of 47%, 40%, 3%, and 10% for the four species, respectively. The ratios of the average to the median (which indicate the influence of very large concentrations if the values are significantly larger than unity) are 1.3, 1.9, 1.5, and 1.7 for organic material, sulfate, nitrate, and ammonium, respectively, indicating organic material was least subject to variability, potentially due to sampling within a forest environment. In general, the aerosol measured during the campaign was not fully neutralized by ammonium, with a slope of 1.6 for a regression between molar ammonium (y variable) and sulfate (x variable) concentrations. Campaign average parameters are shown in Table II.1.

The overall average contributions of specific m/z values to the organic signal over the course of the campaign are presented in Figure II.2a. Of particular note are the strong, nearly equal signals at m/z 43 and 44 and elevated peaks at *m/z* 27 and 29, which are the main spectral features observed for biogenic SOA generated from the oxidation of VOC emissions from live plants (Kiendler-Scharr et al., 2009). The signal at m/z 44 in ambient aerosol MS primarily results from CO_2^+, which is thought typically to represent highly aged OOA, while m/z 43 (primarily $C_3H_7^+$ and $C_2H_3O^+$) is influenced by organic material of both primary and secondary nature (Zhang et al., 2005; 2007). The signals at m/z 41 and 55 result from HOA and, to a lesser extent, less aged OOA, and those at m/z 27 and 29 are thought to result from less aged OOA as well (Zhang et al., 2005; 2007). These spectra were compared to those of Cottrell et al. (2008) for a semi-rural New England location and Allan et al. (2006) for a Finnish boreal forest. The average spectrum shown in Figure II.2a (x variable) correlated with that of Cottrell et al. (2008, not shown, y variable) with a slope and R^2 of 0.98, suggesting very similar spectra. The comparison indicates a slightly increased relative contribution of m/z 44 compared to m/z

43 in the work of Cottrell et al. (2008), indicating that the aerosol sampled in that study was more oxidized and maybe more aged. Similarly, the spectrum presented by Allan et al. (2006) indicates an even larger relative signal of m/z 43, showing that this enhanced signal (without a corresponding increase at m/z 55) can be used to indicate fresh formation of SOA that is potentially biogenic in nature.

The results of a delta analysis across the entire campaign are shown in Figures II.2b and II.2c. Figure II.2b indicates the overall average intensity of specific delta values (Δ = m/z -14n + 1 where n is the nominal number of carbons in the fragment, that is 1 for m/z from 12 to 23, 2 for m/z from 24 to 35, etc. (McLafferty and Turecek, 1993)) and shows the predominance of delta values 2, 0, and 3 (due nominally to m/z 43 and 29, 41 and 27, and 44). Compared to values in southern New Hampshire (Cottrell et al., 2008), the intensities of delta values 0 and 2 at Duke Forest are enhanced, and the intensity at delta value 3 is decreased. These changes correspond to the relative changes in m/z 43 and 44 between the two studies.

Figure II.2c indicates the segregation of average delta values by n. The average delta value for fragments with carbon number between one and four is approximately 0.7 (compared to 0.8 for the study of Cottrell et al. (2008)). The values for fragments with carbon numbers five and six and fragments with carbon numbers between seven and 15 are -1.5 and -1.0 in this study compared to the values of -1.4 and -0.9 from Cottrell et al. (2008). The greater contribution of smaller fragments again indicates the aerosols observed by Cottrell et al. (2008) were more oxidized.

Table II.1. Statistics of measured variables over the campaign and during each event identified in the text.

	Campaign[f]	E1	E2
Date[a]	9/13 – 9/29	9/19 – 9/20	9/24 – 9/25
OM ($\mu g\ m^{-3}$)	1.9 ± 1.6	1.0 ± 0.3	2.2 ± 0.7
HOA ($\mu g\ m^{-3}$)	0.12 ± 0.15	0.06 ± 0.05	0.22 ± 0.16
OOAI ($\mu g\ m^{-3}$)	1.2 ± 1.1	0.54 ± 0.15	1.5 ± 0.5
OOAII ($\mu g\ m^{-3}$)	0.59 ± 0.49	0.45 ± 0.17	0.81 ± 0.35
HOA/OM	0.07	0.06	0.09
OOAI/OM	0.62	0.51	0.59
OOAII/OM	0.31	0.43	0.32
Sulfate ($\mu g\ m^{-3}$)	1.6 ± 1.9	0.3 ± 0.1	1.0 ± 0.7
Ammonium ($\mu g\ m^{-3}$)	0.4 ± 0.4	0.1 ± 0.0	0.3 ± 0.2
Nitrate ($\mu g\ m^{-3}$)	0.1 ± 0.1	0.1 ± 0.0	0.1 ± 0.1
Neutralization[b]	1.6 (0.94)	1.2 (0.92)	1.5 (0.96)
Black Carbon ($ng\ m^{-3}$)	372.0 ± 289.3	162.4 ± 80.8	NA[g]
Ozone (ppbv)	27.9 ± 14.9	31.0 ± 4.8	NA
Nitric Oxide (pptv)	236.8 ± 536.8	163.5 ± 256.1	NA
Isoprene (pptv)	427.0 ± 561.9	190.1 ± 159.1	440.3 ± 386.8
α-Pinene (pptv)	456.6 ± 771.7	91.9 ± 46.0	250.6 ± 220.6
Toluene (pptv)	92.9 ± 62.0	53.1 ± 25.7	91.6 ± 37.4
IPN[c] (pptv)	3.8 ± 2.1	2.3 ± 0.3	5.0 ± 1.5
PAR[d] ($\mu mol\ m^{-2}\ s^{-1}$)	836.8 ± 502.4	1285.2 ± 284.5	NA
Wind Speed ($m\ s^{-1}$)	2.1 ± 0.9	2.4 ± 0.8	NA
Wind Direction (°)[e]	133.8 ± 95.8	87.3 ± 67.5	NA
Temperature (Celsius)	18.7 ± 4.6	14.2 ± 4.5	NA

[a] Events are defined as noon to noon, local time, with campaign dates being general because some equipment were on-line sooner or later than others

[b] expressed as the slope of a regression between molar ammonium and sulfate concentrations (such that 2.0 implies complete neutralization by ammonium) with R^2 given in parentheses

[c] IPN = isopropyl nitrate

[d] PAR values between 0800 and 1600 local time included

[e] 0 degrees = due north

[f] values shown are averages ± one standard deviation

[g] NA = not available for significant fraction of event day

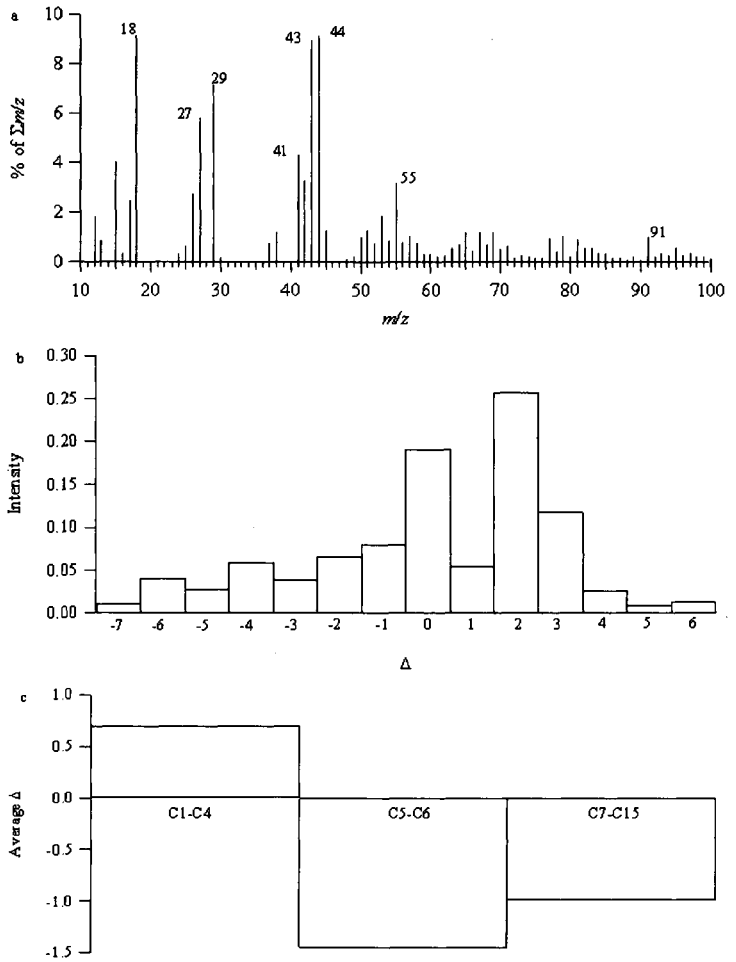

Figure II.2. a.) Campaign average spectrum expressed as the contribution of specific m/z values to the total organic signal; b.) Campaign average intensities at specified delta values; c.) Campaign average delta values segmented by carbon number.

It should be noted that the delta patterns for both studies are similar to those observed for chamber-derived SOA from oxidation of α-pinene (Bahreini et al., 2005) and biogenic SOA produced in a chamber with live plant emissions (Kiendler-Scharr et al., 2009), again suggesting that BVOC played an important role in the formation of SOA at the Duke Forest site.

When the method of Zhang et al. (2007) was applied to the organic aerosol mass spectral matrix, three organic aerosol components were identified: one representing HOA (including contribution from biomass burning aerosol, henceforth termed HOA/BBOA) and two representing OOA in separate states of oxidation/aging (OOAI and OOAII) (Zhang et al., 2007). The spectra representing each of these components are shown in Figure II.3. As would be expected based on previous studies, the HOA/BBOA spectrum shows elevated relative signal at m/z values 41 and 43 as well as 55, 57, and the last two m/z values plus 14 units, representing a CH_2 unit. The spectrum of OOAI, again thought to indicate regional aged SOA, is dominated by signal at m/z 44. Lastly, the spectrum of OOAII, thought to represent less oxidized SOA, potentially of a biogenic nature, shows enhanced relative signals at m/z 27, 29, and 43. To underscore the interpretation of this deconvolution, the time series of HOA/BBOA (y variable) was regressed against the contemporaneous time series of BC (x variable), with a resulting R^2 of 0.50, a value that indicates a statistically relevant relationship (both derived from combustion), though not one that is as strong as that observed in the study of Cottrell et al. (2008) where an R^2 value of 0.76 was found. Similarly, a regression between sulfate aerosol and OOAI yields a R^2 value of 0.71 for this study, compared to 0.74 for the study of Cottrell et al. (2008), underscoring the probable regional nature of sulfate and OOAI. These R^2 values are summarized in Table II.2.

The time series for the calculated concentrations of the organic aerosol components also are shown in Figure II.3; the time series display diurnal patterns similar to those discussed above. The average concentrations of HOA/BBOA, OOAI, and OOAII are 0.12 ± 0.15 (median of 0.06, maximum 0.75), 1.18 ± 1.07 (median of 0.89,

maximum 5.01), and 0.59 ± 0.49 (median of 0.44, maximum of 2.99) μg m^{-3}, respectively. The ratios of the average to the median are 1.9, 1.3, and 1.3, respectively, indicating that the components generally are affected to the same degree by large concentration events except for the surrogate for primary emissions. The average composition of the organic aerosol was 6% HOA/BBOA, 58% OOAI, and 36% OOAII.

Figure II.4 shows the chemically resolved mass-based particle size distribution ($dM/d\log D_{va}$, μg m^{-3}) and the total number-based particle size distribution ($dN/d\log D_{va}$, cm^{-3}) for the campaign and for each event. Organic-equivalent mass-size distributions of organic fragments at m/z = 44 and m/z = 43 are included in Figure II.4 for E1, E2, and the full campaign. It is indicated in Figure II.4c that inorganic aerosol constituents (nitrate and sulfate) exhibit similar behavior, with peaks in $dM/d\log D_{va}$ between 300 and 400 nm in D_{va}. This size likely indicates transport of aged regional aerosol to the site (Marquez et al., 2005). Inorganic mass clearly is dominated by sulfate. In contrast, organic aerosol shows different behavior. The predominant peak is shifted to slightly smaller sizes relative to those of the inorganics; in addition, the distribution is significantly broader, with more pronounced contributions to mass from particles smaller than those at the peak of the distribution (Figure II.4a-II.4c).

Table II.2. R^2 for correlations between organic aerosol components and other measured/derived quantities over the course of the campaign and for each event identified in the text. Values larger than 0.50 are shown in bold.

Campaign	HOA/BBOA	OOAI	OOAII	Sulfate	Nitrate	Ammonium	BC	NO	Toluene	Isoprene	α-Pinene	IPN	O_3	Wind Speed	Wind Direction	Temperature	PAR[a]
HOA/BBOA		**0.50**	**0.67**	0.20	**0.63**	0.29	**0.50**	0.00	0.20	0.00	0.00	0.43	0.18	0.11	0.05	0.07	0.03
OOAI			**0.81**	**0.71**	**0.66**	**0.79**	**0.51**	0.00	0.08	0.05	0.01	**0.84**	0.32	0.15	0.06	0.00	0.16
OOAII				0.22	**0.82**	0.33	0.38	0.01	0.13	0.00	0.02	0.34	0.13	0.09	0.04	0.11	0.04
E1	**HOA/BBOA**	**OOAI**	**OOAII**	**Sulfate**	**Nitrate**	**Ammonium**	**BC**	**NO**	**Toluene**	**Isoprene**	**α-Pinene**	**IPN**	**O_3**	**Wind Speed**	**Wind Direction**	**Temperature**	**PAR**
HOA/BBOA		0.28	**0.53**	0.27	**0.63**	0.34	0.43	0.03	**0.68**	0.36	0.02	0.27	0.11	0.08	0.03	0.42	0.45
OOAI			**0.64**	**0.56**	**0.56**	**0.60**	0.24	0.08	0.25	**0.51**	0.01	**0.62**	**0.50**	0.39	0.00	**0.83**	**0.78**
OOAII				**0.57**	**0.88**	0.21	0.37	0.00	**0.63**	**0.61**	0.03	**0.49**	0.33	0.21	0.00	**0.79**	**0.92**
E2	**HOA/BBOA**	**OOAI**	**OOAII**	**Sulfate**	**Nitrate**	**Ammonium**	**BC**	**NO**	**Toluene**	**Isoprene**	**α-Pinene**	**IPN**	**O_3**	**Wind Speed**	**Wind Direction**	**Temperature**	**PAR**
HOA/BBOA		0.26	**0.54**	0.08	**0.58**	0.11	NA[b]	NA	0.00	0.17	0.00	0.00	NA	NA	NA	NA	NA
OOAI			0.08	**0.85**	0.03	**0.85**	NA	NA	0.03	0.32	0.01	**0.66**	NA	NA	NA	NA	NA
OOAII				0.00	**0.69**	0.01	NA	NA	**0.70**	0.25	0.25	0.01	NA	NA	NA	NA	NA

[a] Values included only between 0800 and 1600 local time

[b] NA = not available for significant fraction of event day

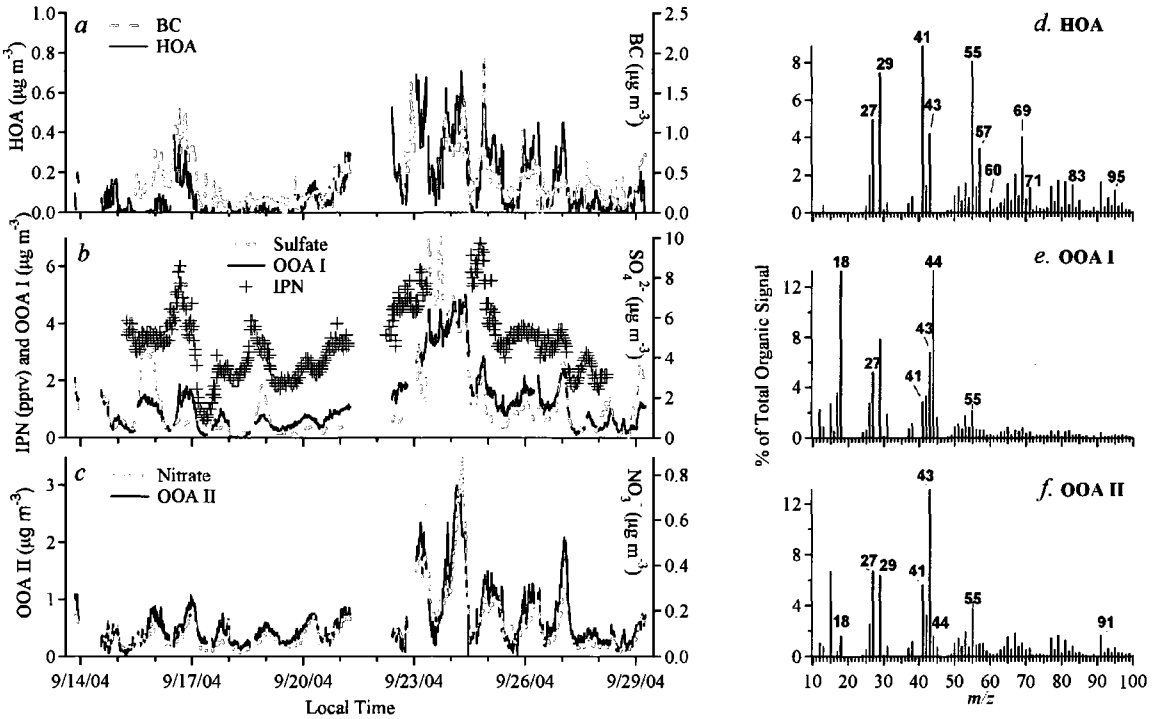

Figure II.3. Time series of concentrations (μg m^{-3}) for derived components (HOA/BBOA (a.), OOAI (b.), and OOAII (c.)) of organic aerosol measured by the Q-AMS. Other measured variables to which the components correlate are included. The corresponding derived average spectra (as in Figure II.2a) are shown in panels (d.), (e.), and (f.) for HOA/BBOA, OOAI, and OOAII, respectively. Spectra determined by the method of Zhang et al. (2007).

$dM/d\log D_{va}$ for m/z = 43 and m/z = 44 exhibited similar distributions although $dM/d\log D_{va}$ for m/z = 43 was broader and greater than that of m/z = 44 at smaller D_{va} (<200 nm) for the full campaign (Figure II.4c). This trend is especially exaggerated during E1 (Figure II.4a), and to a lesser extent during E2 (Figure II.4b).

Calculated total number-based size distributions ($dN/d\log D_{va}$, cm^{-3}) for E1, E2, and the full campaign all have a maximum at 60-70 nm D_{va} (Figure II.4d-II.4f). The magnitude of this peak is significantly increased during both events, by approximately a factor of 3 and 2 for E1 and E2, respectively. Additionally, the minor mode in $dN/d\log D_{va}$ present during the full campaign and during E2 is negligible during E1.

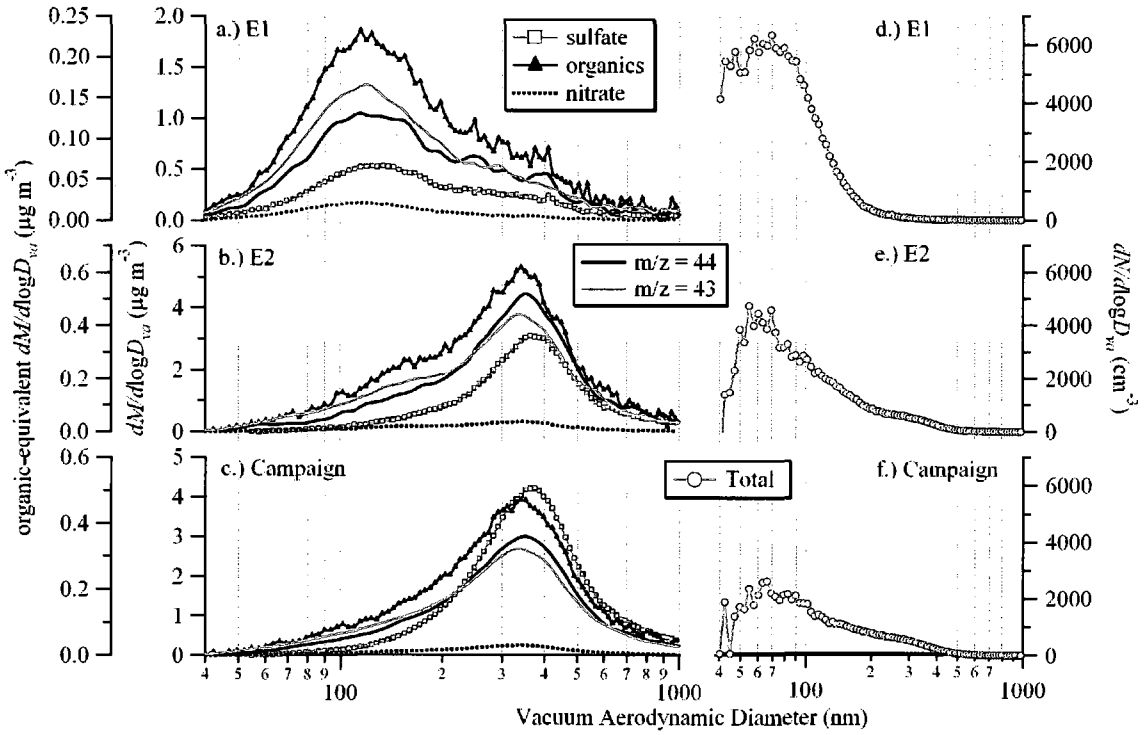

Figure II.4. Average mass-based particle size distribution ($dM/d\log D_{va}$, µg m^{-3}) for a.) E1, b.) E2, and c.) the full campaign and total aerosol average number-based particle size distribution ($dN/d\log D_{va}$, cm^{-3}) for d.) E1, e.) E2, and f.) the full campaign. Note that $dN/d\log D_{va}$ is likely underestimated at D_{va} less than 60 nm due to decreased sampling efficiency by the Q-AMS at this size range.

Data from the impactors can be used to investigate the influence of other aerosol sources on the sub-micron aerosol loading. Sulfate, as discussed above, was used to determine the collection efficiency of the Q-AMS. Here, only the sub-1.1-micron stages of the impactor are composited and averaged. For the 13 ~24-hour impactor samples collected during the campaign, the concentrations of potassium (biomass burning), magnesium (soil/crustal), and chloride (fresh oceanic air) are used as indicators of other sources that may contribute to the sub-micron Q-AMS measurement of organic material. Over the course of the campaign, the blank-corrected concentrations of these three species averaged 12.3 ± 7.3 (median of 11.0, range of 2.5 to 28.7), 2.8 ± 2.1 (median of 2.6, range of 0.1 to 6.4), and 7.2 ± 6.6 (median of 3.8, range of 1.0 to 20.3) ng m^{-3},

respectively. In each case, the average to median ratio is less than two. The uncertainty associated with each measurement is 2.4, 0.6, and 3.1 ng m^{-3}, respectively. Because of these very small concentrations, influence of biomass burning, soil components, and sea salt on sub-micron organic aerosol are considered negligible.

Data from the aethalometer can be used to indicate the typical influence of combustion sources at the site. Over the course of the entire campaign, the average BC concentration was 372 ± 289 (median of 285, range from below LDL of 4 to 1956) ng m^{-3}; on average, this indicates a BC concentration more than five times smaller than the Q-AMS observed organic aerosol and more than 10 times smaller than the total Q-AMS observed submicron aerosol. However, the BC concentrations and the average 7% contribution of HOA/BBOA to the overall organic aerosol mass loading indicate significant (though small and variable, with a ratio of average to median of 1.3) influence of anthropogenic activities at the site. Similarly, enhanced mixing ratios of NO can be used to indicate local combustion sources, despite local soil and biogenic sources (Ludwig et al., 2001; Hari et al., 2003). Over the campaign, the average ± 1σ value of NO mixing ratio was 0.2 ± 0.5 (median of 0.1) ppbv, and the corresponding range was from below the LDL of the instrument (approximately 75 pptv) to 4.7 ppbv, indicating a probable local combustion source. In general, NO mixing ratios were small, and it is likely that O_3 chemistry was NO_x-limited and that low-NOx SOA yield parameters would be most appropriate (Presto et al., 2005; Song et al., 2005). In addition, NO shows no relationship (Table II.2) with any of the organic aerosol components.

As stated previously, four (out of many) VOCs will be used to assess likely precursors to O_3 and SOA in the FACE site during the campaign and within the particle

events, specifically. The campaign average mixing ratios for toluene, isoprene, α-pinene, and isopropyl nitrate were 92.9 ± 62.0 (median of 76.7, range of 17.9 to 378.3), 427.0 ± 561.9 (median of 283.4, range of 2.6 to 6275.6), 456.6 ± 771.7 (median of 219.4, range of 19.2 to 7491.8), and 3.8 ± 2.1 (median of 3.4, range of 0.6 to 10.6) pptv, respectively. For these four compounds, the ratios of the average to the median were 1.2, 1.5, 2.1, and 1.1, respectively, indicating that BVOCs were subject to significantly greater variability, much of it diurnal in nature. Overall, the compound with the largest average and median mixing ratio was ethane, which would be expected due to its long life time. Considering reactivity (combing reaction rate constants and mixing ratios), isoprene and the monoterpene isomers had the greatest in situ impact on chemistry in the FACE site, as would be expected. In fact, α-pinene exhibited the greatest single mixing ratio observed over the course of the campaign.

In an effort to understand any relationship between different types of organic aerosol and these VOCs, regressions were performed; these are summarized in Table II.2. The primary VOCs are not correlated with any of the organic aerosol components (all R^2 less than or equal to 0.20). However, all three organic aerosol components show more significant correlation (R^2 greater than or equal to 0.34) with isopropyl nitrate, particularly OOAI, with an R^2 of 0.84. The study of deGouw et al. (2005) indicated an R^2 of 0.69 for isopropyl nitrate with total organic aerosol thought to be mostly secondary; hence, isopropyl nitrate was used as an indicator of anthropogenic SOA. In this study, the relationships between isopropyl nitrate and OOAI and between OOAI and sulfate indicate the regional anthropogenic nature of the isopropyl nitrate. The strong relationship between HOA/BBOA and isopropyl nitrate indicates that NO_x from

combustion sources is predominantly responsible for the isopropyl nitrate formation. The similar relationship between isopropyl nitrate and OOAII could indicate anthropogenic influence on local biogenic SOA formation as hypothesized by Tsigaridis and Kanakidou (2007).

Ozone mixing ratios also can be used as indicators of photochemistry, though without an indication of the relative influences of biogenic and anthropogenic emissions. Over the course of the Duke campaign, the O_3 mixing ratio ranged from 0.5 to 78.4 ppbv, with an average of 27.9 ± 14.9 and a median of 25.2. The ratio of the average to the median was 1.1. These values are not vastly different than those obtained when considering only the data from between 0800 and 1600 local time in order to account for the diurnal nature of O_3. The relationships between O_3 and the organic aerosol components are weak, with R^2 values all less than 0.33. For HOA/BBOA, this is intuitive as emissions are generally independent of photochemistry. The lack of a relationship with OOAI likely indicates that the airmasses with enhanced OOAI are aged more than a day (because of the diurnal nature of O_3). More interesting is the lack of a relationship between OOAII (thought to be representative of more local formation of SOA) and O_3 as this indicates that only minimal gas-phase photochemical activity is needed to form OOAII at this site. Although nitrogen dioxide (NO_2) is not included in this analysis due to a lack of measurements, it is assumed that its mixing ratios are small based on the relative mixing ratios of O_3 and NO. Therefore, it does not appear that OOAII would exhibit a strong relationship with O_x (O_3 + NO_2) either, which is in contrast to measurements made by Herndon et al. (2008) in Mexico City.

Relationships with meteorological parameters may also provide some insight into the nature/source of the three organic aerosol components; regression coefficients are also shown in Table II.2. Wind speed (generally on the order of 1-2 m s^{-1}), wind direction (predominantly from the east/southeast), temperature (typically around 20°C), and PAR (maximum of 1878.7 μmol m^{-2} s^{-1}) show no relationship with any of the three organic aerosol components, indicating the regional and aged nature of airmasses containing HOA/BBOA and OOAI. It is hypothesized that PAR would show the strongest relationship with OOAII, given that local SOA formation is often driven by local photochemical conditions. However, as with O_3, no strong relationship is shown between OOAII and PAR over the course of the campaign. When only daytime (0800 – 1600 local) PAR is considered (836.8 ± 502.4 mmol m^{-2} s^{-1}, median of 848.2, and range of 38.7 to 1878.7), the relationship between the organic aerosol components and PAR does not strengthen considerably, with R^2 values of 0.03, 0.16, and 0.04 for HOA/BBOA, OOAI, and OOAII, respectively. These poor relationships again indicate the regional/aged nature of HOA/BBOA and OOAI and again point to strong photochemistry not being needed to drive local formation of OOAII at this site. However, it should be pointed out that the correlation with PAR and OOAII could be affected by the coupling between PAR and temperature. Due to its semi-volatile nature (Lanz et al., 2007; Ulbrich et al., 2009), OOAII is expected to evaporate under elevated temperatures.

Events

Over the course of the campaign, two events were identified according to the criteria outlined previously. The corresponding event days were 19 – 20 September (again defined as 1200 to 1200 local) and 24 – 25 September, as shown in Table II.1 and

highlighted in Figure II.1. The average mass concentrations of the aerosol species (both measured and calculated), mixing ratios of gaseous pollutants, and values for meteorological parameters are summarized in Table II.1 for each event. Table II.2 includes the R^2 values for regressions between parameters within a given event.

Events: E1

Compared to the average, E1 exhibited decreased concentrations of OM, HOA/BBOA, OOAI, OOAII, sulfate, ammonium, nitrate, and BC in the observed aerosols. The increased fractional contribution of OOAII to the overall organic mass (OM) is confirmed by the spectrum indicated in Figure II.5a that shows enhancement at m/z 43. In addition, the aerosol in E1 appears to be less neutralized with respect to ammonium. During E1, the mixing ratios of O_3 were comparable to the campaign average, but other gases (NO and VOCs) exhibited mixing ratios that were smaller than the average. Meteorology during E1 indicated a prevailing wind direction from the east, and backward trajectories indicated clean airmass histories from the north. Average temperatures were low (favoring partitioning of secondary material to the aerosol phase) and enhanced PAR (to drive photochemistry) was likely to influence formation of secondary aerosols.

E1 exhibited relationships between the organic aerosol components and the inorganic aerosol components similar to those for the campaign average, as shown in Table II.2. OOAI and OOAII exhibit enhanced correlations with toluene and isoprene and show consistent trends with isopropyl nitrate. OOAI and OOAII both show strong relationships to temperature and daytime PAR.

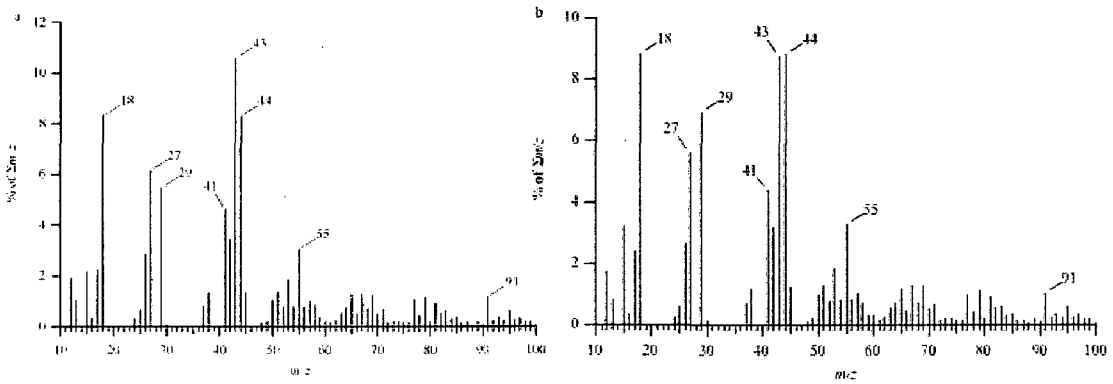

Figure II.5. Average mass spectra as in Figure II.2a for each of the events discussed in the text: a.) E1; b.) E2.

These factors indicate the influence of temperature-driven partitioning of secondary, photochemically derived species from oxidation of both anthropogenic and biogenic parent hydrocarbons. The relationship between OOAII and isopropyl nitrate again points to the enhancement of biogenic SOA formation by the presence of anthropogenic material.

The particle size distribution during E1 was significantly different than the campaign average. The most prominent feature of the mass-based particle size distribution in Figure II.4a was a peak at approximately 120 nm D_{va} that was present, but not distinct, in the campaign average $dM/d\log D_{va}$ shown in Figure II.4c. At this E1 $dM/d\log D_{va}$ peak, organic compounds are the dominant chemical constituent with nearly 3.5 times the mass of sulfate and 10 times that of nitrate. This distribution of mass is nearly unchanged at $dM/d\log D_{va}$ at 60 nm D_{va}. $dM/d\log D_{va}$ for m/z = 43 is enhanced distinctly (compared to $dM/d\log D_{va}$ for m/z = 44) at D_{va} less than 200 nm during E1 (Figure II.4a), consistent with the sub-200 nm organic aerosol during this event being less oxidized and potentially from biogenic sources.

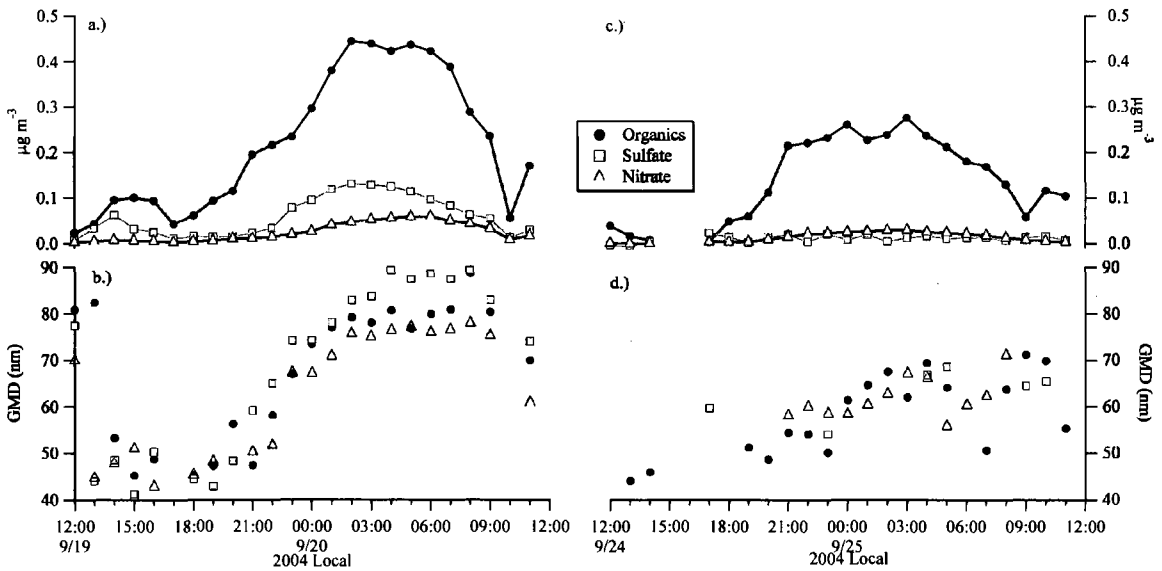

Figure II.6. Evolution of associated particle mass concentration (top panels) and GMD (bottom panels) during E1 (left, panels a and b) and E2 (right, panels c and d) for organic compounds, sulfate, and nitrate. Mass concentrations include only the mass associated with the peak in $dN/d\log D_{va}$ which occurred at sub-100 nm D_{va} during each event.

The most prominent peak in the campaign-average $dM/d\log D_{va}$ between 300 and 400 nm D_{va} is nearly absent during E1. The number-based size distribution during E1 is characterized by an increased magnitude of the sub-100 nm D_{va} peak (by greater than a factor of two) that seems to be present beyond the Q-AMS detection limit to D_{va} smaller than 40 nm. There was negligible contribution to $dN/d\log D_{va}$ at larger D_{va} (>200 nm) during E1. The small particles indicate the importance of recent growth during E1, most likely of biogenic SOA.

Changes in the calculated GMD were used to assess particle mass increases and GR during E1. Additionally, the chemically-resolved mass concentrations associated with the peak at each GMD were calculated. Both GMD and event-associated mass concentrations are shown in Figure II.6a. The calculated GMD was observed to increase linearly with time starting at 1800 on 19 September and ending at 0400 the following

day. This behavior is consistent with observations of aerosol growth in many other regions of the atmosphere. The timing and calculated GR of each chemical constituent were similar, with values of 4.0, 4.9, and 3.6 nm hr^{-1} for organic compounds, sulfate, and nitrate, respectively. Correlation coefficients (R^2) for the calculation of GR were 0.95, 0.98, and 0.96 for each chemical component, respectively, indicating the linear nature of geometric growth. The similar GR values for each component suggest that the organic compounds, sulfate, and nitrate were internally mixed. An average net increase of 37 nm in D_{va} was observed during the growth event. The event-associated mass of organic compounds, sulfate, and nitrate showed increases from 1800 to 0400 local time of 0.38 $\mu g\ m^{-3}$, 0.11 $\mu g\ m^{-3}$, and 0.041 $\mu g\ m^{-3}$, respectively, suggesting that organic compounds contributed the majority, 71%, of the mass during the growth event.

Events: E2

During E2, mass concentrations of inorganic aerosol constituents were also decreased relative to the campaign average (Table II.1) but were larger than concentrations during E1. Concentrations of OM and the individual organic aerosol components were enhanced, though with essentially no change in their relative importance. Neutralization with respect to ammonium was more similar to the campaign average than during E1. The average spectrum of the organic aerosol during E2 (Figure II.5b) was also more similar to the campaign average (including the delta analysis) compared to E1, in that the signals from m/z 43 and m/z 44 were roughly equivalent and contributed approximately 9% each to the total organic signal. Isoprene and toluene mixing ratios were comparable to the campaign average, but that of α-pinene was decreased and that of isopropyl nitrate was enhanced. Enhanced HOA/BBOA and a more

aged spectrum compared to E1 indicate an increased influence of anthropogenic organic aerosol constituents (though not compared to the campaign average). This is supported by HYSPLIT backward trajectories that traveled down the eastern seaboard of the United States for the three days prior to arrival at the sampling site. Unfortunately, BC, NO, O_3, and other meteorological data were unavailable during E2. Inter-relationships shown in Table II.2 are similar to those for E1, particularly for aerosol constituents. The relationships with VOCs are, in general, less strong, and only OOAI is correlated positively to isopropyl nitrate, again indicating its regional nature.

The particle size distribution during E2 (Figure II.4b) was more similar to the campaign-average $dM/d\log D_{va}$ (Figure II.4c) than was the distribution during E1. The most prominent feature of the mass-based particle size distribution in Figure II.4b was not the 120-nm D_{va} peak as in E1 but one at approximately 350 nm D_{va}, indicating the presence of larger aerosol. Still, organic compounds comprise almost twice the sulfate mass during E2. This is in contrast to the campaign-average mass distribution which slightly favors sulfate at the peak $dM/d\log D_{va}$. This distribution is more exaggerated at 60 nm D_{va}, with organic compounds accounting for almost 20 times more mass than sulfate. The nitrate mass concentration was greater than the sulfate concentration by nearly 40%. The sub-200 nm increase in $dM/d\log D_{va}$ of m/z = 43 compared to $dM/d\log D_{va}$ of m/z = 44 is less prominent during E2 (Figure II.4b) and likely indicates that biogenic oxidation products play a decreased role during E2 compared to E1. Clearly, no single factor controls growth of small particles in the suburban forest.

Aerosol growth was also observed during E2, as evidenced by a linear increase in GMD and an increase in associated-particle mass concentration shown in Figure II.6b.

The timing of growth during E2 was very similar to that of E1 (Figure II.6a), with increases in mass and GMD starting at approximately 1800 local time. Calculated GR for organic compounds and nitrate were 2.2 nm hr^{-1} and 1.2 nm hr^{-1} ($R^2 = 0.89$, $R^2 = 0.82$) respectively, with an average change in GMD of 21 nm D_{va}. These values were small compared to those found for E1. Few GMD values could be determined for sulfate due to very low mass concentrations during the event; therefore, no GR determination was made. The associated mass concentrations of both organic compounds and nitrate increased during the event, by 0.27 μg m^{-3} and 0.025 μg m^{-3}, respectively, suggesting that organic compounds contributed 92% of the mass increase. No significant change in associated sulfate mass concentration was observed.

Discussion and Conclusions

As has been stated previously, homogeneous nucleation/growth events have been observed regardless of preexisting particle mass in many different locations throughout the atmosphere (Kulmala, 2003), including both urban or downwind polluted regions (Birmili and Wiedensohler, 2000; Harrison et al., 2000; Alam et al., 2003; Weber et al., 2003; Mozurkewich et al., 2004; Stanier et al., 2004; McMurry et al., 2005; Qian et al., 2007; Smith et al., 2008) and rural or more remote areas (Weber et al., 1995; Clarke et al., 1999; O'Dowd et al., 2002) including the boreal forest (Mäkelä et al., 1997). Boy et al. (2008) present evidence for the role of sesquiterpene oxidation in the formation and growth of new particles in a study that occurred in the Front Range of the Rocky Mountains. In addition, oxidation of fresh plant emissions (VanReken et al., 2006; Kiendler-Scharr et al., 2009) and of single BVOC (Burkholder et al., 2007) in the

laboratory has been shown to lead to new particle formation and growth. Because the Duke FACE site is situated in the vicinity of a conglomerate of three moderately sized cities and experiences abundant biogenic emission of its own, it is interesting to determine if formation and subsequent growth of new particles occurs at this location. While observation of new particle formation is not claimed in this manuscript, it is possible that the elevated calculated particle number concentrations associated with smaller diameters are the result of the growth of newly formed particles to a size measureable by the Q-AMS. Simultaneous consideration of number concentration, size, and composition of such particles is critical for assessing their role in climate.

During late summer, the atmosphere at the Duke FACE site appeared to be influenced to some extent by both anthropogenic and biogenic material. Regional OOAI and sulfate constitute significant fractions of the observed particulate matter, as does HOA/BBOA. In contrast, the OOA components do not appear as aged as those observed in other forested, rural areas (Allan et al., 2006; Cottrell et al., 2008), indicating a stronger local source. This is evidenced by the increased relative importance of OOAII in this study.

One previous study also presents Q-AMS measurements of particulate matter in the Duke Forest (Stroud et al., 2007). This study was conducted during July 2003. Inorganic aerosol constituents appear to have similar concentrations and variability as those presented for the current study, likely implying that anthropogenic influences between the two summer periods of different years were similar. Organic concentrations presented by Stroud et al. (2007) (maxima approaching 20 $\mu g\ m^{-3}$) are significantly larger than those presented in the current study. Although the measurements can not be

compared directly, it is possible that this increase in OM in the study of Stroud et al. (2007) results from increased BVOC emission and chemistry as a result of stronger photochemistry during July relative to September. Unfortunately, an extensive spectral analysis is not presented by Stroud et al. (2007) so that comparisons of OM components, contributions of specific m/z, etc., are not possible. However, based on a closure study focused on prediction of cloud condensation nuclei concentrations, Stroud et al. (2007) inferred a mixed anthropogenic/biogenic influence on the atmosphere above the Duke FACE site, a conclusion in agreement with that of the present study.

Two events were identified over the course of the campaign based on elevated number concentrations and mass concentrations of small particles. Both events exhibited linear increases in GMD and increases in mass concentration consistent with particle growth. Observed GR values between 1.2 and 4.9 nm hr^{-1} are consistent with values of between 1 and 20 nm hr^{-1} observed at other rural mid-latitude sites (Kulmala et al., 2004), and with an average GR of 3 nm hr^{-1} that was observed from eight years of measurements at a boreal forest in southern Finland (Dal Maso et al., 2005). An average GR of 3.8 nm hr^{-1} was observed during summertime observations on the western slope of the Sierra Nevada Mountains of California at a site similarly located in a pine-forest environment (Lunden et al., 2006), a result consistent with the findings presented here. Organic compounds contributed the majority of condensed mass during both events, with minor contribution from sulfate and nitrate. The timing of growth was similar during each event, although little consistency was observed between the two events in terms of concentrations, compositions, mass-based particle size distributions, airmass history, and inter-relationships among both measured and derived quantities compared to the

campaign average. Thus, it appears that particle growth occurred during periods of both local biogenic and regional anthropogenic conditions. This leads to the conclusion that even within forest canopies, different precursors and processes can lead to the formation and growth of small particles. There is no apparent single parameter or group of consistent parameters that controls this process.

References

Alam, A., Shi, J.P., and Harrison, R.M., 2003. Observations of new particle formation in urban air. Journal of Geophysical Research 108, doi:10.1029/2001JD001417.

Allan, J.D., Delia, A.E., Coe, H., Bower, K.N., Alfarra, M.R., Jimenez, J.L., Middlebrook, A.M., Drewnick, F., Onasch, T.B., Canagaratna, M.R., Jayne, J.T., and Worsnop, D.R., 2004. A generalized method for the extraction of chemically resolved mass spectra from Aerodyne aerosol mass spectrometer data. Journal of Aerosol Science 35, 909-922.

Allan, J. D., Jimenez, J.L., Williams, P.I., Alfarra, M.R., Bower, K.N., Jayne, J.T., Coe, H., and Worsnop, D.R., 2003. Quantitative sampling using an Aerodyne aerosol mass spectrometer – 1. Techniques of data interpretation and error analysis. Journal of Geophysical Research 108, doi:10.1029/2002JD002358.

Allan, J.D., Alfarra, M.R., Bower, K.N., Coe, H., Jayne, J.T., Worsnop, D.R., Aalto, P.P., Kulmala, M., Hyötyläinen, T., Cavalli, F., and Laaksonen, A., 2006. Size and composition measurements of background aerosol and new particle growth in a Finnish forest during QUEST 2 using an Aerodyne Aerosol Mass Spectrometer. Atmospheric Chemistry and Physics 6, 315-327.

Bahreini, R., Keywood, M.D., Ng, N.L., Varutbangkul, V., Gao, S., Flagan, R.C., Seinfeld, J.H., Worsnop, D.R., and Jimenez, J.L., 2005. Measurements of secondary organic aerosol from oxidation of cycloalkenes, terpenes, and m-xylene using an Aerodyne aerosol mass spectrometer. Environmental Science and Technology 15, 5674-5688.

Birmili, W., and Wiedensohler, A., 2000. New particle formation in the continental boundary layer: Meteorological and gas phase parameter influence. Geophysical Research Letters 27, 3325-3328.

Boy, M., Karl, T., Turnipseed, A., Mauldin, R.L., Kosciuch, E., Greenberg, J., Rathbone, J., Smith, J., Held, A., Barsanti, K., Wehner, B., Bauer, S., Wiedensolhler, A.,

Bonn, B., Kulmala, M., and Guenther, A., 2008. New particle formation in the Front Range of the Colorado Rocky Mountains. Atmospheric Chemistry and Physics 8, 1577-1590.

Burkholder, J.B., Baynard, T., Ravishankara, A.R., and Lovejoy, E.R., 2007. Particle nucleation following the O_3 and OH initiated oxidation of alpha-pinene and beta-pinene between 278 and 320 K. Journal of Geophysical Research 112, doi:10.1029/JD007783.

Canagaratna, M., Jayne, J., Jimenez, J.L., Allan, J.A., Alfarra, R., Zhang, Q., Onasch, T., Drewnick, F., Coe, H., Middlebrook, A., Delia, A., Williams, L., Trimborn, A., Northway, M., DeCarlo, P., Kolb, C., Davidovits, P., and Worsnop, D., 2007. Chemical and microphysical characterization of ambient aerosols with the Aerodyne aerosol mass spectrometer. Mass Spectrometry Reviews 26, doi:10.1002/mas.20115.

Charlson, R.J., Schwartz, S.E., Hales, J.M., Cess, R.D., Coakley, J.A., Hansen, J.E., and Hofmann, D.J., 1992. Climate forcing by anthropogenic aerosols. Science 255, 423-430.

Clarke, A.D., Eisele, F., Kapustin, V.N., Moore, K., Tanner, D., Mauldin, L., Litchy, M., Lienert, B., Carroll, M.A., and Albercook, G., 1999. Nucleation in the equatorial free troposphere: Favorable environments during PEM-Tropics. Journal of Geophysical Research 104, 5735-5744.

Cottrell, L.D., Griffin, R.J., Jimenez, J.L., Zhang, Q., Ulbich, I., Ziemba, L.D., Beckman, P.J., Sive, B.C., and Talbot, R.W., 2008. Submicron particles at Thompson Farm during ICARTT measured using aerosol mass spectrometry. Journal of Geophysical Research 113, doi:10.1029/2007JD009192.

Cwiertny, D.M., Young, M.A., and Grassian, V.H., 2008. Chemistry and photochemistry of mineral dust aerosol. Annual Review of Physical Chemistry 59, 27-51.

DeBell, L.J., Vozzella, M., Talbot, R.W., and Dibb, J.E., 2004. Asian dust storm events of spring 2001 and associated pollutants observed in New England by the AIRMAP monitoring network. Journal of Geophysical Research 109, doi:10.1029/2003JD003733.

de Gouw, J.A., Middlebrook, A.M., Warneke, C., Goldan, P.D., Kuster, W.C., Roberts, J.M., Fehsenfeld, F.C., Worsnop, D.R., Canagaratna, M.R., Pszenny, AAP., Keene, W.C., Marchewka, M., Bertman, S.B., and Bates, T.S., 2005. Budget of organic carbon in a polluted atmosphere: Results from the New England Air Quality Study in 2002. Journal of Geophysical Research 110, doi:10.1029/2004JD005623.

Dal Maso, M., Kulmala, M., Riipinen, I., Wagner, R., Hussein, T., Aalto, P.P., and Lehtinen, K.E.J., 2005. Formation and growth of fresh atmospheric aerosols: Eight years of aerosol size distribution data from SMEAR II, Hyytiala, Finland. Boreal Environmental Research 10, 323-336.

Draxler, R.R. and Rolph, G.D., 2003. HYSPLIT (HYbrid Single-Particle Lagrangian Integrated Trajectory) Model access via NOAA ARL READY Website (http://www.arl.noaa.gov/ready/hysplit4.html). NOAA Air Resources Laboratory, Silver Spring, MD.

Drewnick, F., Jayne, J.T., Canagaratna, M., Worsnop, D.R., and Demerjian, K.L., 2004. Measurement of ambient aerosol composition during PMTACS-NY 2001 using an aerosol mass spectrometer. Part II: Chemically speciated mass distributions. Aerosol Science and Technology 38, 104-117.

Guenther, A., Hewitt, C.N., ,Erickson, D., Fall, R., Geron, C., Graedel, T., Harley, P., Klinger, L., Lerdau, M., Mckay, W.A., Pierce, T., Scholes, B., Steinbrecher, R., Tallamraju, R., Taylor, J., and Zimmerman, P., 1995. A global-model of natural volatile organic-compound emissions. Journal of Geophysical Research 100, 8873-8892.

Hari, P., Raivonen, M., Vesala, T., Munger, J.W., Pilegaard, K., and Kulmala, M., 2003. Atmospheric science – Ultraviolet light and leaf emission of NO_x. Nature 422, 134.

Harrison, R.M., Grenfell, J.L., Savage, N., Allen, A., Clemitshaw, K.C., Penkett, S., Hewitt, C.N., and Davison, B., 2000. Observations of new particle formation in the atmosphere of a moderately polluted site in eastern England. Journal of Geophysical Research 105, 17819-17832.

Held, A., Nowak, A., Birmili, W., Wiedensohler, A., Forkel, R., and Klemm, O., 2004. Observations of particle formation and growth in a mountainous forest region in central Europe. Journal of Geophysical Research 109, doi:10.1029/2004JD005346.

Herndon, S.C., Onasch, T.B., Wood, E.C., Kroll, J.H., Canagaratna, M.R., Jayne, J.T., Zavala, M.A., Knighton, W.B., Mazzoleni, C., Dubey, M.K., Ulbich, I.M., Jimenez, J.L., Seila, R., de Gouw, J.A., de Foy, B., Fast, J., Molina, L.T., Kolb, C.E., and Worsnop, D.R., 2008. Correlation of secondary organic aerosol with odd oxygen in Mexico City. Geophysical Research Letters 35, doi:10.1029/2008GL034058.

Hock, B.N., Schneider, J., Borrmann, S., Rompp, A., Moortgat, G., Franze, T., Schauer, C., Poschl, U., Plass-Dulmer, C., and Berresheim, H., 2008. Rural continental aerosol properties and processes observed during the Hohenpeissenberg Aerosol

Characterization Experiment (HAZE2002), Atmospheric Chemistry and Physics 8, 603-623.

Hoffmann, T., Odum, J.R., Bowman, F., Collins, D., Klockow, D., Flagan, R.C., and Seinfeld, J.H., 1997. Formation of organic aerosols from the oxidation of biogenic hydrocarbons. Journal of Atmospheric Chemistry 26, 189-222.

Jayne, J.T., Leard, D.C., Zhang, X.F., Davidovits, P., Smith, K.A., Kolb, C.E., Worsnop, D.R., 2000. Development of an aerosol mass spectrometer for size and composition analysis of submicron particles. Aerosol Science and Technology 33, 49-70.

Jimenez, J.L., Jayne, J.T., Shi, Q., Kolb, C.E., Worsnop, D.R., Yourshaw, I., Seinfeld, J.H., Flagan, R.C., Zhang, X.F., Smith, K.A., Morris, J.W., and Davidovits, P., 2003. Ambient aerosol sampling using the aerodyne aerosol mass spectrometer. Journal of Geophysical Research-Atmospheres 108, doi:10.1029/2001JD001213.

Jordan, C.E. and Talbot, R.W., 2000. Direct atmospheric deposition of water-soluble nitrogen to the Gulf of Maine. Global Biogeochemical Cycles 14, 1315-1329.

Kiendler-Scharr, A., Zhang, Q., Hohaus, T., Kleist, E., Mensah, A., Mentel, T., Spindler, C., Tillmann, R., and Wildt, J., 2009. Aerosol Mass Spectrometric Features of Biogenic SOA: Observations from a Plant Chamber and in Rural Atmospheric Environments, Atmospheric Chemistry and Physics, in preparation.

Kroll, J.H., Ng, N.L., Murphy, S.M., Flagan, R.C., and Seinfeld, J.H., 2006. Secondary organic aerosol formation from isoprene photooxidation. Environmental Science and Technology 40, 1869-1877.

Kulmala, M., 2003. How particles nucleate and grow. Science 302, 1000-1001.

Kulmala, M., Vehkamäki, H., Petäjä, T., Dal Maso, M., Lauri, A., Kerminen, V.M., Birmili, W., and McMurry, P.H., 2004. Formation and growth rates of ultrafine atmospheric particles: a review of observations. Journal of Aerosol Science 35, 143-176.

Lanz, V.A., Alfarra, M.R., Baltensperger, U., Buchmann, B., Hüglin, C., and Prévôt, A.S.H., 2007. Source apportionment of submicron organic aerosols at an urban site by factor analytical modelling of aerosol mass spectra, Atmospheric Chemistry and Physics 7, 1503-1522, 2007.

Liu, P., Ziemann, P.J., Kittelson, D.B., and McMurry, P.H., 1995. Generating particle beams of controlled dimensions and divergence. 1. Theory of particle motion in aerodynamic lenses and nozzle expansions. Aerosol Science and Technology 22, 293-313.

Liu, P., Ziemann, P.J., Kittelson, D.B., and McMurry, P.H., 1995. Generating particle beams of controlled dimensions and divergence. 2. Experimental evaluation of particle motion in aerodynamic lenses and nozzle expansions. Aerosol Science and Technology 22, 314-324.

Ludwig, J., Meixner, F.X., Vogel, B., and Forstner, J., 2001. Soil-air exchange of nitric oxide: An overview of processes, environmental factors, and modeling studies. Biogeochemistry 52, 225-257.

Lunden, M.M., Black, D.R., Mckay, M., Revzan, K.L., Goldstein, A.H., and Brown, N.J., 2006. Characteristics of fine particle growth events observed above a forested ecosystem in the Sierra Nevada Mountains of California. Aerosol Science and Technology 40, 373-388.

Mäkelä, J.M., Aalto, P., Jokinen, V., Pohja, T., Nissinen, A., Plamroth, S., Markkanen, T., Seitsonen, K., Lihavainen, H., Kulmala, M., 1997. Observations of ultrafine aerosol particle formation and growth in a boreal forest. Geophysical Research Letters 24, 1219-1222.

Mäkelä, J.M., Koponen, I.K., Aalto, P., and Kulmala, M., 2000. One-year data of submicron size modes of tropospheric background aerosol in southern Finland. Journal of Aerosol Science 31, 595-611.

Mao, H.T., Talbot, R.W., Troop, D., Johnson, R., Businger, S., and Thomposon, A.M., 2006. Smart balloon observations over the North Atlantic: O_3 data analysis and modeling. Journal of Geophysical Research 111, doi:10.1029/2005JD006507.

Marquez, C., Castro, T., Muhlia, A., Moya, M., Martinez-Arroyo, A., and Baez, A., 2005. Measurement of aerosol particles, gases and flux radiation in the Pico de Orizaba National Park, and its relationship to air pollution transport. Atmospheric Environment 39, 3877-3890.

McLafferty, F.W., and Turecek, F., 1993. Interpretation of mass spectra. University Science Books 4th edition.

McMurry, P.H., Fink, M., Sakurai, H., Stolzenburg, M.R., Mauldin, R.L., Smith, J., Eisele, F., Moore, K., Sjostedt, S., Tanner, D., Huey, L.G., Nowak, J.B., Edgerton, E., and Voisin, D., 2005. A criterion for new particle formation in the sulfur-rich Atlanta atmosphere. Journal of Geophysical Research 110, doi:10.1029/2005JD005901.

Mozurkewich, M., Chan, T.W., Aklilu, Y.A., and Verheggen, B., 2004. Aerosol particle size distributions in the lower Fraser Valley: evidence for particle nucleation and growth. Atmospheric Chemistry and Physics 4, 1047-1062.

Naik V., Delire, C., and Wuebbles, D.J., 2004. Sensitivity of global biogenic isoprenoid emissions to climate variability and atmospheric CO_2. Journal of Geophysical Research 109, D06301, doi:10.1029/2003JD004236.

O'Dowd, C.D., Jimenez, J.L., Bahreini, R., Flagan, R.C., Seinfeld, J.H., Hameri, K., Pirjola, L., Kulmala, M., Jennings, S.G., and Hoffmann, T., 2002. Marine aerosol formation from biogenic iodine emissions. Nature 417, 632-636.

Odum, J.R., Jungkamp, T.P.W., Griffin, R.J., Forstner, H.J.L., Flagan, R.C., and Seinfeld, J.H., 1997. Aromatics, reformulated gasoline, and atmospheric organic aerosol formation. Environmental Science and Technology 31, 1890-1897.

Phillips, M.A., Savage, T.J., and Croteau, R., 1999. Monoterpene synthases of loblolly pine (Pinus taeda) produce pinene isomers and enatniomers. Archives of Biochemistry and Biophysics 372, 197-204.

Presto, A.A., Hartz, K.E.H., and Donahue, N.M., 2005. Secondary organic aerosol production from terpene ozonolysis. 2. Effect of NO_x concentration. Environmental Science and Technology 39, 7046-7054.

Qian, S., Sakurai, H., and McMurry, P.H., 2007. Characteristics of regional nucleation events in urban East St. Louis. Atmospheric Environment 41, 4119-4127.

Schichtel, B.A., Husar, R.B., Falke, S.R., and Wilson, W.E., 2001. Haze trends over the United States, 1980-1995. Atmospheric Environment 35, 5205-5210.

Schwartz, J., Dockery, D.W., and Neas, L.M., 1996. Is daily mortality associated specifically with fine particles? Journal of Air and Waste Management Association 46, 927-939.

Seinfeld, J.H., and Pankow, J.F., 2003. Organic atmospheric particulate material. Annual Review of Physical Chemistry 54, 121-140.

Sive, B.C., Zhou, Y., Troop, D., Wang, Y.L., Little, W.C., Wingenter, O.W., Russo, R.S., Varner, R.K., and Talbot, R.W., 2005. Development of a cryogen-free concentration system for measurements of volatile organic compounds. Analytical Chemistry 77, 6989-6998.

Smith, J.N., Dunn, M.J., VanReken, T.M., Iida, K., Stolzenburg, M.R., McMurry, P.H., and Huey, L.G., 2008. Chemical composition of atmospheric nanoparticles formed from nucleation in Tecamac, Mexico: Evidence for an important role of organic species in nanoparticle growth. Geophysical Research Letters 35, doi:10.1029/2007GL032523.

Song, C., Na, K.S., and Cocker, D.R., 2005. Impact of the hydrocarbon to NO_x ratio on secondary organic aerosol formation. Environmental Science and Technology 39, 3143-3149.

Stanier, C.O., Khlystov, A.Y., and Pandis, S.N., 2004. Ambient aerosol size distributions and number concentrations measured during PAQS. Atmospheric Environment 38, 3275-3284.

Stroud, C.A., Nenes, A., Jimenez, J.L., DeCarlo, P.F., Huffman, J.A., Bruintjes, R., Nemitz, E., Delia, A.E., Toohey, D.W., Guenther, A.B., Nandi, S., 2007. Cloud activating properties of aerosol observed during CELTIC. Journal of Atmospheric Sciences 64, 441-459.

Tsigaridis, K., and Kanakidou, M., 2007. Secondary organic aerosol importance in the future atmosphere. Atmospheric Environment 41, 4682-4692.

Ulbrich, I., Canagaratna, M., Zhang, Q., Worsnop, D., and Jimenez, J., 2008. Interpretation of organic components from positive matrix factorization of aerosol mass spectrometric data. Atmospheric Chemistry and Physics 9, 2891-2918.

VanReken, T.M., Greenberg, J.P., Harley, P.C., Guenther, A.B., and Smith, J.N., 2006. Direct measurement of particle formation and growth from the oxidation of biogenic emissions. Atmospheric Chemistry and Physics 6, 4403-4413.

Weber, R.J., McMurry, P.H., Eisele, F.L., and Tanner, D.J., 1995. Measurement of expect nucleation precursor species and 3-500-nm diameter particles at Mauna-Loa-Observatory, Hawaii. Journal of the Atmospheric Sciences 52, 2242-2257.

Weber, R.J., Orsini, D., Wang, B., Scheuer, E., Talbot, R.W., Dibb, J.E., Seid, G.K., DeBell, L., Mauldin, R.L., Kosciuch, C., Cantrell, C., and Eisele, F., 2003. New particle formation in anthropogenic plumes advecting from Asia observed during TRACE-P. Journal of Geophysical Research 108, doi:10.1029/2002JD003112.

White, M. L., Russo, R.S., Zhou, Y., Ambrose, J.L., Haase, K., Frinak, E.K., Varner, R.K., Wingenter, O.W., Mao, H., Talbot, R., and Sive, B.C., 2009. Are biogenic emissions a significant source of summertime atmospheric toluene in the rural Northeastern United States? Atmospheric Chemistry and Physics 9, 81-92.

Zhang, Q., Stanier, C.O., Canagaratna, M.R., Jayne, J.T., Worsnop, D.R., Pandis, S.N., and Jimenez, J.L., 2004. Insights into the chemistry of new particle formation and growth events in Pittsburgh based on Aerosol Mass Spectrometry. Environmental Science and Technology, 38, 4797-4809.

Zhang, Q., Worsnop, D.R., Canagaratna, M.R., Jimenez, J.L., 2005. Hydrocarbon-like and oxygenated organic aerosols in Pittsburgh: Insights into sources and processes of organic aerosols. Atmospheric Chemistry and Physics 5, 3289-3311.

Zhang, Q. et al., 2007. Ubiquity and dominance of oxygenated species in organic aerosols in anthropogenically-influenced Northern Hemispheric midlatitudes. Geophysical Research Letters 34, doi:10.1029/2007GL029979.

CHAPTER III

CHARACTERIZATION OF WATER-SOLUBLE ORGANIC AEROSOL IN COASTAL NEW ENGLAND: IMPLICATIONS OF VARIATIONS IN SIZE DISTRIBUTION

Abstract

Size distributions up to 10-micron aerosol diameter (D_P) of organic carbon (OC) and water-soluble organic carbon (WSOC) were measured at two sites in coastal New England, slightly inland at Thompson Farm (TF) and offshore at Isles of Shoals (IOS). Significant OC concentrations were measured in the accumulation (D_P < 0.7 μm; 1.18 and 1.38 μg m^{-3}), droplet (D_P = 0.7-2.1; 1.11 and 1.48 μg m^{-3}), and coarse (D_P = 2.1-9.0; 2.20 and 1.79 μg m^{-3}) size modes at TF and IOS, respectively. The WSOC fraction (WSOC/OC) was largest in the accumulation mode with values of 0.86 and 0.93, respectively, and smallest in the coarse mode with values of 0.61 and 0.79 at TF and IOS, respectively. Dicarboxylic acids containing up to five carbon atoms (C_5) were concentrated in droplet and accumulation mode aerosol with minor contributions in the coarse mode. C_1-C_3 monocarboxylic acids were generally near or below detection limits. Results from proton nuclear magnetic resonance (HNMR) analyses showed that the organic function group characterized by protons in the alpha position to an unsaturated carbon atoms ([H-C-C=]) was the dominant WSOC functionality at both TF and IOS, constituting 34 and 43% of carbon-weighted HNMR signal, respectively. Size distributions of each HNMR-resolved organic functionality are presented. Source

apportionment using HNMR fingerprints is also presented, and results indicate that nearly all of the WSOC at TF and IOS resembled secondary organic aerosol, regardless of D_P.

Introduction

Organic compounds are ubiquitous in ambient aerosol (Kanakidou et al., 2005) and constitute a large but variable portion of total aerosol mass depending on season, location, time-of-day, and particle size. Based on aerosol mass spectrometric measurements, a large fraction of sub-micron organic aerosol (OA), between 64% and 95% depending on location, has been shown to be oxygenated and likely secondary in nature (Zhang et al., 2007) as a result of gas-to-particle conversion or aqueous processing. Similarly, a large fraction of OA is water soluble. The water-soluble organic carbon (WSOC) content of OA also greatly varies with location and airmass age, from nearly 10% in urban areas to 70-80% in rural areas (Jaffrezo et al., 2005 and references therein) to greater than 90% in the remote Arctic (Hagler et al., 2008).

Although oxalic acid comprises only a few percent of WSOC mass, it is typically the most abundant carboxylic acid found in ambient aerosols because it is the end-product of various oxidation/decomposition pathways (Ervens et al., 2004). Oxalic acid was determined to be principally a secondary product based on a distinct seasonality and strong correlation with ozone (Kawamura and Ikushima, 1993). Strong correlations with sulfate aerosol (Yu et al., 2005) and the prevalence of oxalic acid aerosol in clouds compared to below cloud (Crahan et al., 2004; Sorooshian et al., 2006) suggest that aqueous processing is the dominant pathway for secondary oxalic acid formation. However, evidence regarding oxalic acid as a primary pollutant from combustion processes is inconclusive (Kawamura and Kaplan, 1987; Huang and Yu, 2007).

Modeling has identified two pathways of aqueous-phase oxalic acid formation: 1.) sequential dicarboxylic acid decarboxylation of glutaric acid to succinic, malonic, and

oxalic acids (Ervens et al., 2004) by simplified reaction (R1) and 2.) hydroxylation of pyruvic acid through glyoxylic acid (Lim et al., 2005) by reaction simplified (R2):

$$\text{Glutarate } (C_5) \xrightarrow{OH} \text{Succinate } (C_4) \xrightarrow{OH} \text{Malonate } (C_3) \xrightarrow{OH} \text{Oxalate } (C_2) \qquad \text{(R1)}$$

$$\text{Pyruvate } (C_3) \xrightarrow{OH} \text{Acetate } (C_2) \xrightarrow{OH} \text{Glyoxylate } (C_2) \xrightarrow{OH} \text{Oxalate } (C_2) \qquad \text{(R2)}$$

Acids are shown above as dissociated ions. Glutaric acid is present in the aqueous phase due to partitioning of gas-phase oxidation products of alkenes (Kalberer et al., 2000; Ervens et al., 2004) that have both biogenic and anthropogenic sources. Glyoxylic acid is an aqueous-phase product of the oxidation of methylglyoxal, pyruvic acid, acetic acid, glycolic acid, and hydroxyacetaldehyde (Lim et al., 2005), which arise from oxidation of precursors of both biogenic and anthropogenic origin.

The bulk functionality of WSOC has been determined by proton nuclear magnetic resonance (HNMR) (Decesari et al., 2000) and Fourier transfer infrared spectroscopy (Gilardoni et al., 2007) techniques. These analyses are particularly useful because they are able to resolve a large fraction of WSOC that cannot be speciated by other methods and may be most applicable to modeling applications. HNMR can be applied to assess the oxidative aging (Moretti et al., 2008) and source apportionment (Decesari et al., 2007) of atmospheric WSOC.

Size distributions are useful to elucidate sources and formation mechanisms of ambient aerosol. On a mass basis, three modes exist for sub-micron aerosol. The nucleation/Aitken mode describes particles that were recently formed or emitted into the

atmosphere and is typically observed at particle diameters (D_P) smaller than 0.1 μm (Mäkelä et al., 2000). The accumulation mode is characteristic of aged aerosol and secondary processing and is typically observed at a mode D_P between 0.2 and 0.7 μm (Zhang et al., 2005). The droplet mode exists due to aqueous processing of water-soluble compounds in fogs and clouds and subsequent evaporation, resulting in particles with a modal D_P that is larger than that for particles that grow by gas-to-particle conversion (Meng and Seinfeld, 1994; Kerminen and Wexler, 1995). For example, Huang et al. (2006) used positive matrix factorization to isolate the accumulation and droplet modes and determine that they had characteristic mean medium aerodynamic diameters (MMAD) of 0.4 μm and 1.0 μm, respectively. Water-soluble constituents of the droplet mode either are present in the aerosol phase prior to water uptake or are present through uptake of gas-phase compounds to the water droplets themselves.

Methods

Sample Collection and Site Descriptions

Sampling was carried out using two cascade impactors manufactured by Graseby Anderson (Smyrna, GA). Collection of aerosols by inertial impaction has been employed previously in a variety of environments from urban (Venkataraman et al., 1994) to Arctic (Kerminen et al., 1999). The impactors used here employ eight size bins to sample aerosol up to 10 μm in D_P: 0.4 - 0.7 μm, 0.7 - 1.1 μm, 1.1 - 2.1 μm, 2.1 - 3.3 μm, 3.3 - 4.7 μm, 4.7 - 5.8 μm, 5.8 - 9.0 μm, and 9.0 - 10.0 μm. Additionally, particles with D_P smaller than 0.4 μm are collected by a filter at the exit of the impactor. For the discussion below, the < 0.4 μm and 0.4 - 0.7 μm size bins together are referred to as the accumulation

mode, the 0.7 - 1.1 μm and 1.1 - 2.1 μm size bins together are referred to as the droplet mode, and the 2.1 - 3.3 μm, 3.3 - 4.7 μm, 4.7 - 5.8 μm, 5.8 - 9.0 μm, and 9.0 - 10.0 μm size bins together are referred to as the coarse mode. Consistent air flow rate of 28.5 L min^{-1} was maintained using MKS (Andover, MA) mass flow controllers. Pre-fired quartz-fiber filters were used to collect aerosol on each impactor stage and samples were stored below 0°C until analysis.

Appledore Island is part of an island group in the Atlantic Ocean known as the Isles of Shoals (IOS) and is located at 42.97°N, 70.62°W, approximately 10 kilometers offshore of New Hampshire and Maine. Sampling was performed in conjunction with the AIRMAP program (DeBell et al., 2004) atop a 23-meter-tall tower located centrally on Appledore Island. Twelve samples were taken at the site from 08 July 2005 through 03 August 2005, resulting in an average sampling duration of approximately two days. Most samples were changed between 0800 and 1200 local time.

Thompson Farm (TF) also is operated by the AIRMAP program. It is a rural site located at 43.11°N, 70.95°W, approximately 25 kilometers from IOS, and is 24 meters above sea level. Measurements were made midway up a permanent walk-up tower at approximately eight meters above ground. Twenty-three impactor samples were taken from 22 August 2005 through 20 November 2005, resulting in an average sample-duration of approximately 3.7 days. The actual sample duration ranged from two to 13 days, with the majority of samples (14) having a duration of approximately three days. Most impactor samples were changed between 0800 and 1200 local time.

OC Analysis

OC analyses were performed directly on 1.5-cm^2 filter punches from each impactor stage using a commercially available instrument (Sunset Labs, Tigard, OR) based on Birch and Cary (1996). Briefly, OC is determined by incrementally heating each sample to 870°C, converting all vaporized species to carbon dioxide (CO_2), completely reducing all CO_2 to methane, and quantifying methane by flame ionization detection. OC concentrations were determined for all TF and IOS samples.

A total of 56 field blanks were taken during sampling at the sites, 14 from IOS and 42 from TF. Blank filters were cleaned, stored, and installed by the same procedure as each sample but were removed from the impactor prior to the start of air flow. The average blank OC concentration of 0.29 μgC cm^{-2} was subtracted from each sample OC concentration prior to all other calculations. OC detection limits (DL) per volume of air were determined for each sample based on the average blank concentration per area of filter. The average DL for OC at IOS was 0.20 μgC m^{-3} and varied from 0.12 to 0.34 μgC m^{-3}. The average DL for OC at TF was 0.11 μgC m^{-3} and varied from 0.03 to 0.20 μgC m^{-3}. The values for twice the standard deviation of the OC blanks were smaller than the corresponding average OC blank concentrations. Therefore, the average blank OC air concentrations can also be thought of as the uncertainty of the measurement.

Sample Extraction

For a subset of impactor samples selected based on large concentrations of OC, a fraction of each impactor filter was extracted in Milli-Q (18 MΩ) water for subsequent WSOC, ion chromatography (IC), and HNMR analyses. Five 1.5-cm^2 punches from each impactor stage were soaked in 15 ml of 18 MΩ water for 10 minutes followed by 10

minutes in a centrifuge to remove fragments of quartz filter. Aliquots were saved in capped vials and stored at approximately 5°C prior to WSOC, IC, and HNMR analyses. For HNMR analyses, a solvent exchange was performed prior to analysis by freeze drying water extracts completely and rehydrating in deuterated water (D_2O).

WSOC

WSOC was determined from extracted aliquots using a Sievers (Boulder, CO) 800 carbon analyzer. This method is described in Peltier et al. (2007). Briefly, WSOC is determined by the difference between total inorganic carbon (TIC) and total carbon (TC). TC is determined by completely oxidizing organic molecules to carbon dioxide (CO_2) using ultraviolet light and ammonium persulfate and subsequently measuring the concentration of dissolved CO_2. TIC is determined in the absence of oxidizing agents. For both measurement channels, CO_2 is detected by conductance across a selectively permeable membrane. Detection limits for WSOC are on the order of 50 ppb (in water) for the Sievers 800 model. An average blank concentration per filter area of 0.075 μgC cm^{-2} was subtracted from each sample. The standard deviations of blanks at both sites were larger than the corresponding average blank concentration, leading to an average DL (and uncertainty value) at IOS of 0.074 μgC m^{-3} and of 0.061 μgC m^{-3} at TF. WISOC is determined by difference between OC and WSOC. WISOC and WSOC were determined for four impactor samples from each site, selected based on relatively large concentrations of OC on all impactor stages.

Low Molecular Weight Carboxylic Acids (LMWCA)

Concentrations of LMWCA were determined by IC based on the method of Jaffrezo et al. (1998). Three saturated monocarboxylic acids were quantified (formic

(C_1), acetic (C_2), and propionic (C_3)) as were glycolic (hydroxy C_2), lactic (hydroxy C_3), and pyruvic (keto C_3) acids. Four saturated dicarboxylic acids were quantified (oxalic (C_2), malonic (C_3), succinic (C_4), and glutaric (C_5)), as were maleic (unsaturated C_4), malic (hydroxy C_4), and methanesulfonic (MSA) acids. The IC system consisted of a Dionex TAC-ULP1 ultra-low pressure trace anion preconcentrator, a Dionex AS11 column, and chemical suppression using a Dionex ASRS-300 suppressor with 23-mM H_2SO_4 as the regenerant. All analyses were performed with a 10%-methanol (by volume) sodium hydroxide (NaOH) eluent at two strengths (3.1 mM NaOH and 0.15 mM NaOH) to improve the separation of early-eluting compounds and to shorten the run time necessary to elute compounds with greater affinity for the column. Calibrations were performed using standard solutions prepared either from sodium salts or commercially available standard solutions. All samples were blank-subtracted. Average DL values (which can also be thought of as uncertainty values) for both sites are based on the larger of the blank concentration and the standard deviation of the blank concentrations and are as follows: formic acid, 0.0023 μg m^{-3}; acetic acid, 0.0095 μg m^{-3}; propionic acid, 0.0003 μg m^{-3}; glycolic acid, 0.056 μg m^{-3}; lactic acid, 0.0055 μg m^{-3}, pyruvic acid, 0.00087 μg m^{-3}; oxalic acid, 0.0013 μg m^{-3}; malonic acid, 0.0005 μg m^{-3}; succinic acid, 0.0015 μg m^{-3}; glutaric acid, 0.0013 μg m^{-3}; maleic acid, 0.0010 μg m^{-3}; malic acid, 0.0073 μg m^{-3}; and MSA, 0.0003 μg m^{-3}. LMWCA concentrations were determined for the same eight samples (4 from each site) that were used for WSOC analysis.

HNMR

HNMR analyses were performed using a Varian (Palo Alto, CA) 500 MHz instrument. Preconcentration was performed to reduce the mono-deuterated water signal,

and 1024 scans were collected for each sample, resulting in an analysis time of approximately one hour. A line-broadening technique was applied post-processing to improve signal-to-noise in the spectra. One impactor sample from each site was selected for HNMR analysis based on large OC concentrations and presence of a bimodal distribution.

The integrated HNMR signal over specific ranges in chemical shift has been used previously to quantify the contribution of organic functional groups in aerosol and fog samples. The HNMR scheme used here is a combination of those used in Decesari et al. (2000) and Tagliavini et al. (2005) to quantify concentrations of the following: methyl-group protons ([-CH_3]), 0.7 - 1.0 ppm; methylene protons ([-CH_2-]), 1.2 - 1.8 ppm; protons in an α-position to an unsaturated carbon atom ([H-C-C=]), 1.8 - 3.2 ppm; protons associated with alcohols, ethers, or esters ([H-C-O]), 3.2 - 4.0 ppm; aromatic protons ([Ar-H]), 6.5 - 8.2 ppm; and aldehydic protons ([H-C=O]), 9.0 - 10 ppm.

HNMR signal (which is based on proton mass) is converted to OC mass ($HNMR_{OC}$) based on the expected stoichiometry of each functional group by the method described in Decesari et al. (2007). The signal originally allocated to [H-C-C=] is further separated to unsaturated oxygenated species ([H-C-C=O]) and [H-C-C=] associated with aromatic rings ($[H\text{-}C\text{-}C{=}]_{Ar}$) according to Decesari et al. (2007). The total aliphatic carbon content is defined as the sum of the $HNMR_{OC}$ for [-CH_3], [-CH_2-], [H-C-C=], and [H-C-O] (Decesari et al., 2007). Because an internal standard was not used during analysis, calculation of atmospheric concentrations of each functional group was not possible and concentrations are presented as ratios to total aliphatic carbon.

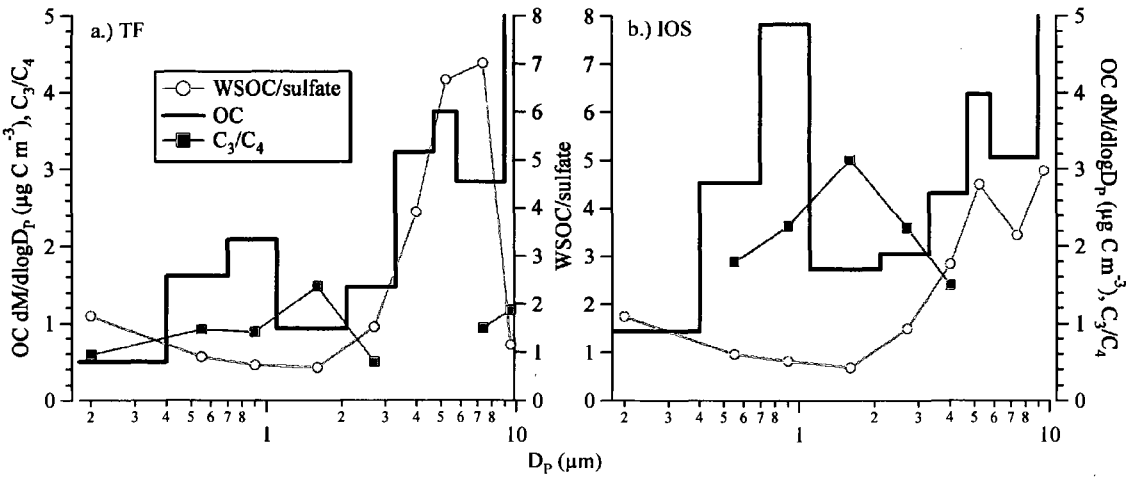

Figure III.1. Average size distributions for OC at a.) TF and b.) IOS. Ratios of WSOC/sulfate and C_3/C_4 also are shown. Note that the 9.0-10-µm-stage concentration for both sites is truncated.

Table III.1. Average Concentrations of OC, WSOC, LMWCA

	TF			IOS		
	Accum.[1]	Droplet[2]	Coarse[3]	Accum.	Droplet	Coarse
OC	1.18(0.22)	1.11(0.23)	2.20(0.21)	1.38(0.26)	1.48(0.25)	1.79(0.14)
WSOC	1.10(0.26)	0.92(0.31)	1.24(0.19)	1.27(0.17)	1.30(0.28)	1.38(0.07)
f_{WSOC}	0.86(0.15)	0.86(0.20)	0.61(0.30)	0.93(0.08)	0.88(0.17)	0.79(0.21)
Oxalate	0.0411	0.0475	0.0347	0.0550	0.0535	0.0321
Malate	0.0738	0.1113	0.0220	0.0412	0.0426	0.0100
Malonate	0.0026	0.0031	0.0008	0.0106	0.0142	0.0043
Succinate	0.0036	0.0033	0.0023	0.0111	0.0127	0.0079
Glutarate	0.0062	0.0028	BDL[4]	0.0091	0.0086	0.0069
Maleate	0.0026	0.0023	BDL	0.0037	0.0055	BDL
Formate	0.0046	0.0037	BDL	0.0036	0.0047	BDL
Pyruvate	BDL	BDL	BDL	0.0034	0.0041	0.0092
MSA	0.0050	0.0047	0.0014	0.0066	0.0036	0.0005
Lactate	BDL	0.0087	BDL	BDL	BDL	BDL
Glycolate	BDL	BDL	BDL	BDL	BDL	BDL
Acetate	BDL	BDL	BDL	BDL	BDL	BDL
Propionate	0.0009	0.0021	0.0006	BDL	BDL	BDL
Sulfate	0.8391	1.285	0.4587	0.7984	1.2788	0.3660
Nitrate	0.0187	0.0289	0.2055	0.0357	0.0389	0.3889
Chloride	0.0301	0.0255	0.0511	BDL	0.0106	0.2529

All units in µg m^{-3} (OC and WSOC in C) except f_{WSOC} which is unitless
OC, WSOC, and f_{WSOC} standard deviations are given in parentheses
[1]impactor stages <0.4 and 0.4-0.7 µm
[2]impactor stages 0.7-1.1 µm and 1.1-2.1 µm
[3]impactor stages from 2.1-10 µm
[4]below detection limits, described in text

Additionally, no replicates were performed and thus no determination of sample-to-sample uncertainty is reported.

Results

Average mass-based size distributions of OC at each site are shown in Figure III.1; statistics are presented in Table III.1. The average OC_{10}, the sum of OC measured on all impactor stages, was 4.49 μgC m^{-3} at TF and 4.65 μgC m^{-3} at IOS. A visually identified bimodal distribution in $dM/dlogD_P$ was observed for a majority of samples at both sites, which is reflected in the average distributions in Figure III.1, with peaks in OC $dM/dlogD_P$ on the 0.7 - 1.1-μm and 4.7 - 5.8-μm stages. Accumulation-mode OC constituted 26.3 and 29.7% of OC_{10} at TF and IOS, respectively. Droplet-mode OC constituted 24.7 and 31.8% of OC_{10} at TF and IOS, respectively, and coarse-mode OC constituted 49.0 and 38.5% of OC_{10} TF and IOS, respectively. Sample-to-sample variability was similar at the two sites, as the standard deviation in OC_{10} was 0.22 μgC m^{-3} and 0.20 μgC m^{-3} at TF and IOS, respectively. Note that large values for $dM/dlogD_P$ were typically observed on the 9.0 - 10-μm stage, in Figure III.1 for example. This is likely both an artifact of the bin-width normalization method for plotting size distributions and a result of an uncertain upper bounds to the 9.0 - 10-μm stage. Thus, the 9.0 - 10-μm stage is not considered in this discussion or in subsequent sections.

Mass-based size distributions of WSOC and WISOC for four samples at TF (panels a-d) and IOS (panels e-h) are shown in Figure III.2. WSOC was the dominant component of OC_{10} with average water-soluble fractions of OC_{10}, $f_{WSOC,10}$, of 0.72 and 0.84 at TF and IOS, respectively (Table III.1). The range of $f_{WSOC,10}$ was 0.47 (TF-12) to 1.03 (IOS-8).

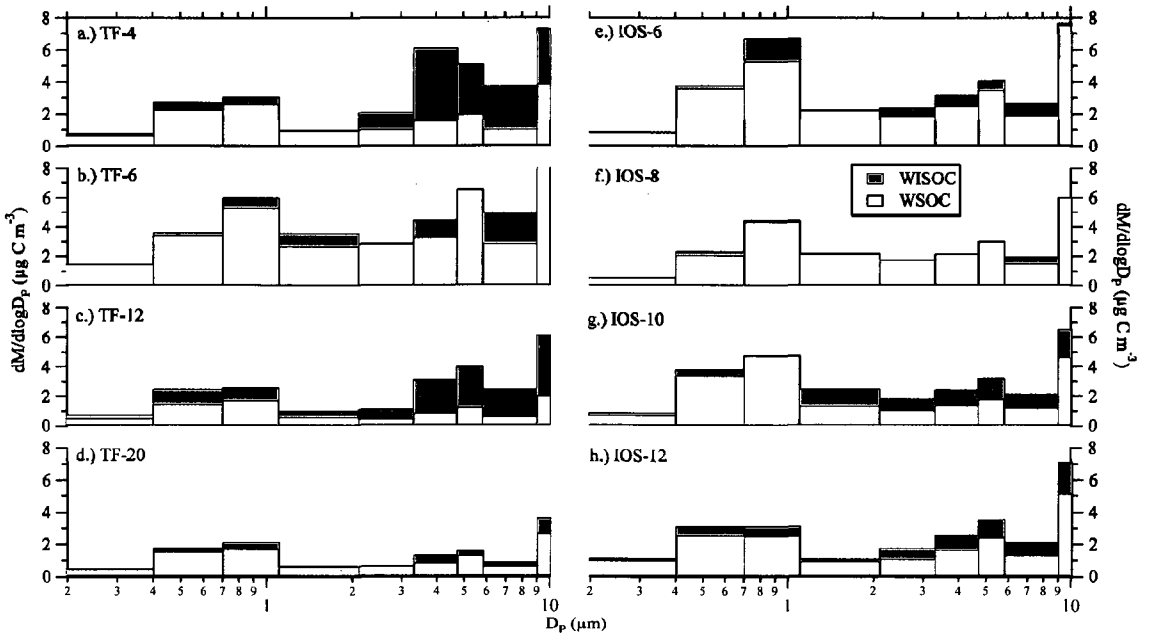

Figure III.2. Mass-based size distributions of WSOC and WISOC for four samples at TF (panels a-d) and at IOS (panels e-h). Note that WSOC and WISOC are stacked for each impactor stage so the top of each bar represents the total OC concentration. Start times, start dates, and durations for each sample are as follows: TF-4, 1255 local time (LT), 1 September 2005, 2.8 days; TF-6, 0859 LT, 10 September 2005, 1.9 days; TF-12, 1516 LT, 28 September 2005, 4.7 days; TF-20, 1420 LT, 25 October 2005, 6.0 days; IOS-6, 0953 LT, 14 July 2005, 1.9 days; IOS-8, 1215 LT, 17 July 2005, 2.8 days; IOS-10, 0940 LT, 23 July 2005, 3.0 days; and IOS-12, 0900 LT, 28 July 2005, 3.0 days. Note that the top of the 9.0-10-µm bar (13.8 µg C m^{-3}) is truncated in panel b.

The WSOC-dominant composition is more exaggerated for accumulation- and droplet-mode OC, where the f_{WSOC} values were 0.86 and 0.86, respectively, at TF and 0.93 and 0.88, respectively, at IOS. Because WSOC comprised a consistently significant fraction of OC, WSOC showed a similar bimodal distribution as OC, with peaks on the 0.7 - 1.1-µm and 4.7 - 5.8-µm stages, while WISOC was more prevalent in the coarse mode, especially at TF (Figure III.2).

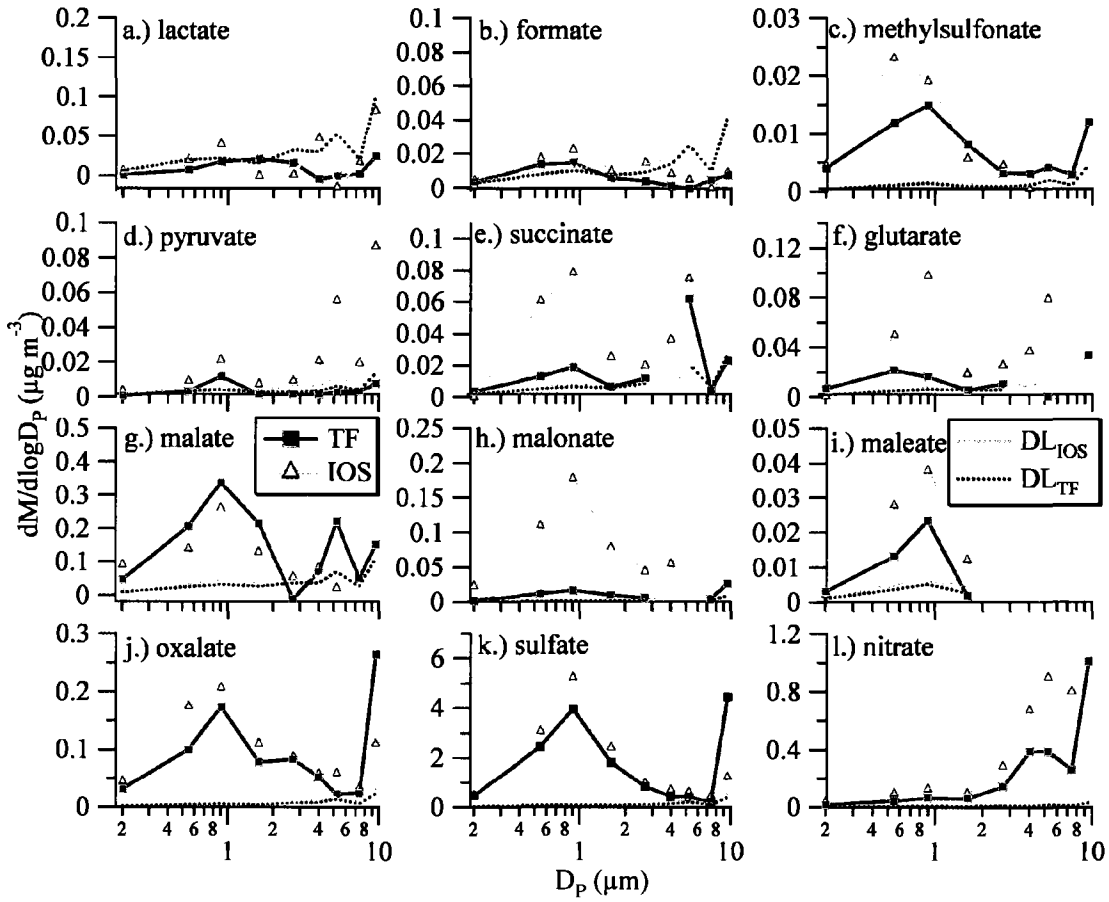

Figure III.3. Average mass-based size distributions of identified LMWCA (panels a-j), sulfate (panel k), and nitrate (panel l) at TF and IOS. $dM/dlogD_P$ is shown as a continuous line and the DL for each species is shown as a dotted line. $dM/dlogD_P$ is plotted as a function of the midpoint D_P of each stage. Note the different y-axis scales for each species and that the point for IOS-nitrate concentration at 9.5-μm D_P (2.68 μg m^{-3}) is truncated in panel l.

Average mass-based size distributions and average mass concentrations for LMWCA from the four selected impactor samples at each site are presented in Figure III.3 and Table III.1. Mass-based size distributions for two inorganic species, nitrate and sulfate, are included in Figure III.3 for comparison with the organic acids, and average mass concentrations for nitrate, sulfate, and chloride are included in Table III.1. Note that the LMWCA are listed by generally decreasing concentrations in Table III.1. Oxalate was the most concentrated LMWCA at IOS with an average sub-10-micron

concentration of 0.141 μg m^{-3} while malate had the largest concentration at TF (0.207 μg m^{-3}). The size distribution of each was dominated by accumulation- and droplet-mode concentrations at both sites (Figure III.3g and III.3j). Oxalate was observed predominantly in the droplet and accumulation modes at TF and IOS (total of 72 and 77% of observed oxalate mass for each location, respectively), as was malate (89% of observed malate in the droplet and accumulation modes at both sites). Average accumulation and droplet-mode concentrations were similar at both sites. Oxalate concentrations were larger at IOS, as the TF to IOS concentration ratios were 0.75 and 0.89 for the accumulation and droplet modes, respectively. Malate concentrations were greater at TF, and the TF to IOS ratios were 1.79 and 2.61 for the accumulation and droplet modes, respectively.

The dicarboxylic acids malonate, glutarate, succinate, and maleate were observed at smaller concentrations (Table III.1), were consistently dominated by accumulation- and droplet-mode mass (Figure III.3), and were all more concentrated at IOS. Accumulation and droplet mode-mass constituted 88, 89, 75, and 100% of the sub-10-micron mass for each species, respectively, at TF, and constituted 85, 72, 75, and 100% of the sub-10-micron mass for each species, respectively, at IOS. Each was observed with a 0.7 - 1.1-μm-stage maximum. Sub-10-micron concentrations were enhanced by a factor of 4.5, 2.4, 3.4, and 1.9 at IOS compared to TF for each species, respectively. Glutarate, malate, and succinate exhibited a notable peak in $dM/dlogD_P$ in the coarse mode (Figure III.3f, III.3g, III.3e), unlike the distribution of oxalate, maleate, and malonate (Figure III.3j, III.3i, III.3h).

Monocarboxylic acids were generally observed at concentrations near detection limits at both sites. Average lactate concentrations were below DL (BDL) for the majority of impactor stages and displayed no variation with particle size, as shown in Figure III.3a. Pyruvate concentrations were BDL for all stages except the 0.7 - 1.1-μm stage at TF but were above detection limits for all stages at IOS, where the mass-based size distribution showed a minor peak on the 0.7 - 1.1-μm stage and a dominant coarse mode (Figure III.3d). Formate concentrations were above DL in the accumulation and

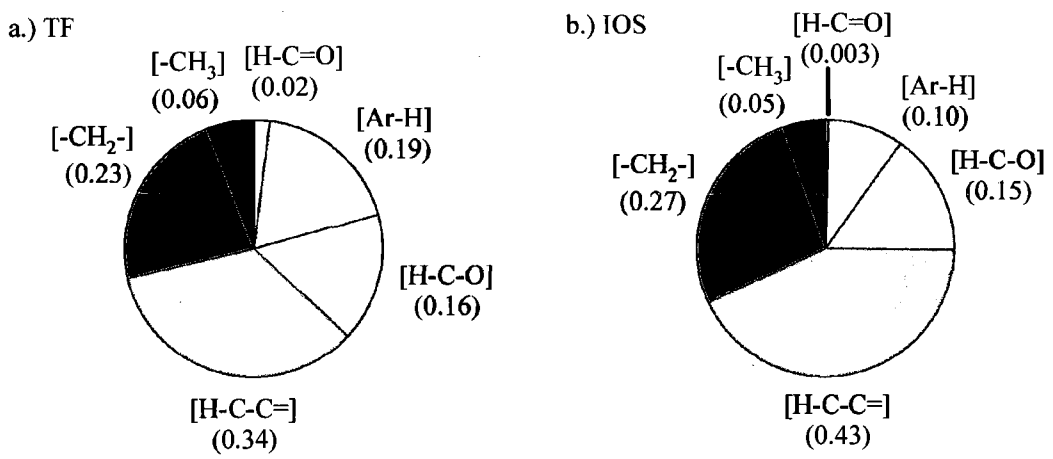

Figure III.4. Fractional distribution of carbon mass for sub-10-micron aerosol sampled at a.) TF and b.) IOS.

droplet modes but BDL for all samples with D_P greater than 3.3 μm at both sites (Figure III.3b). Glycolate, acetate, and propionate were generally BDL and exhibited no variation with particle size at either site, similar to lactate, and thus are not shown.

Accumulation- and droplet-mode mass dominated the size distribution of MSA (Figure III.3c). At IOS, MSA peaked on the 0.4-0.7-μm size bin as opposed to the 0.7 -

1.1 μm size bin, where maximum concentrations of all other dicarboxylic acids were observed, and the MSA concentration was 83% greater in the accumulation mode than in the droplet mode at IOS. The average accumulation-mode MSA concentration was only 8.0% greater than the droplet-mode concentration at TF. Coarse-mode mass contributed only 12.0 and 4.2% of sub-10-micron MSA at TF and IOS, respectively.

The average distribution of organic functionality for sub-10-micron aerosol sampled at both sites is presented in Figure III.4 as the fraction of total carbon measured by HNMR (estimated from proton signal). Saturated aliphatic carbon (the sum of [$-CH_3$]

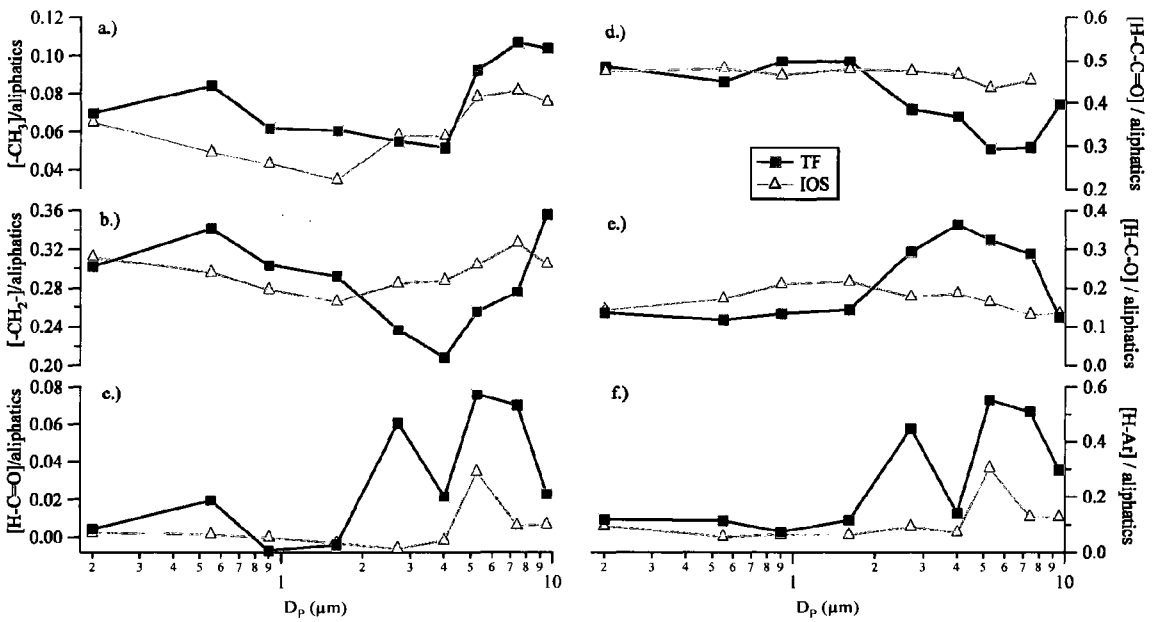

Figure III.5. Size distributions of a.) [$-CH_3$], b.) [$-CH_2-$], c.) [H-C=O], d.) [H-C-C=O], e.) [H-C-O], and f.) [Ar-H] at TF (TF-12) and IOS (IOS-10). The size distributions are expressed as ratios to the sum of aliphatics. Note that y-axis scales differ for each.

and [$-CH_2$-]) was similarly distributed at both sites, and constituted 29 and 32% of measured carbon at TF and IOS, respectively. The [$-CH_2$-] was approximately a factor of 5.5 greater than [$-CH_3$]. The [H-C-O] also was distributed evenly between sites, constituting 16 and 15% at each site, respectively. The [H-C-C=] constituted the largest fraction at both sites and represented a larger carbon-fraction at TF than at IOS: 43 and 34% at IOS and TF, respectively. The fractional contribution of [Ar-H] was larger at TF than at IOS, making up 19 and 9.5%, at each site, respectively. The [H-C=O] contributed only a minor carbon fraction at both sites. Overall, IOS is characterized by an increased contribution from [H-C-C=] and a decreased contribution from [Ar-H] compared to TF.

Normalized size distributions of HNMR organic functional groups are shown in Figure III.5 for TF and IOS. Generally, the size dependence of identified functional groups is similar at both sites. Saturated aliphatic carbon, both [$-CH_3$] and [$-CH_2$-], showed a bimodal distribution with maxima in the accumulation and coarse modes (Figure III.5a and III.5b). The accumulation-mode peak at IOS was in the <0.4 μm size bin while that at TF was shifted to the 0.4-0.7 μm size bin for both [$-CH_3$] and [$-CH_2$-]. The distribution of [H-C-C=] at TF was similar to that of saturated aliphatic carbon, with less enhancement in the coarse mode (Figure III.5d). The maximum for [H-C-C=] at IOS was also in the accumulation mode, although very little dependence on D_P was observed. The most noticeable difference between TF and IOS was observed in the size distribution of [H-C-O] (Figure III.5e). At TF, this distribution was weighted heavily towards the coarse mode, while at IOS a distinct peak for [H-C-O] was observed in the droplet mode, with decreasing importance at larger and smaller D_P. The size distribution of [Ar-H] and

[H-C=O] at both sites was enhanced in the coarse mode, with minor contribution on accumulation-mode stages (Figure III.5c and III.5f).

Discussion

Characteristics of OC and WSOC

The average size distribution of OC (Figure III.1) and all size distributions of WSOC (Figure III.2) observed at TF and IOS exhibited bimodal character, with peaks on the 0.7 - 1.1-μm bin and on the 4.7 - 5.8-μm bin. The bimodal trend is consistent with WSOC MMAD observations of 0.7 and 4.0 μm from measurements in coastal Hong Kong (Yu et al., 2004) and with marine observations during ACE-Asia (Mochida et al., 2007). For both studies, the bimodal character of OC is explained by aqueous processing in the droplet mode and sea-spray or dust particles in the coarse mode. The dominant droplet mode is also consistent with observations of WSOC in an urban atmosphere (Huang et al., 2006).

The ratio of WSOC/sulfate also is shown in Figure III.1. In the droplet mode, both WSOC and sulfate presumably have the same source, aqueous-phase reactions, and the average WSOC/sulfate ratios were very consistent between sites: 0.73 and 0.82 for TF and IOS, respectively, in the 0.7 - 1.1-μm size bin and 0.68 and 0.69 for TF and IOS, respectively, in the 1.1 - 2.1-μm size bin. The similarity in the droplet-mode between sites suggests that WSOC and sulfate have similar precursor source strengths and/or processing kinetics. In the coarse mode on the 4.7 - 5.8-μm size bin where WSOC peaks, WSOC/sulfate values were 6.7 and 4.5 for TF and IOS, respectively. This increase from droplet to coarse modes represents a factor of 10 change at TF and a factor of 6.5 change

at IOS, suggesting that there exists a significant source of WSOC in coarse-mode particles compared to droplet-mode particles and that the source is stronger at TF compared to IOS. A marine influence cannot be ruled to explain enhanced WSOC/sulfate values in the coarse mode. Significant enrichment of WSOC (compared to inorganic constituents including sulfate) has been observed in sea salt particles compared to the bulk composition of seawater (Keene et al., 2007). Primary biological aerosol particles (PBAPs) could contribute to coarse-mode OC and are linked to water-soluble sugars and sugar alcohols (Graham et al. 2003; Yttri et al., 2007). This may explain the enhanced coarse-mode WSOC at TF (located in a mixed forest) compared to the offshore IOS site.

Characteristics of LMWCA and Oxalate Formation Mechanisms

Although the majority of mass was observed in the accumulation and droplet modes, the majority of the dicarboxylic acids identified at TF and IOS exhibited some bimodal characteristics with respect to mass-based size distributions. This is especially the case for succinate and glutarate at IOS and succinate and malate at TF. Oxalate showed only a weak enhancement in the coarse mode, and neither maleate nor malonate was significantly present in particles larger than 2.1 micron. A strong bimodal trend in oxalate, succinate, and malonate was observed by Mochida et al. (2003) off the coast of Asia with a much more distinct super-micron influence, especially for succinate and malonate. For that study, the larger mode was likely due to either uptake or heterogeneous reaction of the dicarboxylic acids on sea salt, based on the similarity between sea-salt surface area and dicarboxylic acid size distributions (Mochida et al., 2003). Sea salt also may influence the partitioning and size distribution of dicarboxylic

acids at TF and IOS because sea salt was clearly observed at D_P greater than 1.1 μm (increases in nitrate (Figure III.3l and Table III.1) through displacement reactions and chloride (Table III.1)).

Size distribution observations at an urban coastal site by Yao et al. (2002) found a dominant droplet mode for oxalate, succinate, malonate, and sulfate that was presumably due to aqueous reactions, with only a minor influence in the accumulation mode. Concentrations of malonate observed by Yao et al. (2002) at larger D_P were attributed to sea salt. Hsieh et al. (2007) observed similar bimodal characteristics for succinate, malate, maleate, malonate, and oxalate, where increases in the droplet mode were enhanced during the wetter, mid-summer season, suggesting that the dicarboxylic acids are related by aqueous formation/decomposition reactions. For this study from suburban Taiwan, only succinate was linked to sea-salt emissions.

Tedetti et al. (2006) identified oxalate, malonate, succinate, glutarate, and maleate, along with C_6 – C_9 dicarboxylic acids, fumaric acid, phthalic acid, glyoxylic acid, and 4-oxobutanoic acid in seawater samples from the Mediterranean Sea. The sum of these acids constituted between 0.9 and 2.1% of total dissolved OC in the seawater, and a general decreasing trend in mass concentration with water depth was observed, suggesting a light-dependent source (Tedetti et al., 2006). Thus, emission of sea salt from surface ocean water is a viable source for the observed coarse mode LMWCA at TF and IOS.

The average oxalate concentrations observed at TF and IOS, 0.15 and 0.19 μg m^{-3}, respectively, are similar in magnitude to observations in other coastal/rural locations, which range from 0.057 to 0.34 μg m^{-3} (Huang et al., 2006 and references therein), in

comparison to larger oxalate concentrations of 0.46 and 0.50 μg m^{-3} from urban Shanghai, China and Los Angeles, CA, USA, respectively, and 0.0046 μg m^{-3} from remote Antarctica (Huang et al., 2007). Other dicarboxylic acids are in general agreement with previous studies in terms of the magnitude of concentrations, with the exception of malate, which was observed in significantly higher concentrations at TF and IOS. The high concentrations of malate at TF and IOS are not unprecedented and have been observed previously at levels near that of oxalate, especially in more remote atmospheres (Kawamura and Ikushima, 1993). Malic acid is likely a side-product of succinic acid reactions in (R1) (Kawamura and Ikushima, 1993) and has also been identified as a product of isoprene oxidation by hydrogen peroxide (Claeys et al., 2004).

Because oxalic acid is the end-product of several known aqueous-phase oxidation pathways, precursor molecules can be used to assess the relative extent of aerosol processing. For example, the ratio of malonate to succinate (or C_3/C_4) indicates the extent of processing with respect to glutaric acid decomposition to oxalic acid (Kawamura and Ikushima, 1993; Sorooshian et al., 2007b; Aggarwal and Kawamura, 2008). Because succinate is oxidized to malonate, an increase in the C_3/C_4 ratio indicates increased processing, assuming that malonate does not have an additional source and that succinate does not have an additional sink in the aqueous phase. The C_3/C_4 ratios at TF and IOS are shown in Figure III.1. Average C_3/C_4 values at TF and IOS were 0.93 and 2.19, respectively. In comparison, the C_3/C_4 ratio for fresh emissions in Los Angeles was 0.35 (Kawamura and Kaplan, 1987), for urban Tokyo was approximately 1.0, for marine aerosol at Chichi-jima Island was 2.0, and for the remote Pacific was 3.9 (Aggarwal and Kawamura, 2008). This suggests that the relative extent of processing is greater at IOS

by a factor of two compared to TF. The relative extent of processing with respect to oxalate at TF is relatively fresh and closer to that of an urban site, while that at IOS implies more aging, similar to the marine site.

The C_3/C_4 ratios also exhibited a distinct dependence on particle size, shown in Figure III.1, with a peak at both sites in the 1.1 - 2.2-μm size bin. This suggests that oxalate production by the glutaric acid decomposition pathway is most efficient in the droplet mode and is due to aqueous reactions. Interestingly, the peak at the 1.1-2.2-μm size is shifted compared to all dicarboxylic acid concentrations that peak at 0.7 - 1.1 μm. In-cloud carboxylic acid processing increases with increasing liquid water content and decreasing sulfate concentration (Figure III.3k), as the uptake of oxalate precursors and reaction kinetics depend on pH (Lim et al., 2005; Sorooshian et al., 2007a). This dependence likely explains the shift in size distribution of the C_3/C_4 ratios observed at TF and IOS compared to the peak in WSOC and OC concentrations.

Monocarboxylic acids were observed in very small concentrations at TF and IOS, consistent with generally higher vapor pressures and lower water solubilities compared to dicarboxylic acids. Still, Fisseha et al. (2006) report average summertime concentrations from online sampling in urban Zurich (formate, 0.023 μg m^{-3}; acetate, 0.0025 μg m^{-3}; pyruvate, 0.012 μg m^{-3}; and lactate, 0.0071 μg m^{-3}) that are similar in magnitude to those at TF and IOS.

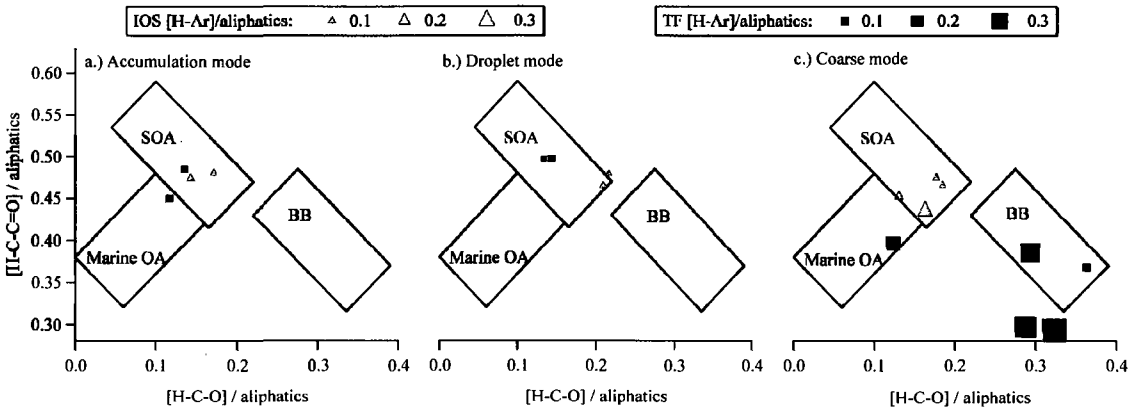

Figure III.6. H-NMR fingerprint analysis for one size distribution measured at TF (TF-12) and at IOS (IOS-10). Source-apportionment boxes are plotted according to Table 2 in Decesari et al. (2007) where SOA is secondary organic aerosol, marine OA is organic aerosol derived from marine sources, and BB is organic aerosol from biomass burning.

HNMR Source Apportionment

Decesari et al. (2007) showed that HNMR spectra could be interpreted as fingerprints for source contribution analysis by evaluating the carbon-weighted ratios of H-C-C=O/aliphatics, H-C-O/aliphatics, and H-Ar/aliphatics. These fingerprints are shown in Figure III.6 as a function of D_P at TF and IOS. The source boxes are reproduced from Decesari et al. (2007) and represent regions characteristic of secondary organic aerosol (SOA), marine OA, and biomass burning aerosol (BB). All impactor stages from the sample taken at IOS reside inside, or very close to the SOA region, suggesting that all of the HNMR-resolved WSOC at IOS is similar to OA that is secondary in nature. Because it is likely that the HNMR-resolved mass constitutes a majority of total WSOC (Decesari et al. (2007) were able to resolve approximately 86% of the total WSOC by an analytical method identical to the one used here), it appears that

the majority of WSOC at IOS, even in the coarse size mode, is formed (or at least altered) by secondary processing.

At TF, the source for WSOC on all of the impactor stages varies between the SOA/Marine OA and a potential BB source (Figure III.6). The HNMR fingerprint of accumulation-mode-mode aerosol at TF closely resembles that at IOS and is likely SOA/aged OA. HNMR fingerprints for droplet-mode aerosol at both sites could be characterized as SOA, but they showed different [H-C-O]/aliphatics values; droplet-mode [H-C-O]/aliphatics values at IOS were near the values characteristic of BB aerosol. The four TF stages in the coarse mode from 2.1-9.0 μm were in close proximity to the BB source, though two exhibited depleted [H-C-C=O]/aliphatics. The fifth coarse TF stage (9 – 10 μm) was consistent with a marine source. [H-Ar]/aliphatics were also enhanced only in the coarse mode, especially at TF, consistent with the BB source shown in Decesari et al. (2007). Backward trajectory analysis was inconclusive in indentifying a specific source region during this TF sample, as airmass history varied considerably throughout the nearly five-day duration. Although differences in collection-time resolution make conclusions strictly qualitative, average potassium concentrations from bulk aerosol collected at TF during this sample were not different from the season average and were inconsistent with a biomass burning source.

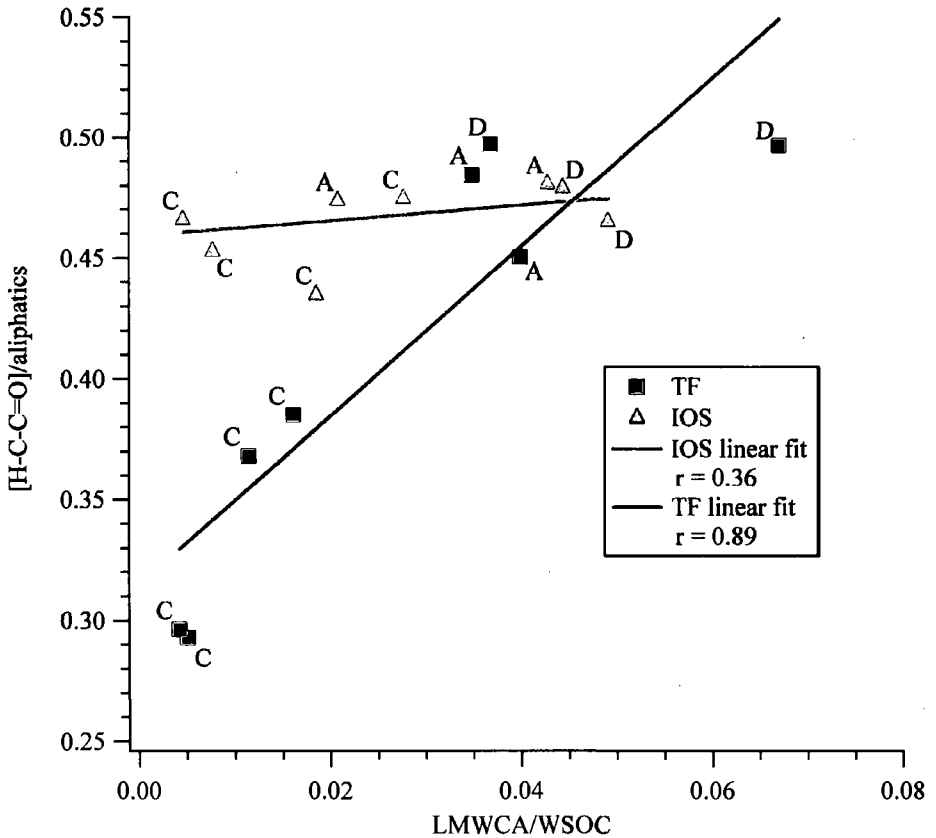

Figure III.7. Relationship between [H-C-C=O]/aliphatics and LMWCA/WSOC for TF-12 and IOS-10 samples. Linear regression fits and Pearson's correlation coefficients are shown for each sample. Each point is labeled by size-mode: A, accumulation; D, droplet; and C, coarse.

HNMR/IC Comparison

Because the concentration of [H-Ar] was very small at both sites, $[H\text{-}C\text{-}C{=}]_{Ar}$ was also very small. The $[H\text{-}C\text{-}C{=}]_{Ar}$ only accounted for 0.85 to 4.4% of the total [H-C-C=] signal at IOS and 0.98 to 11% at TF, with the largest contribution occurring in the coarse mode where the [H-Ar] contribution was largest. Thus, 89-99% of the [H-C-C=] signal was attributed to [H-C-C=O], and [H-C-C=O] constituted the largest fraction of carbon-weighted, HNMR-resolved WSOC ($WSOC_{HNMR}$) at both TF and IOS: 33 and 42%, respectively. The [H-C-C=O] could be attributed to ketones, esters, aldehydes, or

carboxylic acids, though it is assumed that the aldehyde contribution is negligible based on small [H-C=O] contributions (Figure III.4) and esters would contribute mainly to [H-C-O] (Tagliavini et al., 2006). Because ketones were not quantified by IC, [H-C-C=O] could only be compared to the sum of identified LMWCA at each site, where [H-C-C=O] and LMWCA are normalized to total aliphatics and WSOC, respectively (Figure III.7). Very little variation in [H-C-C=O] and its ratio to aliphatics was observed as a function of particle size at IOS (Figure III.5d, Figure III.6), resulting in a poor r value for [H-C-C=O]/LMWCA of 0.36. Much more variability in the normalized [H-C-C=O] and LMWCA was observed at TF, and linear regression analysis resulted in a r value of 0.89 (Figure III.7). This indicates that the majority of the variability in [H-C-C=O] can be attributed to variations in LMWCA (or compounds with similar sources/sinks) at TF.

At TF and IOS, however, LMWCA constituted only a small fraction, between 0.42% (TF, 5.8 - 9.0-μm size bin) and 6.7% (TF, 0.7 - 1.1-μm size bin), of total WSOC. The [H-C-C=O] accounted for between 18% (TF, 4.7 - 5.8-μm size bin) and 47% (TF, 0.7 - 1.1-μm size bin) of $WSOC_{HNMR}$. If WSOC and $WSOC_{HNMR}$ are similar in magnitude, compounds other than LMWCA must be responsible for the majority of the [H-C-C=O] signal. In previous HNMR studies (Tagliavini et al., 2006; Decesari et al., 2007), $WSOC_{HNMR}$/WSOC is 60-80% and 85%, respectively. Thus, HNMR resolves a major fraction of total WSOC. The concentration of unresolved [H-C-C=O] signal ($[H-C-C=O]_{unresolved}$) (μg C m^{-3}) can be calculated by:

$$[H-C-C=O]_{unresolved} = \left\{ WSOC \cdot \frac{WSOC_{HNMR}}{WSOC} \cdot f_{[H-C-C=O]} \right\} - LMWCA \qquad (E1)$$

using measured concentrations of WSOC (μg C m^{-3}), LMWCA (converted to carbon-based units (μg C m^{-3}) using MWs), and $f_{[H\text{-}C\text{-}C=O]}$, and assuming a $WSOC_{HNMR}$/WSOC ratio of 0.8. Calculated $[H\text{-}C\text{-}C=O]_{unresolved}$ concentrations were 0.17, 0.09, and 0.05 μg C m^{-3} in the accumulation-, droplet-, and coarse-mode at TF, respectively and 0.42, 0.38, and 0.26 μg C m^{-3}, respectively at IOS. This equates to 23, 17, and 9% of WSOC at TF, respectively, and 31, 28, and 26% of WSOC at IOS, respectively. $[H\text{-}C\text{-}C=O]_{unresolved}$ was, on average, a factor of 2.5 and 7.5 greater than oxalate concentrations at TF and IOS, respectively.

Humic-like substances (HULIS) may contribute a large fraction of $[H\text{-}C\text{-}C=O]_{unresolved}$ because these compounds are not typically identified by traditional speciation techniques due to acidic character and high molecular weights (Graber and Rudich, 2006). Other compounds previously identified in aerosol speciation studies are unlikely to account for a majority of $[H\text{-}C\text{-}C=O]_{unresolved}$. The sum of aromatic acids likely only contribute approximately the same mass as oxalic acid alone based on WSOC speciation of Amazonian aerosol (Decesari et al., 2006). Tricarboxylic and tetracarboxylic acids also likely contribute a negligible mass fraction to WSOC. Graham et al. (2003) report negligible concentrations of longer-chain fatty acids compared to LMWCA in the Amazon. Specific compounds from the oxidation of biogenic volatile organic compounds like pinonic acid, pinic acid, and norpinone have also been identified in aerosol but at maximum concentrations (Cahill et al., 2006) lower than average oxalate concentrations at TF and IOS. Oxidation of aromatic compounds leads to the formation of unsaturated anhydrides (Forstner et al., 1997), though the concentrations of these species are unknown here.

$[H\text{-}C\text{-}C{=}O]_{unresolved}$ was observed at all sub-10-micron D_P and was especially concentrated in the accumulation and droplet modes. If HULIS indeed makes up the majority of $[H\text{-}C\text{-}C{=}O]_{unresolved}$, because [H-C-C=O] and LMWCA are well correlated (Figure III.7), HULIS likely has similar sources as LMWCA. At IOS, this source is likely secondary in nature based on the HNMR source apportionment discussed above. This is consistent with aqueous-phase processing and polymer formation (Krivácsy et al., 2000). At TF, $[H\text{-}C\text{-}C{=}O]_{unresolved}$ likely is due to secondary processing in the accumulation and droplet modes.

Conclusions

Size distributions of OC and WSOC at TF and IOS are consistent with other coastal measurements and suggest that aqueous processing and processes related to sea-salt aerosol are important in WSOC dynamics. The size distribution of WSOC/sulfate suggests that an additional source (such as sea salt or PBAPs) beyond aqueous processing is important for coarse-mode WSOC, especially at TF.

Dicarboxylic acids were observed to peak in the droplet mode due presumably to aqueous-phase processing. A minor contribution in the coarse mode observed for several dicarboxylic acids was most likely associated with sea-salt aerosol, although the role of these compounds in marine processing is not clear. Average concentrations of mono- and dicarboxylic acids were consistent with other observations. The C_3/C_4 ratios indicate that the amount of processing of organic aerosol at IOS is roughly twice that at TF. A peak in the size distribution of C_3/C_4 in the droplet mode confirms the hypothesis that aqueous-phase reactions are most efficient at this D_P.

Significant variability in organic functionality was observed as a function of sub-10-micron D_P at both sites, consistent with assertions of Tagliavini et al. (2005). Source apportionment analysis using HNMR suggested that the majority of WSOC at IOS is similar to SOA, independent of D_P. At TF, accumulation and droplet mode aerosol is likely formed by secondary processes, but coarse mode WSOC had a similar HNMR fingerprint to that of biomass burning aerosol. Because no coincident increase in potassium was observed, the observed HNMR fingerprint may be characteristic of an additional source not identified by Decesari et al. (2007), potentially PBAPs. By comparing HNMR and LMWCA results, a significant fraction of OA at both sites likely is composed of unspeciated compounds containing carboxylic acid groups.

References

Aggarwal, S.G. and Kawamura, K., 2008. Molecular distributions and stable carbon isotope compositions of dicarboxylic acids and related compounds in aerosols from Sapporo, Japan: Implications for photochemical aging during long-range transport. Journal of Geophysical Research 113, doi:10.1029/2007JD009365.

Birch, M.E. and Cary, R.A., 1996. Elemental carbon-based method for monitoring occupational exposures to particulate diesel exhaust, Aerosol Science and Technology 25, 221-241.

Cahill, T.M., Seaman, V.Y., Charles, M.J., Holzinger, R., and Goldstein, A.H., 2006. Secondary organic aerosols fromed from oxidation of biogenic volatile organic compounds in the Sierra Nevada Mountains of California. Journal of Geophysical Research 111, doi:10.1029/2006JD007178.

Carlton, A.G., Turpin, B.J., Lim, H.-J., Altieri, K.E., and Seitzinger, S., 2006. Geophysical Research Letters 33, doi:10.1029/2005GL025374.

Claeys, M., Wang, W., Ion, A.C., Kourtchev, I., Gelencser, A., and Maenhaut, W., 2004. Formation of secondary organic aerosols from isoprene and its gas-phase oxidation products through reaction with hydrogen peroxide. Atmospheric Environment 38, 4093-4098.

Crahan, K.K., Hegg, D., Covert, D.S., and Jonsson, H., 2004. An exploration of aqueous oxalic acid production in the coastal marine atmosphere. Atmospheric Environment 38, 3757-3764.

DeBell, L.J., Vozzella, M., Talbot, R.W., and Dibb, J.E., 2004. Asian dust storm events of spring 2001 and associated pollutants observed in New England by the Atmospheric Investigation, Regional Modeling, Analysis, and Prediction (AIRMAP) monitoring network. Journal of Geophysical Research 109, doi:10.1029/2003JD003733.

Decesari, S., Facchini, M.C., Fuzzi, S., and Tagliavini, E., 2000. Characterization of water-soluble organic compounds in atmospheric aerosol: A new approach. Journal of Geophysical Research 105, 1481-1489.

Decesari, S., Fuzzi, S., Facchini, C., Mircea, M., Emblico, L., Cavalli, F., Maenhaut, W., Chi, X., Schkolnik, G., Falkovich, A., Rudich, Y., Claeys, M., Pashynska, V., Vas, G., Kourtchev, I., Vermeylen, R., Hoffer, A., Andreae, M.O., Tagliavini, E., Moretti, F., and Artaxo, P., 2006. Characterization of the organic composition of aerosols from Rondonia, Brazil, during the LBA-SMOCC 2002 experiment and its representation through model compounds. Atmospheric Chemistry and Physics 6, 375-402.

Decesari, S., Mircea, M., Cavalli,, F., Fuzzi, S., Moretti, F., Tagliavini, E., and Facchini, M.C., 2007. Source attribution of water-soluble organic aerosol by nuclear magnetic resonance spectroscopy. Environmental Science and Technology 41, 2479-2484.

Ervens, B., Feingold, G., Frost, G.J., and Kreidenweis, S.M., 2004. A modeling study of aqueous production of dicarboxylic acids: Chemical pathways and speciated organic mass production. Journal of Geophysical Research 109, doi:1029/2003JD004387.

Fisseha, R., Dommen, J., Gaeggeler, K., Weingartner, E., Samburova, V., Kalberer, M., and Baltensperger, U., 2006. Online gas and aerosols measurements of water soluble carboxylic acids in Zurich. Journal of Geophysical Research 111, doi:10.1029/2005JD006782.

Forstner, H.J.L., Flagan, R.C., and Seinfeld, J.H., 1997. Secondary organic aerosol from the photooxidation of aromatic hydrocarbons: Molecular composition. Environmental Science and Technology 31, 1345-1358.

Fry, B., Peltzer, E.T., Hopkinson Jr., C.S., Nolin, A., and Redmond, L., 1996. Analysis of marine DOC using a dry combustion method. Marine Chemistry 54, 191-201.

Gilardoni, S., Russell, L.M., Sorooshian, A., Flagan, R.C., Seinfeld, J.H., Bates, T.S., Quinn, P.K., Allan, J.D., Williams, B., Goldstein, A.H., Onasch, T.B., and

Worsnop, D.R., 2007. Regional variation of organic functional groups in aerosol particles on four U.S. east coast platforms during the ICARTT 2004 campaign. Journal of Geophysical Research 112, doi:10.1029/2006JD007737.

Graber, E.R. and Rudich, Y., 2006. Atmospheric HULIS: How humic-like are they? A comprehensive and critical review. Atmospheric Chemistry and Physics 6, 729-753.

Graham, B., Guyon, P., Taylor, P.E., Artaxo, P., Maenhaut, W., Glovsky, M.M., Flagan, R.C., and Andreae, M.O., 2003. Organic compounds present in the natural Amazonian aerosol: Characterization by gas chromatography – mass spectrometry. Journal of Geophysical Research 108, doi:10.1029/2003JD003990.

Hagler, G.S.W., Bergin, M.H., Smith, E.A., and Dibb, J.E., 2008. A summer time series of particulate carbon in the air and snow at Summit, Greenland. Journal of Geophysical Research 112, doi:10.1029/2007JD008993.

Hsieh, L.-Y., Kuo, S.-C., Chen, C.-L., and Tsai, Y.I., 2007. Origin of low-molecular-weight dicarboxylic acids and their concentration and size distribution variation in suburban aerosol. Atmospheric Environment 41, 6648-6661.

Huang, X.-F. and Yu, J.Z., 2007. Is vehicle exhaust a significant primary source of oxalic acid in ambient aerosols? Geophysical Research Letters 34, doi:10.1029/2006GL028457.

Huang, X.-F., Yu, J.Z., He, L.-Y., and Yuan, Z., 2006. Water-soluble organic carbon and oxalate in aerosols at a coastal urban site in China: Size distribution characteristics, sources, and formation mechanisms. Journal of Geophysical Research 111, doi:10.1029/2006JD007408.

Jaffrezo, J.L., Calas, N., and Bouchet M., 1998. Carboxylic acids measurements with ion chromatography, Atmospheric Environment 32, 2705-2708.

Jaffrezo, J.L., Aymoz, G., Delaval, C., and Cozie, J., 2005. Seasonal variation of the water soluble organic carbon mass fraction of aerosol in two valleys of the French Alps. Atmospheric Chemistry and Physics 5, 2809-2821.

Kalberer, M., Yu, J., Cocker, D.R., Flagan, R.C., and Seinfeld, J.H., 2000. Aerosol formation in the cyclohexene-ozone system. Environmental Science and Technology 34, 4894-4901.

Kanikidou, M. et al., 2005. Organic aerosol and global climate modeling: a review. Atmospheric Chemistry and Physics 5, 1053-1123.

Kawamura, K. and Ikushima, K., 1993. Seasonal changes in the distribution of dicarboxylic acids in the urban atmosphere. Environmental Science and Technology 27, 2227-2235.

Kawamura, K., and Kaplan, I.R., 1987. Motor exhaust emissions as a primary source for dicarboxylic acids in Los Angeles ambient air. Environmental Science and Technology 21, 105-110.

Keene, W.C., Maring, H., Maben, J.R., Kieber, D.J., Pszenny, A.A.P., Dahl, E.E., Izaguirre, M.A., Davis, A.J., Long, M.S., Zhou, X., Smoydzin, L., and Sander, R., 2007. Chemical and physical characteristics of nascent aerosols produced by bursting bubbles at a model air-sea interface. Journal of Geophysical Research 112, doi:10.1029/2007JD008464.

Kerminen, V.-M., Teinilä, K., Hillamo, R., and Mäkelä, T., 1999. Size-segregated chemistry of particulate dicarboxylic acids in the Arctic atmosphere, Atmospheric Environment 33, 2089-2100.

Kerminen, V.-M., and Wexler, A.S., 1995. Growth laws for atmospheric aerosol particles: An examination of the bimodality of the accumulation mode. Atmospheric Environment 29, 3263-3275.

Krivácsy, Z., Kiss, G., Varga, B., Galambos, I., Sárvári, Z., Gelencsér, A., Molnár, Á., Fuzzi, S., Facchini, M.C., Zappoli, S., Andracchio, A., Alsberg, T., Hansson, H.C., and Persson, L., 2000. Study of humic-like substances in fog and interstitial aerosol by size-exclusion chromatography and capillary electrophoresis. Atmospheric Environment 34, 4273-4281.

Lim, H.J., Carlton, A.G., and Turpin, B.J., 2005. Isoprene forms secondary organic aerosol through cloud processing: Model simulations. Environmental Science and Technology 39, 4441-4446.

Mäkelä, J.M., Koponen, I.K., Aalto, P., and Kulmala, M., 2000. One-year data of submicron size modes of tropospheric background aerosol in Southern Finland. Journal of Aerosol Science 31, 595-611.

Meng, Z., and Seinfeld, J.H., 1994. On the source of the submicrometer droplet mode of urban and regional aerosols. Aerosol Science and Technology 20, 253-265.

Mochida, M., Umemoto, N., Kawamura, K., Lim, H.-J., and Turpin, B.J., 2007. Bimodal size distributions of various organic acids and fatty acids in the marine atmosphere: Influence of anthropogenic aerosols, Asian dusts, and sea spray off the coast of East Asia. Journal of Geophysical Research 112, doi:10.1029/2006JD007773.

Mochida, M., Umemoto, N., Kawamura, K., Uematsu, M., 2003. Bimodal size distribution of C_2-C_4 dicarboxylic acids in the marine aerosols. Geophysical Research Letters 30, doi:10.1029/2003GL017451.

Moretti, F., Tagliavini, E., Decesari, S., Facchini, M.C., Rinaldi, M., and Fuzzi, S., 2008. NMR determination of total carbonyls and carboxyls: A tool for tracing the evolution of atmospheric oxidized organic aerosols. Environmental Science and Technology 42, 4844-4849.

Peltier, R.E., Weber, R.J., and Sullivan, A.P., 2007. Investigating a liquid-based method for online organic carbon detection in atmospheric particles, Aerosol Science and Technology 12, 1117-1127.

Sorooshian, A., Lu, M.-L., Brechtel, F.J., Jonsson, H., Feingold, G., Flagan, R.C., and Seinfeld, J.H., 2007a. On the source of organic acid aerosol layers above clouds. Environmental Science and Technology 41, 4647-4654.

Sorooshian, A., Ng, N.L., Chan, A.W.H., Feingold, G., Flagan, R.C., and Seinfeld, J.H., 2007b. Particulate organic acids and overall water-soluble aerosol composition measurements from the 2006 Gulf of Mexico Atmospheric Composition and Climate Study (GoMACCS). Journal of Geophysical Research 112, doi:10.1029/2007JD008537.

Sorooshian, A., Varutbangkul, V., Brechtel, F.J., Ervens, B., Feingold, G., Bahreini, R., Murphy, S.M., Holloway, J.S., Atlas, E.L., Buzorius, G., Jonsson, H., Flagan, R.C., and Seinfeld, J.H., 2006. Oxalic acid in clear and cloudy atmospheres: Analysis of data from ICARTT 2004. Journal of Geophysical Research 111, doi:10.1029/2005JD006880.

Tagliavini, E., Moretti, F., Decesari, S., Facchini, M.C., Fuzzi, S., and Maenhaut, W., 2005. Functional group analysis by H NMR/chemical derivatization for the characterization of organic aerosol from the SMOCC field campaign. Atmospheric Chemistry and Physics 6, 1003-1019.

Tedetti, M., Kawamura, K., Charrière, B., Chevalier, N., and Sempéré, R., 2006. Determination of low molecular weight dicarboxylic and ketocarboxylic acids in seawater samples. Analytical Chemistry 78, 6012-6018.

Venkataraman, C., Lyons, J.M., and Friedlander, S.K., 1994. Size distributions of polycyclic aromatic hydrocarbons and elemental carbon. 1. Sampling, measurement methods, and source characterization, Environmental Science and Technology 28, 555-562.

von Glasow, R., and Crutzen, P.J., 2004. Model study of multiphase DMS oxidation with a focus on halogens. Atmospheric Chemistry and Physics 4, 589-608.

Yao, X., Fang, M., and Chan, C.K., 2002. Size distributions and formation of dicarboxylic acids in atmospheric particles. Atmospheric Environment 36, 2099-2107.

Yttri, K.E., Dye, C., and Kiss. G., 2007. Ambient aerosol concentrations of sugars and sugar-alcohols at for different sites in Norway. Atmospheric Chemistry and Physics 7, 4267-4279.

Yu, J.Z., Hong, Y., Zhang, H., and Lau, A.K.H., 2004. Size distributions of water-soluble organic carbon in ambient aerosols and its size-resolved thermal characteristics. Atmospheric Environment 38, 1061-1071.

Yu, J.Z., Huang, X.-F., Xu, J., and Hu, M., 2005. When aerosol sulfate goes up, so does oxalate: Implications for the formation mechanisms of oxalate. Environmental Science and Technology 39, 128-133.

Zhang, Q., Worsnop, D.R., Canagaratna, M.R., and Jimenez, J.L., 2005. Hydrocarbon-like and oxygenated organic aerosols in Pittsburg: insights into sources and processes of organic aerosols. Atmospheric Chemistry and Physics 5, 3289-3311.

Zhang, Q. et al., 2007. Ubiquity and dominance of oxygenated species in organic aerosols in anthropogenically-influenced Northern Hemisphere midlatitudes. Geophysical Research Letters 34, doi:10.1029/2007GL029979.

CHAPTER IV

HETEROGENEOUS CONVERSION OF NITRIC ACID TO NITROUS ACID ON THE SURFACE OF PRIMARY ORGANIC AEROSOL IN AN URBAN ATMOSPHERE

Abstract

Nitrous acid (HONO), nitric acid (HNO_3), and organic aerosol were measured simultaneously atop an 18-story tower in Houston, TX during August and September of 2006. HONO and HNO_3 were measured using a mist chamber/ion chromatographic technique, and aerosol size and chemical composition was determined using an Aerodyne quadrupole aerosol mass spectrometer. Observations indicate the potential for a new HONO formation pathway: heterogeneous conversion of HNO_3 on the surface of primary organic aerosol (POA). Significant HONO production was observed, with an average of 0.97 ppbv (event^{-1} and a maximum increase of 2.2 ppb in four hours. Nine identified events showed clear HNO_3 depletion and well-correlated increases in both HONO concentration and POA-dominated aerosol surface area (SA). Linear regression analysis results in correlation coefficients (r^2) of 0.82 for HONO/SA and 0.92 for HONO/HNO_3. After correction for established HONO formation pathways, molar increases in excess HONO ($HONO_{excess}$) and decreases in HNO_3 were nearly balanced, with an average $HONO_{excess}/HNO_3$ value of 0.97. Deviations from this mole balance indicate that the residual HNO_3 formed aerosol-phase nitrate. Aerosol mass spectral analysis suggests that the composition of POA could influence HONO production. Several previously

identified aerosol-phase PAH compounds were enriched during events, suggesting their potential importance for heterogeneous HONO formation.

Introduction

Nitrous acid (HONO) plays an important role in the cycling of both hydrogen (HO_X) and nitrogen (NO_X) oxides through the photolytic production of hydroxyl radical (OH) and nitrogen oxide (NO) (reaction (R1)) (Harrison et al., 1996; Alicke et al., 2003), especially during the early morning:

$$HONO + h\upsilon \xrightarrow{\lambda=290-400nm} OH + NO \qquad (R1)$$

The sources of HONO in urban atmospheres currently are not well understood. HONO formation was thought to occur heterogeneously by the hydrolysis of nitrogen dioxide (NO_2) (Finlayson-Pitts et al., 2003), a reaction that also produces nitric acid (HNO_3) (reaction (R2)):

$$2NO_2 + H_2O \xrightarrow{\text{surface}} HONO + HNO_3 \qquad (R2)$$

The kinetic details regarding this reaction are not conclusive (Finlayson-Pitts et al., 2003 and references therein) but the reaction is likely first-order in NO_2.

Various environmentally relevant surfaces may contribute to HONO formation through reactions of NO_2. Soot aerosol has been identified as a likely reaction surface for HONO production by reaction (R3) (Ammann et al., 1998):

$$NO_2 + red_{ads} \rightarrow HONO + ox_{ads} \qquad (R3)$$

where red_{ads} and ox_{ads} represent reduced and oxidized states, respectively, of the adsorbing soot surface. This reaction likely is favored compared to reaction (R2) because laboratory studies fail to detect HNO_3 as a major product (Ammann et al., 1998; Kalberer et al., 1999) and because of kinetic limitations of reaction (R2) compared to reaction (R3). Kalberer et al. (1999) reported reaction potentials (f_{soot}) for reaction (R3) that

depend on relative humidity (RH), are insensitive to ozone (O_3) or NO_2 concentration, and are very fast. The maximum f_{soot} measured by Kalberer et al. (1999) was $1x10^{15}$ molec cm^{-2} at a RH of 30%. At a RH of 70%, Kalberer et al. (1999) report a decreased value for f_{soot} of approximately $0.2x10^{15}$ molec cm^{-2}. This is similar to the reaction potential of $0.25x10^{15}$ molec cm^{-2} reported later by Arens et al. (2001). The relevance of a net surface reaction such as reaction (R3) without a mechanism to recycle active surface sites is still unknown (Kalberer et al., 1999; Kleffmann et al., 1999). Such a mechanism has been proposed through additional soot-surface NO_2 reduction by water-soluble organic compounds such as phenols that better represent real automobile emissions (Gutzwiller et al., 2002; Ammann et al., 2005). Photo-dependent NO_2 reduction also has been observed on humic acid films (Stemmler et al., 2006) and films of aromatic organic compounds (George et al., 2005).

Nitric acid has been identified as a precursor to HONO in various atmospheres (Clemitshaw, 2006). Laboratory work suggests the potential for HNO_3 surface photolysis resulting in HONO and NO_2 production by reaction (R4) (Zhou et al., 2003):

$$\begin{aligned} &HNO_{3(ads)} \xrightarrow{h\nu} [HNO_3]^*_{(ads)} \\ &[HNO_3]^*_{(ads)} \rightarrow HNO_{2(ads)} + O(^3P)_{(ads)} \\ &[HNO_3]^*_{(ads)} \rightarrow NO_{2(ads)} + OH_{(ads)} \end{aligned} \qquad \text{(R4)}$$

where $O(^3P)$ is the oxygen atom. Photolysis of HNO_3 on surfaces occurs at a much faster rate than in the gas phase or in bulk solution. Using a HNO_3-coated flow reactor, Zhou et al. (2003) derived a photolysis rate constant ($j_{HNO3\text{-}HONO}$) for HONO production of $1.2x10^{-5}$ s^{-1} at 50% RH. At 80% RH, $j_{HNO3\text{-}HONO}$ increased to $1.4x10^{-5}$ s^{-1} due to intermediate production of NO_2 and subsequent conversion to HONO. Modeling has

suggested that a HNO_3 photolysis mechanism was important for HONO production during the 2001 Northeast Oxidant and Particle Study (Sarwar et al., 2008). Inclusion of renoxification processes on surfaces enhanced HONO concentrations significantly (by an order of magnitude), and improved O_3 model performance, in the South Coast Air Basin of California (Knipping and Dabdub, 2002).

Another mechanism of HONO formation involves the reaction of HNO_3 with NO (Rivera-Figueroa et al., 2003) on hydrated glass surfaces by reaction (R5) via a photochemically independent heterogeneous pathway for HONO formation:

$$HNO_3 + NO \xrightarrow{\text{surface}} HONO + NO_2 \qquad \text{(R5)}$$

Additionally, laboratory work has shown that dissolved nitrate ion (NO_3^-), not simply adsorbed HNO_3, contributes to HONO and NO_2 formation on organic films (Handley et al., 2007). While HONO formation has been observed in laboratory experiments and mechanisms for these processes have been suggested, modeling studies consistently underestimate ambient HONO concentrations (Moussiopoulos et al., 2000; Vogel et al., 2003) despite emphasizing the importance of heterogeneous processing.

This work indicates significant HONO production in the Houston, TX atmosphere correlated strongly with depletion of HNO_3 and enhanced hydrocarbon-like organic aerosol (HOA) surface area. Such events, which typically occurred during early morning, indicate a potential new HONO formation pathway: heterogeneous conversion of HNO_3 to HONO on primary HOA. Because of the many co-dependent variables in question, the mechanism of HONO formation can not be determined explicitly. However, it is clear that the magnitude of observed HONO can not be explained without a currently unidentified source.

Methods

Measurements

All gas- and aerosol-phase measurements were made between 20 August 2006 and 27 September 2006 during the Texas Air Quality Study II Radical and Aerosol Measurement Project (TRAMP). Sampling instrumentation was located atop the North Moody Tower, an 18-story building on the campus of the University of Houston. Nitric and nitrous acid observations were made by a mist chamber/ion chromatographic (MC/IC) technique (Scheuer et al., 2003; Dibb et al., 2004). Air was sampled through a heated inlet designed specifically to eliminate loss of HNO_3 during sampling. Acidic gases (HNO_3, HONO, and hydrochloric acid) were removed over five-minute periods from the air by the MC, collected into 13-15 ml (depending on ambient RH) of pure water, and immediately and automatically quantified by IC. Two identical MC/IC systems were used alternately to obtain continuous measurements. Direct comparison between this measurement and HONO measured by long-path differential optical absorption spectroscopy yielded excellent agreement (Stutz et al., in preparation), especially during the early morning period of focus in this study.

Aerosol mass concentrations and mass size distributions of non-refractory aerosol between 40 and 1000 nm in vacuum aerodynamic diameter (D_{VA}) were measured by an Aerodyne quadrupole aerosol mass spectrometer (Q-AMS). Specific information regarding instrument design, quantification, and field deployment has been well documented previously (Jayne et al., 2000; Jimenez et al., 2003; Canagaratna et al., 2007). The quantification of particle-phase nitrate is based on the sum of mass spectral

signal at mass-to-charge ratio (m/z) = 30 and m/z = 46 (the fragments NO^+ and NO_2^+, respectively) measured by the Q-AMS. This quantification is complicated by potential contribution of organic compounds (Bae et al., 2007), or other nitrogen-containing compounds such as amines, to signal at m/z = 30. Therefore, particle-phase nitrate could be overestimated here, as the average ambient m/z 30 to 46 ratio was 5.0 compared to a value of 2.15 for pure ammonium nitrate (NH_4NO_3) measured during calibrations. However, the contribution of organic fragments to m/z = 30 signal was less significant during the HONO events discussed below (compared to measurements made during the afternoon): the measured m/z 30 to 46 ratio was 4.2 during these periods.

The mass spectral signal at m/z = 44 has been used as a tracer for oxidized organic aerosol (OOA), and the signal at m/z = 57 has been used as a tracer for HOA (Zhang et al., 2005a). Additionally, organic mass spectra were compared by normalizing each m/z signal to the total mass loading for that time period. These values are denoted by X, where, for example, X_{44} is the fraction of the total organic mass spectral signal that was observed at m/z = 44. These comparisons are discussed further below.

Additional supporting data were collected as follows (Lefer et al., in preparation): NO and NO_X were measured using a modified trace-level Thermo Environmental (TEI) 42c NO + O_3 chemiluminescence instrument. The instrument was modified with an externally mounted light-emitting diode-based blue light converter that selectively dissociates NO_2 to NO. Carbon monoxide (CO) was measured using a TEI 48c trace-level enhanced gas filter correlation wheel instrument. Acetylene was measured together with a large suite of other volatile organic compounds (VOC) online every hour using a

Perkin-Elmer VOC-system (Leuchner and Rappenglück, in preparation). Supplemental meteorological data were also available (Lefer et al., in preparation).

Total Aerosol Surface Area

Aerosol mass size distributions measured by the Q-AMS in particle time-of-flight mode were used to calculate total aerosol surface area (SA) for each 10-minute sampling period. Calculations were based on summed Q-AMS aerosol mass (sulfate + nitrate + ammonium + organics + chloride) assuming spherical particles of a uniform density of 1.2 g cm^{-3}. SA was calculated by

$$SA = \sum_{D_{VA}=40nm}^{D_{VA}=1000nm} \left[\frac{Aerosol\ Mass_{AMS(D_{VA})}}{Aerosol\ density} \cdot \frac{6}{D_{VA}} \right] \left(\mu m^2\, cm^{-3}\right) \qquad (1)$$

Rush Hour Definition

To focus on the morning hours during which the events (described in more detail subsequently) generally occurred, the full dataset was segregated into two subsets. Data collected between 0500 and 0850 CST are henceforth termed 'morning rush hour' (MRH) data while data from the remainder (0900 – 0450 CST) will be referred to as 'non morning rush hour' (non-MRH) data. Selection of the MRH interval was based solely on the diurnal profile of CO, a tracer of urban combustion. Carbon monoxide peaked at a median concentration of 308 ± 185 ppb (90th percentile of 682 ppb) at 0700 CST. During non-MRH periods, the median CO concentration was 186 ± 85 ppb. The average acetylene mixing ratio during MRH was 924 ppt, compared to a full-campaign median value of 586 ppt, indicating that combustion sources are likely important during this time (Harley et al., 1992). Because of timing and association with increased CO and acetylene, MRH air masses likely are dominated by local automobile exhaust although

possible influence of the nearby Houston Ship Channel (HSC) on MRH chemistry can not be excluded.

Results

Interaction between HONO, Particle-Phase Nitrate, and HNO_3

The diurnal patterns of HONO, particle-phase nitrate, and HNO_3 exhibited very different characteristics. Figure IV.1 shows a diurnal box plot of these three species over the full campaign. Both HONO and particle-phase nitrate had clear peaks in median, 75th percentile, and 95th percentile concentrations between 0600 and 0800 CST, with a HONO median concentration of 23.2 nmol m^{-3} and a median particle-phase nitrate concentration of 0.590 $\mu g\ m^{-3}$. Contrarily, minimum median concentrations of HNO_3 were observed during these hours (22.3 nmol m^{-3}), and a clear daytime median peak of 84.9 nmol m^{-3} was observed at 1200 CST.

The daytime maximum in HNO_3 is consistent with dominant photochemical production by the reaction between NO_2 and OH. Decreased daytime concentrations of HONO likely are explained by the dominance of photolytic loss (reaction (R1)) over production by all mechanisms including the reverse of reaction (R1). An anti-correlation between HONO and HNO_3 for the full measurement campaign is clearly shown in Figure IV.1. Time-series data (not shown) indicated that morning decreases in HNO_3 were more often than not accompanied by increases in HONO. Small daytime concentrations of particle-phase nitrate are likely due to both the relatively high vapor pressure of NH_4NO_3

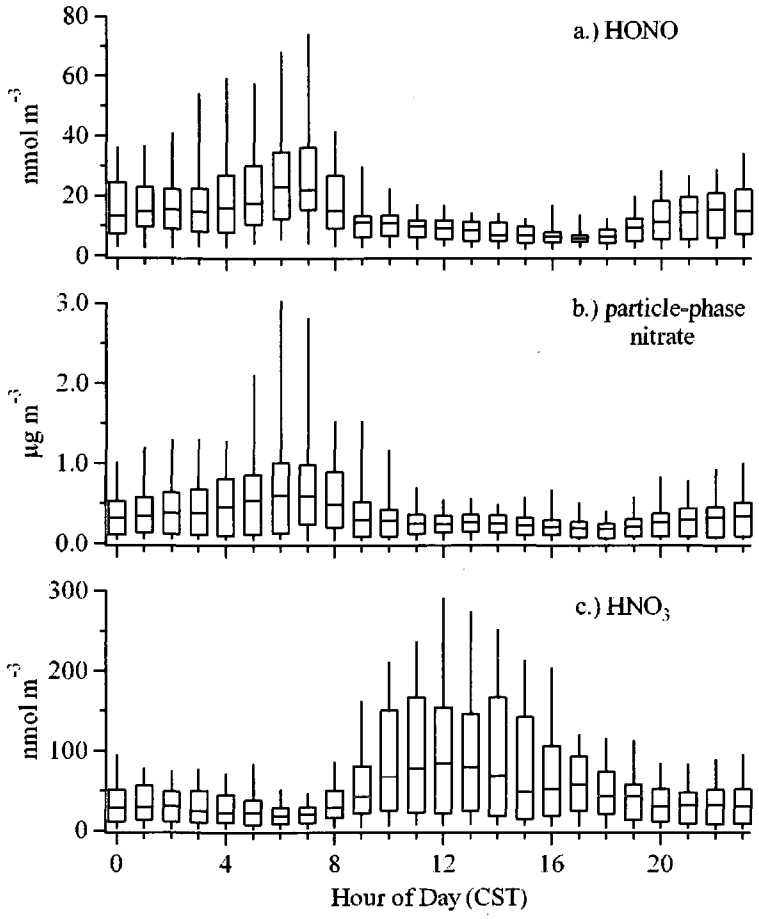

Figure IV.1. Full campaign diurnal plots for a.) HONO, b.) particle-phase nitrate, and c.) HNO_3. The line inside of each box represents the median concentration, the top and bottom of each box represent the 75th and 25th percentile concentrations, respectively, and the top and bottom of each whisker represent the 95th and 5th percentile concentrations, respectively.

and a lack of available ammonia. Non-MRH aerosols were not fully neutralized, with an average sulfate to ammonium molar ratio of 1.36, making NH_4NO_3 formation thermodynamically unfavorable.

Surface Area Dependence

Significant increases in calculated SA were observed during MRH and were driven by variability in organic aerosol. Calculated median aerosol surface area was increased by 24% during MRH (287 $\mu m^2\ cm^{-3}$) compared to the SA for non-MRH

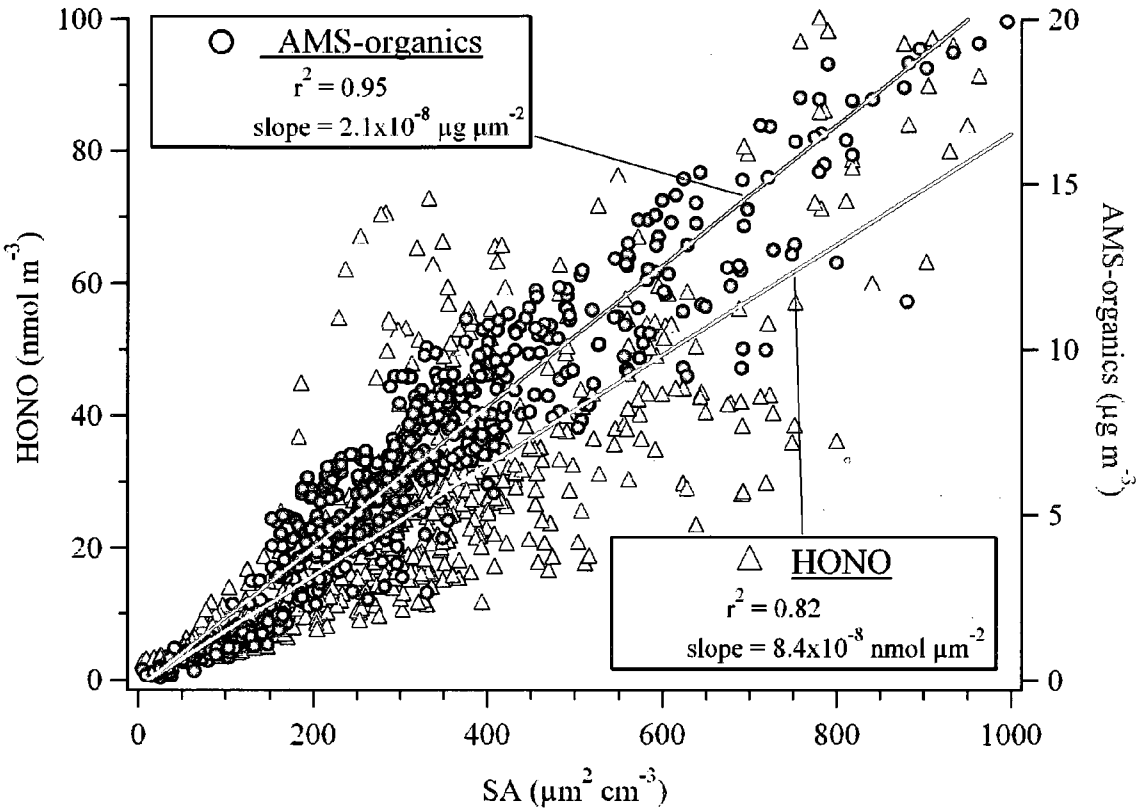

Figure IV.2. Linear regression of HONO and organic aerosol versus SA for only MRH data. Slopes include appropriate unit conversions.

periods (232 $\mu m^2\ cm^{-3}$). The difference between 90th percentile aerosol surface area for MRH and non-MRH periods, an increase of over 40%, is even larger. The peak in SA occurs at 0700 CST, similar to the diurnal profile of HONO and particle-phase nitrate. A linear regression (Figure IV.2) shows a strong correlation between organic aerosol and SA during MRH, with a correlation coefficient (r^2) of 0.95, indicating that almost all of the variability in SA during MRH can be explained by changes in organic aerosol. By contrast, sulfate aerosol (not shown in Figure IV.2 but included in Figures IV.3 and IV.4) was not well correlated with SA (r^2 = 0.54), especially at high SA. MRH HONO concentrations were also well correlated with SA, with a correlation coefficient of 0.82

and a slope (the HONO reaction potential with respect to SA) of 5.0×10^{15} molecules cm^{-2} (Figure IV.2).

Aerosols During MRH

Significant chemical differences were observed between MRH and non-MRH aerosol. The median aerosol mass concentration during MRH periods (11.8 μg m^{-3}) was 25% larger than the mass concentration during non-MRH periods (9.45 μg m^{-3}). Aerosol mass during MRH was dominated by organics, which constituted 59% of the total aerosol mass, compared to a composition of 51% organic mass during non-MRH sampling. This difference is driven by an average MRH increase of 2.0 μg m^{-3} in organic concentration with no corresponding change in sulfate or ammonium concentration (-0.03 and 0.02 μg m^{-3}, respectively). The constant sulfate concentrations during MRH (clearly evident during the events in Figures IV.3 and IV.4) are consistent with a traffic fleet dominated by gasoline fueled cars and light duty trucks (McGaughey et al., 2004) that do not emit significant quantities of sulfur dioxide. Median particle-phase nitrate concentrations increased by 120% during MRH periods compared to the non-MRH periods, which is also seen in the diurnal analysis in Figure IV.1.

Significant differences between MRH and non-MRH aerosols were observed in the Q-AMS mass spectra. The median ratio of m/z = 44/57, was largest during times when photochemistry dominated (9.1 for the 1500 CST hour) and was smallest during MRH (2.6 for the 0700 CST hour), an indication that MRH organic aerosol is less oxidized and more like HOA. Elevated CO and acetylene concentrations coincident with decreased m/z = 44/57 strongly indicate that HOA is primary in nature.

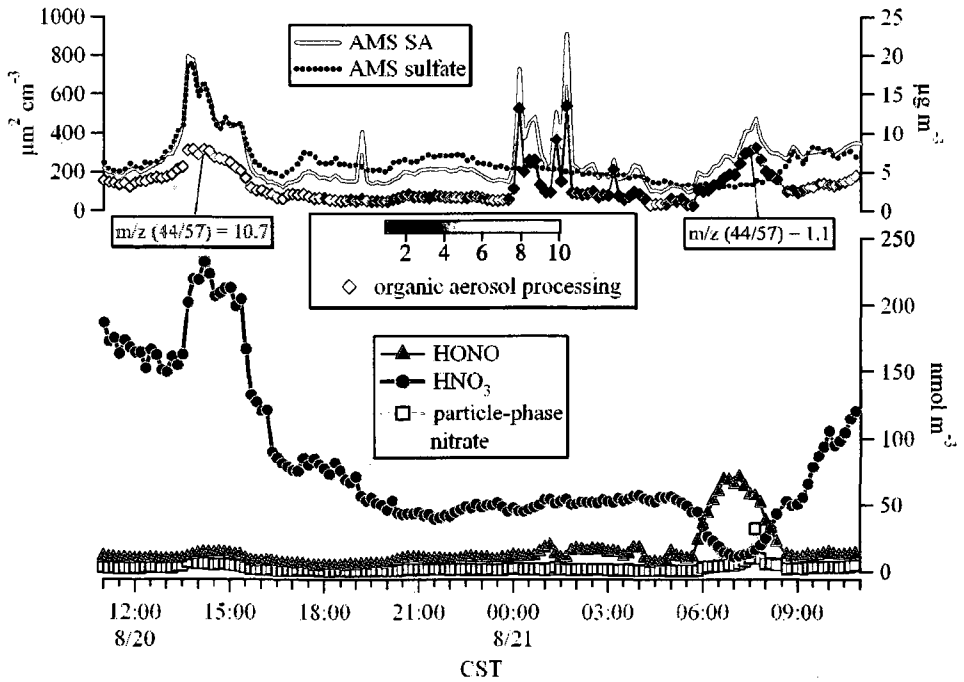

Figure IV.3. 21 August event. Organic processing is described by m/z = 44/57, as described in the text.

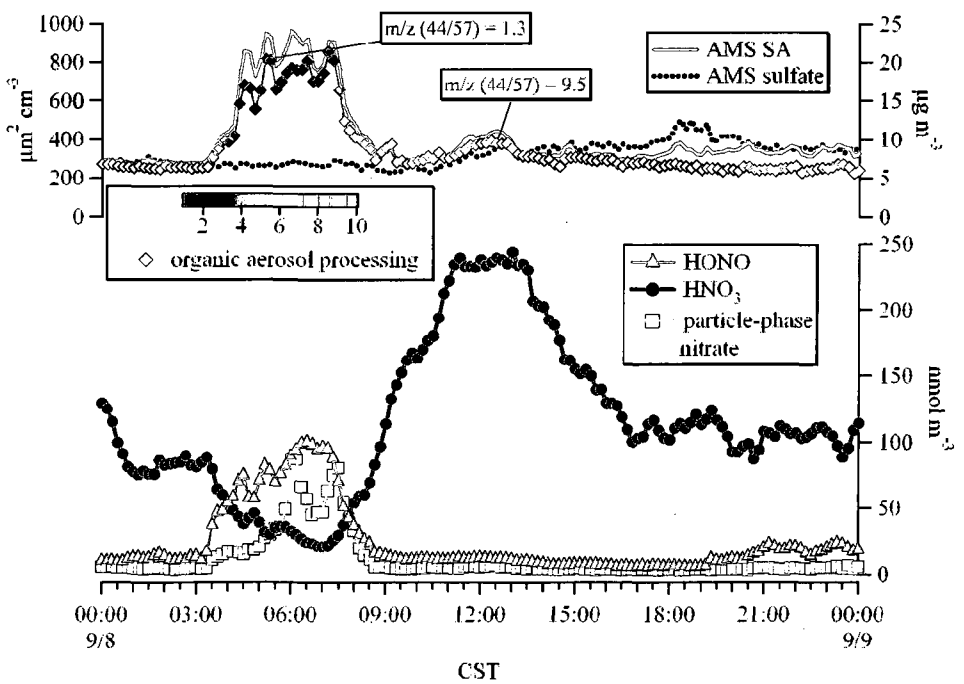

Figure IV.4. 8 September event. Organic processing is described by m/z = 44/57, as described in the text.

Mass spectra measured by the Q-AMS for MRH organic aerosol were compared to non-MRH organic aerosol using the ratio of X_{MRH}/X_{nMRH} shown in Figure IV.5a (m/z < 200) and Figure IV.6a (m/z > 200). MRH organic aerosol was enriched at larger m/z fragments, exclusively after m/z = 114, and depleted in smaller m/z. MRH aerosol was enriched by more than 38% at m/z = 57 (highlighted in Figure IV.5), which likely represents the $C_4H_9^+$ fragment (Zhang et al., 2005b). Other notably enriched m/z signals were observed at larger m/z in intervals of approximately 12 and 14 m/z units, at m/z = 69, 71, 81, 83, 93, and 95. These signals likely are due to the addition of C^+ and CH_2^+ fragments to $C_4H_9^+$ fragments. All of the MRH-enriched m/z signals mentioned above have been observed prominently in diesel exhaust (Canagaratna et al., 2004) and ambient urban aerosol (Alfarra et al., 2004; Zhang et al., 2005b). Contrary to observations during the previously mentioned studies of diesel and urban aerosol, m/z = 43 was enriched by less than 5% during MRH. This is likely due to the prominence of m/z = 43 in oxidized organic aerosol during the daytime as well as during MRH. Signal at m/z = 44 (highlighted in Figure IV.5), the fingerprint often used to identify oxidized (and likely processed) organic aerosol, was depleted during MRH by approximately 14%. Laboratory work involving diesel exhaust processing has shown that m/z = 44 becomes increasingly important with photochemical age (Sage et al., 2008), suggesting that MRH aerosol is less processed and relatively fresh photochemically. Signal at m/z = 60 (potentially $C_2H_4O_2^+$) and signals at m/z associated with subsequent additions of CH_n^+ fragments (at m/z = 73, 87, 100, and 114) were also observed to be depleted during MRH. These fragments were similarly not observed in diesel and urban aerosols (Zhang

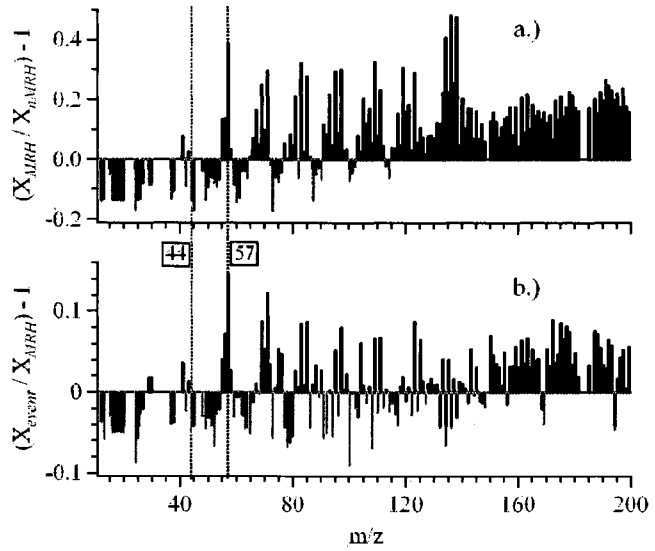

Figure IV.5. Comparison of organic aerosol mass spectra (up to m/z = 200) for a.) MRH (X_{MRH}) and non-MRH (X_{nMRH}) and b.) the event-average mass spectra (X_{event}) and X_{MRH}. Values above zero (in black) indicate m/z signals that were enriched. Values below zero (in gray) indicate m/z signals that were depleted. Signals at m/z = 44 and 57 are highlighted. Note that the scale is reduced for b.).

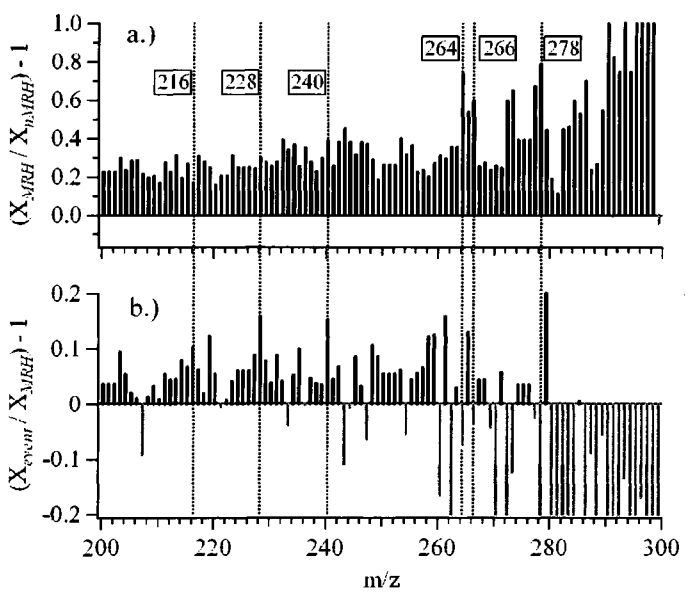

Figure IV.6. Comparison of organic aerosol mass spectra (m/z from 200 to 300) for a.) MRH (X_{MRH}) and non-MRH (X_{nMRH}) and b.) the event-average mass spectra (X_{event}) and X_{MRH}. Values above zero (in black) indicate m/z signals that were enriched. Values below zero (in gray) indicate m/z signals that were depleted. Signals at m/z = 216, 228, 240, 264, 266, and 278 are highlighted. Note that the scale is reduced for b.).

et al., 2005a). Thus, the mass spectral signature observed during MRH and documented in Figure IV.5 is consistent with HOA that was emitted.

Discussion

Observation of Heterogeneous HONO Formation Events

Concentrations of HONO in the Houston urban atmosphere were enhanced significantly during MRH periods. This time period was dominated by vehicular emissions that significantly increased aerosol SA, nearly entirely due to increased abundance of primary HOA. This correlation indicates the potential importance of heterogeneous processes driving HONO formation. The good correlation between HONO and SA suggests that aerosol surface is the dominant reaction substrate and that stationary sources (buildings, soils, etc.) are likely unimportant, a supposition supported by modeling (Stutz et al., in preparation). Boundary layer dynamics can be ruled out as a complicating factor because other atmospheric components with negligible MRH sources, such as sulfate aerosol, showed no correlated increase (Figures IV.3 and IV.4).

Enhanced HONO concentrations during MRH frequently were accompanied by significant depletion in HNO_3. To explore the possibility that HNO_3 is a potential precursor to HONO, events were identified that were characterized by both an increase in HONO concentration and a decrease in HNO_3 concentration. Two examples of such events are presented in Figures IV.3 and IV.4. Start and end times for all events (Table IV.1) were defined based on visual inspection of HNO_3 data such that the events on 21 August and 8 September (Figures IV.3 and IV.4) start at 0540 and 0320 CST,

respectively. These events show clearly the anti-correlation between HONO and HNO_3, as well as the coincident enhancement of less-processed organic aerosol and SA during MRH. The contrast between HOA-dominant and OOA-dominant organic aerosol between MRH and mid-afternoon is emphasized.

Linear regression analysis was preformed for each event to assess the dependence of HONO on SA and of HONO on HNO_3. To isolate potential heterogeneous processing, only data from the onset of HNO_3 depletion to the maximum observed HONO concentration were used for linear regression analysis, as measurements after the HONO peak likely are complicated by increasing photolytic HONO loss (by reaction (R1)) and photochemical HNO_3 production (from OH and NO_2). Nine events were observed throughout the campaign, and slopes and correlation coefficients for each of these events are reported in Table IV.1. The change in HONO during each event (ΔHONO) is also included in Table IV.2 and was calculated as the difference between the peak HONO concentration and the concentration at the start of the event. Each event exhibited significant ΔHONO, especially the 21 August and 8 September events (shown in Figures IV.3 and IV.4) during which ΔHONO was 1.48 and 2.18 ppb (60.5 and 89.2 nmol m^{-3}), respectively.

Excellent correlation was found for both HONO/SA and HONO/HNO_3 during all events (Table IV.1). The average HONO/SA slope for the nine events was $6.6 \pm 2.0 \times 10^{15}$ molec cm^{-2}, slightly larger than the MRH slope shown in Figure IV.2. The absolute value of the slope of a regression between HONO and HNO_3 can be interpreted as a mole balance between precursor and product. Here, it is assumed that one mole of HNO_3

Table IV.1. Linear regression analysis for HNO_3 depletion events. Slopes presented here include relevant unit conversions.

	Linear regression: HONO/SA ($x10^{15}$ molec. cm^{-2})	**Linear regression: HONO/ HNO_3 (nmol/nmol)**	**Linear regression: $HONO_{excess}$/ HNO_3 (nmol/nmol)[1]**
21-Aug (0540-0840)[2] SR[3] = 0552	Slope = 18(5.5)[4] r^2 = 0.92	Slope = -1.6(0.22) r^2 = 0.98	Slope = -1.0(0.18) r^2 = 0.97
22-Aug (0630-0830) SR = 0553	Slope = 9.6(1.4) r^2 = 0.99	Slope = -3.6(0.66) r^2 = 0.98	Slope = -1.9(0.64) r^2 = 0.96
31-Aug (0230-0510) SR = 0558	Slope = 4.1(2.2) r^2 = 0.80	Slope = -1.1(0.45) r^2 = 0.87	Slope = -0.70(0.66) r^2 = 0.73
2-Sep (0110-0240) SR = 0559	Slope = 7.2(2.3) r^2 = 0.88	Slope = -0.55(0.28) r^2 = 0.77	NA[5]
2-Sep (0450-0820) SR = 0559	Slope = 3.4(1.4) r^2 = 0.81	Slope = -0.65(0.12) r^2 = 0.95	Slope = -0.37(0.33) r^2 = 0.60
4-Sep (0350-0710) SR = 0600	Slope = 2.3(2.1) r^2 = 0.57	Slope = -0.75(0.18) r^2 = 0.94	Slope = -0.79(0.44) r^2 = 0.76
7-Sep (0350-0730) SR = 0602	Slope = 5.0(0.90) r^2 = 0.95	Slope = -1.1(0.26) r^2 = 0.92	Slope = -0.40(0.34) r^2 = 0.61
8-Sep (0320-0820) 0602	Slope = 4.9(1.2) r^2 = 0.89	Slope = -1.2(0.19) r^2 = 0.95	Slope = -1.0 (0.23) r^2 = 0.91
15-Sep (0700-0900) SR = 0606	Slope = 2.9(1.6) r^2 = 0.86	Slope = -2.6(0.67) r^2 = 0.96	Slope = -1.6 0.30) r^2 = 0.98

[1] corresponding to the likely scenario described in the text
[2] start and stop time of event in CST
[3] time of sunrise (SR) in CST
[4] twice standard deviation of computed slope in parentheses
[5] sufficient data not available to calculate $HONO_{excess}$

produces one mole of HONO and that no other species contribute to HONO formation. This assumption is likely incorrect, so the HONO/HNO_3 slopes are not expected to be unity (Table IV.1). The average HONO/HNO_3 slope for all nine observed events was 1.5

Table IV.2. Supporting measurements during HNO_3 depletion events.

	m/z = 44/57	Particle-phase nitrate ($\mu g\ m^{-3}$)	Ave. RH (%)	Ave. NO_2, Peak NO_X (ppb)	Δ HONO (ppb)
21-Aug	1.1	0.39	78	29, 161	1.5
22-Aug	1.2	0.28	76	26, 149	1.0
31-Aug	2.5	0.95	65	49, 139	0.60
2-Sep	7.6	0.94	76	NA[3]	0.43
2-Sep	3.6	1.9	76	39, 96	0.98
4-Sep	5.3	0.83	74	21, 36	0.17
7-Sep	3.8	1.7	78	46, 91	0.87
8-Sep	3.6	2.2	74	50, 174	2.2
15-Sep	1.8	0.61	80	31, 107	0.44
Event Average	3.5	1.3	75	38, 119	0.91
Full campaign[1]	5.8	0.38	65	20,77	--
MRH[2]	3.6	0.73	75	27,77	--

[1] 20 August through 27 September
[2] 0500-0850 of full campaign
[3] NA: not available

± 0.34, indicating that the moles of depleted HNO_3 (on average) can not account for every mole of HONO formed. This suggests the likelihood of additional pathways contributing to HONO formation that do not involve HNO_3. A HONO-HNO_3 slope smaller than unity, during events on 2 September and 4 September, for example, indicates that the molar magnitude of HNO_3 depletion is larger than that of HONO formed. Thus, additional coincident HNO_3 loss pathways must exist. The observation of coincident increases in particle-phase nitrate during events could explain a portion of this excess HNO_3 and will be discussed further below. The observed HONO-HNO_3 slopes likely result from a combination of both scenarios.

Estimation of $HONO_{theoretical}$ and a $HONO_{excess}$ /HNO_3 Mole Balance

To assess the potential contribution of HNO_3 to HONO formation, production from established mechanisms were considered quantitatively first. A theoretical HONO

concentration ($HONO_{theoretical}$) was determined based on known formation mechanisms outlined previously using measured NO_X (NO_{Xobs}), NO_2 (NO_{2obs}), and SA (SA_{obs}) concentrations. Along with direct emissions, three heterogeneous reactions were considered as HONO sources: NO_2 hydrolysis by reaction (R2), NO_2 redox reactions on soot aerosol by reaction (R3), and HNO_3 surface photolysis by reaction (R4). Homogeneous reaction mechanisms were neglected based on modeling results (Moussiopoulos et al., 2000; Vogel et al., 2003; Sarwar et al., 2008) that suggest gas-phase reactions contribute negligibly to HONO formation compared to heterogeneous reactions and direct emissions. HONO production by reaction (R5) was also neglected because reaction kinetics are likely too slow (Rivera-Figeroa et al., 2003). Also, gas- and aqueous-phase HNO_3 photolysis is neglected due to rates approximately two orders of magnitude smaller than the surface photolysis rate reported by Zhou et al. (2003). The calculation of $HONO_{theoretical}$ is given by:

$$\begin{aligned} \mathrm{HONO}_{theoretical} = & \left[f_{soot} \times \mathrm{SA}_{\mathrm{obs}}\right] + \left[\mathrm{NO}_{\mathrm{Xobs}} \times f_{emiss}\right] \\ & + \left[\Delta\mathrm{HNO}_{3\mathrm{obs}} \times \left\{1 - \exp\left(-j_{HNO_3-HONO} \times t\right)\right\}\right] \\ & + \left[\mathrm{NO}_{2\mathrm{obs}} \times \left\{1 - \exp\left(-k_2 \times t\right)\right\}\right] \end{aligned} \tag{2}$$

where f_{emiss} is the emission ratio of HONO to NO_x (ppb/ppb), ΔHNO_{3obs} is the change in observed HNO_3 concentration compared to the previous data point, k_2 is the reaction rate coefficient for reaction (R2), and t is the sampling duration for each data point (10 min).

Table IV.3. Values used for calculated $HONO_{theoretical}$ scenarios.

Parameter	Mechanism	Likely	Upper limit
f_{soot} (molec. cm^{-2})	NO_2 reduction on soot aerosol[1]	$0.2x10^{15}$	$1.0x10^{15}$
f_{emiss} (ppb/ppb)	HONO emission factors[2,3]	0.003	0.008
$j_{HNO3-HONO}$ (s^{-1})	HONO from surface HNO_3 photolysis[4]	$0.2x10^{-5}$	$1.4x10^{-5}$
k_2 (min^{-1} m^{-1})[5]	NO_2 hydrolysis[3]	0.003x(S/V)	0.003x(S/V)

[1](Kalberer et al., 1999)
[2](Kirchstetter et al., 1996)
[3](Kurtenbach et al., 2001)
[4]results from (Zhou et al., 2003) at 1200 CST (upper limit) and 0700 CST (likely)
[5](S/V) = aerosol surface to volume ratio between observed ($HONO_{obs}$) and $HONO_{theoretical}$

The excess HONO concentration ($HONO_{excess}$), or the concentration formed in excess of that generated by established mechanisms, was calculated as the difference concentrations by equation (3):

$$HONO_{excess} = HONO_{obs} - HONO_{theoretical} \quad (3)$$

$HONO_{theoretical}$ and $HONO_{excess}$ were calculated for each data point used previously for determination of HONO/SA and HONO/HNO_3 in Table IV.1. It should be noted that the above calculation is meant to serve as a comparison to HNO_3 depletion, not a quantitative HONO formation model.

Two scenarios regarding $HONO_{theoretical}$ were computed according to the values listed in Table IV.3. The likely scenario is meant to be most applicable to conditions during observed Houston MRH events (high NO_2, high RH, and suitable aerosol surface area, reported in Table IV.2). The upper-limit scenario considers parameters that would

result in maximum HONO production but were derived from less realistic conditions. The upper-limit f_{emiss} value used here is taken from the study of Kurtenbach et al. (2001) that was based on a traffic distribution weighted more heavily by diesel and heavy-duty vehicles. The likely f_{emiss} is taken from Kirchstetter et al. (1996) and is based on tunnel studies of mostly light-duty, gasoline motor vehicles (similar to the assumed distribution during Houston MRH). Values for f_{soot} are from Kalberer et al. (1999) and are based on 70% RH for the likely scenario and on 30% RH for the upper limit scenario. Only reaction potential, and not kinetic limitations, was considered for reaction (R3). Values for $j_{HNO3\text{-}HONO}$ are from Zhou et al. (2003) and are based on photolysis at 0700 CST for the likely scenario and on photolysis at 1200 CST for the upper limit scenario. The value for k_2 is based on results from Kurtenbach et al. (2001).

For the likely scenario, the average $HONO_{theoretical}$ was 23% of average $HONO_{obs}$, with a contribution range of 4.1 – 43%. Even when assessing the upper-limit $HONO_{theoretical}$ concentration, which is unrealistic for the conditions during events, the average contribution of $HONO_{theoretical}$ to $HONO_{obs}$ was just 78%. This is shown in Figure IV.7, and indicates that the majority of the observed HONO could not be attributed to the major sources considered. Thus, an additional source must exist. For the likely scenario, direct emissions accounted for 90% of $HONO_{theoretical}$, and soot redox reaction accounted for 10%. Surface HNO_3 photolysis and NO_2 hydrolysis were negligible. The distribution is shifted slightly for the upper-limit scenario, with 71% of $HONO_{theoretical}$ due to emissions and 29% due to soot redox reactions.

Linear regressions for $HONO_{excess}$ (using the likely scenario) and HNO_3 for each event are described in Table IV.1. Excellent correlation coefficients were obtained for all

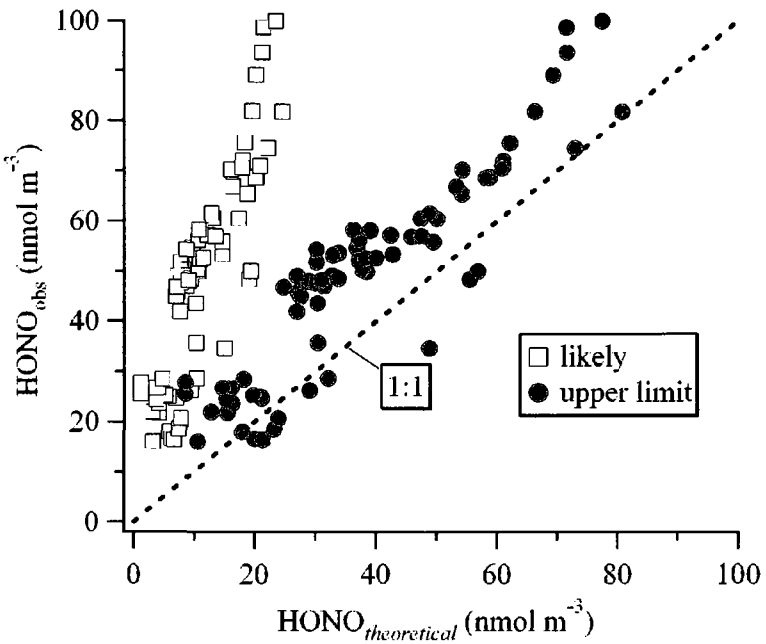

Figure IV.7. Observed HONO concentrations versus theoretical HONO concentrations calculated using equation (2). The likely and upper limit calculations are described in the text and Table IV.3. Note that $HONO_{theoretical}$ does not include a potential heterogeneous HNO_3 source.

events, with all $r^2 > 0.60$. The event average $HONO_{excess}/HNO_3$ slope of 0.97 indicates that, overall, the depleted HNO_3 is nearly balanced by the HONO gained during MRH events, suggesting that HNO_3 is the missing source discussed above. Four of the eight applicable events are statistically (within 2 standard deviations) unity while two event slopes are greater than unity and two are smaller. Both events with $HONO_{excess}/HNO_3$ less than unity (2 September and 7 September) exhibited weaker correlations (0.60 and 0.61, respectively), suggesting a potential missing HNO_3 sink during these events. In fact, these events were marked by notably enhanced particle-phase nitrate concentrations (Table IV.2; 1.9 and 1.7 μg m^{-3}, respectively), suggesting that much of the depleted HNO_3 that did not form HONO could have remained in the aerosol phase. Excluding the event on 8 September which exhibited very high particle-phase nitrate, the

$HONO_{excess}/HNO_3$ mole balance was anti-correlated (r^2 = 0.78) with particle-phase nitrate, supporting the idea that particle-phase nitrate contributed to the $HONO_{excess}/HNO_3$ mole balance discrepancy. Inclusion of the outlying point for 8 September results in a weaker, but still significant, anti-correlation (r^2 = 0.65). The quantitative contribution of particle-phase nitrate to depleted HNO_3 is unknown, as speciation of the m/z = 30 signal from the Q-AMS is uncertain. Still, this anti-correlation seems to indicate strongly that particle-phase nitrate plays a role in HONO formation during MRH events.

The two events with $HONO_{excess}/HNO_3$ slopes greater than unity (22 August and 15 September) likely are due to underestimation of HONO formed from NO_2 reactions. Both events were characterized by very high NO_X concentrations. One distinguishing characteristic of these events is decreased m/z = 44/57 signal (from Table IV.2; 1.2 and 1.8, respectively) from the Q-AMS, indicating that aerosol during these events was even less oxidized than in other MRH events. This could have resulted in more efficient reduction of NO_2 to HONO by reaction (R3) and an underestimation of $HONO_{theoretical}$, resulting in the calculated $HONO_{excess}/HNO_3$ slope that is greater than unity.

While no mechanistic information regarding the formation of $HONO_{excess}$ can be derived from the current observations, the process likely is not photo-dependent. This hypothesis is based on the observation of HONO formation prior to sunrise (Table IV.1) during several events (31 August, 2 September, 4 September, and 7 September). The lack of photo-dependence is most notable on 8 September (Figure V.4) when the HONO increase and HNO_3 depletion started well before the 0603 CST sunrise.

Organic aerosol composition during HONO events

Some evidence for a dependence of $HONO_{excess}$ production on organic aerosol composition exists. Mass spectral signals typical of HOA (m/z = 57, 71, etc.) discussed previously are enhanced in MRH compared to non-MRH as well as during events compared to MRH. Additionally, some correlation exists between X_{event}/X_{MRH} (for individual events) with ΔHONO and with computed HONO/SA slopes. For example, 21 August exhibited the largest $X_{57,event}/X_{57,MRH}$ for any event (an increase of 92%), a ΔHONO of 1.5 ppbv (61 nmol m^{-3}, Table IV.2), and the largest HONO/SA observed (Table IV.1). Likewise, the $X_{57,event}/X_{57,MRH}$ for 4 September was -0.34 (a decrease in m/z = 57 signal compared to the average m/z = 57 signal during MRH), corresponding to a minor ΔHONO of 0.17 ppbv (7.0 nmol m^{-3}, Table IV.2) and HONO/SA slope of 2.3 (Table IV.1). A chemical composition dominated by m/z = 57 likely represents a more reduced aerosol surface (compared to a composition dominated by m/z = 44). Thus, these results suggest a dependence of HONO production on the composition of HOA and potentially on the oxidation state of the HOA surface.

A recent study in Mexico City, another highly polluted urban center, identified several polycyclic aromatic hydrocarbons (PAH) in the aerosol phase using a Q-AMS (Dzepina et al., 2007). To explore the potential influence of PAH during MRH and HONO events, X_{MRH}/X_{nMRH} and X_{event}/X_{MRH} spectra were compared to the PAH spectra obtained by Dzepina et al. (2007). Since most of the PAH signal is observed at m/z > 200, this mass spectral region is the focus of Figure IV.6. Out of the eight molecular ion signals (or groups of signals) identified by Dzepina et al. (2007), three were distinctly enriched during HONO events (Figure IV.6b); m/z = 216, 228, and 240 by 10%, 16%,

and 15%, respectively. These signals were also enriched during MRH (Figure IV.6a), but not significantly compared to surrounding signals, and are identified as the following PAH compounds: 1,2-benzofluorene, 3,4-benzofluorene, and 1-methylpyrene (m/z = 216); benz[α]anthracene, chrysene, and triphenylene (m/z = 228); and methylbenzo[*ghi*]fluoranthrene (m/z = 240). The distinct X_{event}/X_{MRH} signals suggests that the PAH compounds listed above may be important during events and may contribute to the conversion of HNO_3 to HONO.

PAH compounds having larger m/z were generally enriched during MRH (compared to nMRH) but depleted during HONO events (compared to MRH). Notably, m/z = 264, 266, and 278 were enriched during MRH (Figure IV.6a) by 74%, 60%, and 78%, respectively, but were depleted during HONO events (Figure IV.6b) by 7.3%, 3.6%, and 25%, respectively. These signals likely represent 11H-cyclopenta[*ghi*]perylene, 4H-benzo[*hi*]chrysene, and an unidentified PAH, respectively (Dzepina et al., 2007). Signal at m/z = 202 accounted for the highest fraction of the total PAH identified by Dzepina et al. (2007) (the parent ion for pyrene, fluoranthene, and acephenanthrylene) but was not distinctly enriched during either MRH or events in Houston. Several signals that were significantly enhanced during events could not be attributed to previously identified PAH compounds, notably m/z = 203, 219, 235, 261, and 279. These could represent fragments associated with organic compounds of different functionality (including those that are not PAH). While most of the signals at m/z > 200 are consistent with PAH identified previously, the emissions contributing to MRH in Houston may differ from those in Mexico City given the proximity of the sampling site to the HSC.

Marr et al. (2006) identified vehicle emissions as the major source for all of the above PAH compounds in Mexico City, based on maximum diurnal concentrations observed during the early morning and good correlation with CO and gas-phase naphthalene. Benzo[*ghi*]perylene is commonly used as a tracer for gasoline vehicles (Zielinska et al., 2004) and was significantly enhanced during the Mexico City morning (Marr et al., 2006). Benzo[*ghi*]perylene was enriched during MRH in this study by 39% (m/z = 276 in Figure IV.6a) but only slightly enriched during HONO events (by 3.5%, from Figure IV.6b). This may indicate that the organic aerosol composition, and thus HONO formation, was influenced by a more complicated source than simply automobile emissions. Benzo[*ghi*]perylene could also explain the distinctly high values for X_{MRH}/X_{nMRH} at m/z = 134, 136, and 138, which exceeded the X_{MRH}/X_{nMRH} at m/z = 57 (Figure IV.5a). The mass spectrum for benzo[*ghi*]perylene has strong fragmentation peaks at m/z = 134 through 139 (Dzepina et al., 2007) and no other match for these signals was found in Q-AMS spectra published previously (Ulbrich et al., 2008). However, m/z = 134, 136, 138 were depleted by 6.6, 4.4, and 3.1%, respectively, in Figure IV.5b, supporting the hypothesis that gasoline-powered vehicles are not the sole source that influences HONO events.

The significantly enriched m/z signals during events (Figure IV.6b) suggest that PAH compounds may influence heterogeneous HONO formation. The potential for heterogeneous reactions involving PAH compounds is supported by Marr et al. (2006), who suggest that OH is the main oxidant contributing to surface PAH reactions. The enrichment of several PAH parent-ion signals during HONO events (compared to MRH)

described here suggests that HNO_3 chemistry also may contribute significantly to PAH processing.

Conclusions

Strong temporal correlation was observed between SA and HONO during the early morning, coincident with significant depletion of HNO_3. Molar concentration ratios of HONO to HNO_3 and coincidence with enhanced SA suggest that heterogeneous reactions of HNO_3 are a source of HONO. Mass spectral analysis and strong correlations between SA, organic aerosol, and CO suggest that primarily emitted HOA surface is driving the heterogeneous reactions. HONO concentrations predicted by several heterogeneous mechanisms (using likely conditions) and direct emissions account for only a fraction of those observed. On average, observed HONO was more than a factor of four greater than predicted concentrations using the likely scenario. Predicted HONO concentrations using an upper estimate scenario still result in significant underestimation of HONO concentrations compared to observations. By assuming that all depleted HNO_3 is converted to HONO during nine identified events, the discrepancy between observed and predicted HONO is diminished, as average calculated $HONO_{excess}/HNO_3$ slopes were approximately unity. Deviations from unity likely are due to HNO_3 partitioning into the aerosol phase and due to underestimation of the contribution of NO_2 to HONO formation under certain conditions. Thus, heterogeneous HNO_3 reactions on primary HOA are likely an important source of HONO in urban atmospheres. Observations of HONO formation events prior to sunrise suggest a mechanism that is not photo-dependent. Several PAH compounds were enriched during HONO events, suggesting their

importance for HNO_3 conversion. Laboratory work is necessary to investigate HONO formation rates as a function of the chemical composition and oxidation state of HOA. Extrapolation of these results to other urban areas is uncertain, as the influence of the HSC on the observed HONO formation events is not understood. Still, this phenomenon is likely to occur in any urban area where significant HNO_3 is produced or survives through the night and where there is significant emission of HOA

References

Alfarra, M.R., et al., 2004. Characterization of urban and rural organic particulate in the Lower Fraser Valley using two Aerodyne aerosol mass spectrometers. Atmospheric Environment 38 (34), 5745-5758.

Alicke, B., Geyer, A., Hofzumahaus, A., Holland, F., Konrad, S., Patz, H.W., Schafer, J., Stutz, J., Voltz-Thomas, A., and Platt, U., 2003. OH formation by HONO photolysis during the Berlioz experiment. Journal of Geophysical Research-Atmospheres 108 (D4), 8247, doi:10.1029/2001JD000579.

Ammann, M., Kalberer, M., Jost, D.T., Tobler, L., Rossler, E., Piguet, D., Gaggeler, H.W., Baltensperger, U., 1998. Heterogeneous production of nitrous acid on soot in polluted air masses. Nature 395 (6698), 157-160.

Ammann, M., Rossler, E., Strekowski, R., George, C., 2005. Nitrogen dioxide multiphase chemistry: Uptake kinetics on aqueous solutions containing phenolic compounds. Physical Chemistry Chemical Physics 7 (12), 2513-2518.

Arens, F., Gutzwiller, L., Baltensperger, U., Gäggeler, H.W., and Ammann, M., 2001. Heterogeneous reaction of NO_2 on diesel soot particles. Environmental Science and Technology 35 (11), 2191-2199.

Bae, M.S., Schwab, J.J., Zhang, Q., Hogrefe, O., Demerjian, K.L., Weimer, S., Rhoads, K., Orsini, D., Venkatachari, P., and Hopke, P.K., 2007. Interference of organic signals in highly time resolved nitrate measurements by low mass resolution aerosol mass spectrometry. Journal of Geophysical Research-Atmospheres 112 (D22), doi:10.1029/2007JD008614.

Canagaratna, M.R., Jayne, J.T., Ghertner, D.A., Herndon, S., Shi, Q., Jimenez, J.L., Silva, P.J., Williams, P., Lanni, T., Drewnick, F., Demerjian, K.L., Kolb, C.E.,

and Worsnop, D.R., 2004. Chase studies of particulate emissions from in-use New York City vehicles. Aerosol Science and Technology 38 (6), 555-573.

Canagaratna, M.R., et al., 2007. Chemical and microphysical characterization of ambient aerosols with the Aerodyne aerosol mass spectrometer. Mass Spectrometry Reviews 26 (2), 185-222.

Clemitshaw, K.C., 2006. Coupling between the tropospheric photochemistry of nitrous acid (HONO) and nitric acid (HNO_3). Environmental Chemistry 3 (1), 31-34.

Dibb, J.E., Scheuer, E., Whitlow, S.I., Vozella, M., Williams, E., Lerner, B.M., 2004. Ship-based nitric acid measurements in the gulf of Maine during New England Air Quality Study 2002. Journal of Geophysical Research-Atmospheres 109 (D20), doi:10.1029/2004JD004843.

Dzepina, K., Arey, J., Marr, L.C., Worsnop, D.R., Salcedo, D., Zhang, Q., Onasch, T.B., Molina, L.T., Molina, M.J., and Jimenez, J.L., 2007. Detection of particle-phase polycyclic aromatic hydrocarbons in Mexico City using an aerosol mass spectrometer. International Journal of Mass Spectrometry 263, 152-170.

Finlayson-Pitts, B.J., Wingen, L.M., Sumner, A.L., Syomin, D., Ramazan, K.A., 2003. The heterogeneous hydrolysis of NO_2 in laboratory systems and in outdoor and indoor atmospheres: An integrated mechanism. Physical Chemistry Chemical Physics 5 (2), 223-242.

George, C., Strekowski, R.S., Kleffmann, J., Stemmler, K., and Ammann, M., 2005. Photoenhanced uptake of gaseous NO_2 on solid organic compounds: a photochemical source of HONO. Faraday Discussions 130, 195-210.

Gutzwiller, L., Arens, F., Baltensperger, U., Gaggeler, H.W., Ammann, M., 2002. Significance of semivolatile diesel exhaust organics for secondary HONO formation. Environmental Science & Technology 36 (4), 677-682.

Handley, S.R., Clifford, D., Donaldson, D.J., 2007. Photochemical loss of nitric acid on organic films: A possible recycling mechanism for NO_X. Environmental Science & Technology 41 (11), 3898-3903.

Harley, R.A., Hannigan, M.P., Cass, G.R., 1992. Respeciation of organic gas emissions and the detection of excess unburned gasoline in the atmosphere. Environmental Science & Technology 26 (12), 2395-2408.

Harrison, R.M., Peak, J.D., Collins, G.M., 1996. Tropospheric cycle of nitrous acid. Journal of Geophysical Research-Atmospheres 101 (D9), 14429-14439.

Jayne, J.T., Leard, D.C., Zhang, X.F., Davidovits, P., Smith, K.A., Kolb, C.E., Worsnop, D.R., 2000. Development of an aerosol mass spectrometer for size and

composition analysis of submicron particles. Aerosol Science and Technology 33 (1-2), 49-70.

Jimenez, J.L., Jayne, J.T., Shi, Q., Kolb, C.E., Worsnop, D.R., Yourshaw, I., Seinfeld, J.H., Flagan, R.C., Zhang, X.F., Smith, K.A., Morris, J.W., and Davidovits, P., 2003. Ambient aerosol sampling using the aerodyne aerosol mass spectrometer. Journal of Geophysical Research-Atmospheres 108 (D7), doi:10.1029/2001JD001213.

Kalberer, M., Ammann, M., Arens, F., Gaggeler, H.W., Baltensperger, U., 1999. Heterogeneous formation of nitrous acid (HONO) on soot aerosol particles. Journal of Geophysical Research-Atmospheres 104 (D11), 13825-13832.

Kirchstetter, T.W., Harley, R.A., Littlejohn, D., 1996. Measurement of nitrous acid in motor vehicle exhaust. Environmental Science & Technology 30 (9), 2843-2849.

Kleffmann, J., Becker, K.H., Lackhoff, M., Wiesen, P., 1999. Heterogeneous conversion of NO_2 on carbonaceous surfaces. Physical Chemistry Chemical Physics 1 (24), 5443-5450.

Knipping, E.M., Dabdub, D., 2002. Modeling surface-mediated renoxification of the atmosphere via reaction of gaseous nitric oxide with deposited nitric acid. Atmospheric Environment 36 (36-37), 5741-5748.

Kurtenbach, R., Becker, K.H., Gomes, J.A.G., Kleffmann, J., Lorzer, J.C., Spittler, M., Wiesen, P., Ackermann, R., Geyer, A., and Platt, U., 2001. Investigations of emissions and heterogeneous formation of HONO in a road traffic tunnel. Atmospheric Environment 35 (20), 3385-3394.

Marr, L.C., Dzepina, K., Jimenez, J.L., Reisen, F., Bethel, H.L., Arey, J., Gaffney, J.S., Marley, N.A., Molina, L.T., and Molina, M.J., 2006. Sources and transformations of particle-bound polycyclic aromatic hydrocarbons in Mexico City. Atmospheric Chemistry and Physics 6, 1733-1745.

McGaughey, G.R., Desai, N.R., Allen, D.T., Seila, R.L., Lonneman, W.A., Fraser, M.P., Harley, R.A., Pollack, A.K., Ivy, J.M., and Price, J.H., 2004. Analysis of motor vehicle emissions in a Houston tunnel during the Texas Air Quality Study 2000. Atmospheric Environment 38 (20), 3363-3372.

Moussiopoulos, N., Papalexiou, S., Lammel, G., Arvanitis, T., 2000. Simulation of nitrous acid formation taking into account heterogeneous pathways: Application to the Milan metropolitan area. Environmental Modeling & Software 15 (6-7), 629-637.

Rivera-Figueroa, A.M., Sumner, A.L., Finlayson-Pitts, B.J., 2003. Laboratory studies of potential mechanisms of renoxification of tropospheric nitric acid. Environmental Science & Technology 37 (3), 548-554.

Sage, A.M., Weitkamp, E.A., Robinson, A.L., Donahue, N.M., 2008. Evolving mass spectra of the oxidized component of organic aerosol: Results from aerosol mass spectrometer analyses of aged diesel emissions. Atmospheric Chemistry and Physics 8 (5), 1139-1152.

Sarwar, G., Roselle, S.J., Mathur, R., Appel, W., Dennis, R.L., Vogel, B., 2008. A comparison of CMAQ HONO predictions with observations from the Northeast Oxidant and Particle Study. Atmospheric Environment 42 (23), 5760-5770.

Scheuer, E., Talbot, R.W., Dibb, J.E., Seid, G.K., DeBell, L., Lefer, B., 2003. Seasonal distributions of fine aerosol sulfate in the North American Arctic basin during TOPSE. Journal of Geophysical Research-Atmospheres 108 (D4), doi:10.1029/2001JD001364.

Stemmler, K., Ammann, M., Donders, C., Kleffmann, J., George, C., 2006. Photosensitized reduction of nitrogen dioxide on humic acid as a source of nitrous acid. Nature 440 (7081), 195-198.

Ulbrich , I.M., Canagaratna, M.R., Zhang, Q., Worsnop, D.R., and Jimenez, J.L., 2008. Interpretation of organic components from positive matrix factorization of aerosol mass spectrometric data. Atmospheric Chemistry and Physics Discussions, 8, 6729-6791.

Vogel, B., Vogel, H., Kleffmann, J., Kurtenbach, R., 2003. Measured and simulated vertical profiles of nitrous acid - part II. Model simulations and indications for a photolytic source. Atmospheric Environment 37 (21), 2957-2966.

Zhang, Q., Alfarra, M.R., Worsnop, D.R., Allan, J.D., Coe, H., Canagaratna, M.R., Jimenez, J.L., 2005a. Deconvolution and quantification of hydrocarbon-like and oxygenated organic aerosols based on aerosol mass spectrometry. Environmental Science & Technology 39 (13), 4938-4952.

Zhang, Q., Worsnop, D.R., Canagaratna, M.R., Jimenez, J.L., 2005b. Hydrocarbon-like and oxygenated organic aerosols in Pittsburgh: Insights into sources and processes of organic aerosols. Atmospheric Chemistry and Physics 5 3289-3311.

Zhou, X.L., Gao, H.L., He, Y., Huang, G., Bertman, S.B., Civerolo, K., Schwab, J., 2003. Nitric acid photolysis on surfaces in low-NO_X environments: Significant atmospheric implications. Geophysical Research Letters 30 (23), doi:10.1029/2003GL018620.

Zielinska, B, Sagebiel, J., McDonald, J.D., Whitney, K., and Lawson, D.R., 2004. Emission rates and comparative chemical composition from selected in-use diesel and gasoline-fueled vehicles. Journal of Air and Waste Management 54, 1138-1150.

CHAPTER V

OBSERVATIONS OF PARTICLE GROWTH AT A REMOTE, ARCTIC SITE

Abstract

Observations of aerosol size distributions suggest that aerosols grow significantly just above the snow surface at a remote, Arctic site. Measurements were made at Summit, Greenland (71.38° N and 31.98° W) at approximately 3200 m above sea level. No new particle formation was observed locally, but growth of ultrafine aerosol was identified by continuous evolution of the geometric mean diameter (GMD) during four events. The duration of the growth during events was between 24 and 115 hours, and calculated event-average growth rates (GR) were 0.089, 0.297, 0.265, and 0.183 nm hr^{-1} during each event, respectively. Four-hour GR were observed up to 0.963 nm hr^{-1}. Events occurred during below- and above-average temperatures and were independent of wind direction. Correlation analysis of hourly-calculated GR suggested that aerosol growth was limited by the availability of photochemically-produced precursor gases. Sulfuric acid played a very minor role in aerosol growth, which was likely dominated by condensation of organic compounds, the source of which was presumably the snow surface. The role of boundary layer dynamics is not conclusive, although some mixing at the surface is necessary for the observation of aerosol growth. Due to the potentially large geographic extent of events, observations described here may provide a link between the long-range transport of mid-latitude pollutants and climate regulation in the remote Arctic.

Introduction

Much scientific attention in the last 30 years has focused on understanding Arctic haze, an accumulation of aerosol mass in the polar regions during the late winter and early spring which is characterized by an alteration of the Arctic radiation balance and visibility degradation (Quinn et al., 2007). This phenomenon can be attributed directly to transport of anthropogenic pollutants from populated mid-latitude regions, the trapping of those pollutants by strong, stable temperature inversions near the surface, and reduced wet deposition rates. The breakup of Arctic haze, brought on by surface heating and increased wet deposition in the late spring (Quinn et al., 2007), is followed by a much cleaner atmospheric boundary layer in the summer months typified by depleted aerosol mass concentrations and enhanced ultrafine particle number concentrations with an aerosol size distribution that is shifted towards smaller diameters (Ström et al., 2003; Engvall et al., 2008).

Particle nucleation and growth events have been studied extensively throughout much of the globe (Kulmala et al., 2004) due to both the potential health effects (Oberdörster 2000) and climate implications (Kerminen et al., 2005) of ultrafine particles. Nucleation has been observed in both the remote (Vehkamäki et al., 2004) and urban (Alam et al., 2003) lower troposphere, due to natural (O'Dowd et al., 2002) and anthropogenic (Weber et al., 2003) emissions, and in the free troposphere/lower stratosphere (Young et al., 2007). For newly formed particles to become climatically significant, growth to sizes relevant to direct scattering of solar radiation and activation as cloud condensation nuclei (CCN) or ice nuclei (IN) is necessary.

Observations suggest that CCN activity is most sensitive to particle size (Dusek et al., 2006). Garrett et al. (2004) showed that new particle formation produced little effect on low-level, Arctic-cloud microphysics while larger, more aged, haze aerosol resulted in smaller, more numerous cloud droplets. Thus, the processes that govern the growth of newly formed particles (on the order of 1-nm in diameter) to larger sizes that are more active CCN/IN are extremely important to climate regulation. Arctic aerosol/cloud/climate interactions are unique compared to lower latitudes due to low surface temperatures, high surface albedo, and prevalence of stable conditions (Curry, 1995), and due to the highly water-soluble nature of the aerosol (Hagler et al., 2007a). This results in a climate system that is likely more sensitive to aerosol dynamics (Garrett et al., 2004).

In this work, aerosol size distribution measurements were made at an extremely remote, high-elevation site during an Arctic summer. New particle formation was not observed, but the following analysis is focused on observations of sustained geometric growth of ultrafine aerosol near the snow surface. Several particle growth events were observed, and the conditions favorable for these events are described.

Methods

Field Site

Summit, Greenland is located at 71.38° N and 31.98° W and approximately 3,200 m above sea level atop the Greenland ice cap. With the nearest coastline approximately 400 km from the site, Summit is extremely remote and is subject to no influence from any (non-camp) local pollution sources. Sampling was carried out from 15 May 2007

through 16 June 2007 during which time the sun was always above the horizon. Still, the average intensity of incoming solar radiation, approximated by the photolysis rate constant of nitrogen dioxide, was a factor of 17 greater at noon than that at midnight local time.

Instrumentation

A scanning mobility particle sizer (SMPS, TSI, Inc., Shoreview, MN, model 3080) was used to measure particle number size distributions. The SMPS consisted of a nano-differential mobility analyzer (DMA, TSI, Inc, model 3085) coupled with an ultrafine condensation particle counter (UCPC, TSI, Inc., model 3076). Electrical differential mobility analysis has been used extensively for measuring ambient particle size distributions (Winklmayr et al., 1991; Kulmala et al., 2004). For this system, sample air is first introduced through a pre-impactor to remove aerosol larger than one micron in diameter. The sample is then passed through a neutralizer which gives the aerosol population a known charge distribution using a radioactive ^{85}Kr source. Aerosols then enter a cylindrical column surrounding an inner, charged rod. Using an applied potential across the inner rod and the outside walls of the cylinder, aerosol particles of a specific electrical mobility are selected. Assuming particles are spherical, electrical mobility is a function of particle diameter. Upon column exit, the resulting monodisperse aerosol is counted by the UCPC (described below). By varying the applied potential, a number-based distribution of electrical mobility diameter is observed.

Condensation particle counters were used both as a detector in the SMPS system and as an external quality control during ambient measurements. As part of the SMPS, the TSI, Inc. model 3076 (referred to as the UCPC) has a detection range of 5 to 3000

nm. The external TSI, Inc., model 3022A (referred to as the CPC) has a detection range of 8 to 3000 nm. In both instruments, sample enters the instrument at a known flow rate and continues into a chamber containing 2-butanol at 30°C. The sample and saturated 2-butanol enter a condenser held at 10°C, where the 2-butanol condenses on the surface of each particle, increasing the diameter up to several micron. The particles are then counted optically with a laser, and number concentrations are determined. Number concentrations obtained from the external CPC (N_{CPC}) were saved with 1-minute resolution and averaged to 5-minute resolution to compare with SMPS measurements.

Size-detection limits of the SMPS are a function of the DMA operating specifications and the ambient conditions. Sheath and excess flow rates in the DMA were controlled at 3.0 L min^{-1} and the aerosol (inlet) flow rate was 0.3 L min^{-1}. The monodisperse flow rate leaving the DMA is matched to the inlet flow rate of the UCPC, which was 0.3 L min^{-1} in low flow mode. Manufacturer-developed software was used for data collection and processing. Values of 1.632×10^{-5} g cm^{-1} s^{-1}, 9.122×10^{-8} m, and 7.8×10^{-4} g cm^{-3} for the average ambient gas viscosity, mean free path (λ), and density, respectively, were used to account for the decreased temperature and pressure at Summit. These parameters resulted in measurement of number-based size distributions of 5.52-nm (midpoint) diameter to 195-nm diameter aerosol, across 100 measurement channels. The full size range was scanned in 285 seconds with a 10 second retrace time and 5 second dead time resulting in a sampling resolution of 5 minutes. Size calibrations were performed in the field using National Institute of Standards and Technology-traceable 81-nm and 151-nm diameter polystyrene latex spheres. All flow rates were verified prior to sampling with a bubble flow meter. Post-processing options for 'multiple charge

correction' and 'diffusion correction' were employed according to manufacturer specifications.

Both the SMPS and the CPC were operated inside a small heated structure on the snow surface. Each instrument sub-sampled air through 0.635 cm-inner diameter silicone conductive tubing approximately 20-cm in length from a common manifold made of 1.27 cm-inner diameter silicone conductive tubing. The manifold was 1 m in length, approximately 1 m above the snow surface, and was operated at a flow rate of 10 L min^{-1}.

A multitude of other gas-, aerosol-, and snow-phase atmospheric variables, along with meteorological conditions, were measured at Summit during this campaign. Most relevant to this work were gas-phase observations of sulfuric acid (H_2SO_4), measured by chemical ionization-mass spectrometry, and nitric oxide (NO) and ozone (O_3), measured by chemiluminescence (Sjostedt et al., 2007). Meteorological conditions (temperature, pressure, wind speed, wind direction, and relative humidity) were measured at a height of 10-m above the snow surface at a site approximately 1 km from the gas- and aerosol-phase measurements. Temperature was also measured at 2-m above the snow surface. Aerosol-phase ^{7}Be and ^{210}Pb activity was measured from 48-hr bulk (no-size cut) filter samples by gamma spectroscopy (Dibb, 2007).

Analysis

Analysis: Local Anthropogenic Influence

Despite extensive efforts to increase efficiency and decrease emissions, anthropogenic influence to the local environment from camp activities at Summit is inevitable (Hagler et al., 2008). Electricity is available through the continuous operation of diesel fuel-burning generators, and intermittent use of heavy-duty maintenance

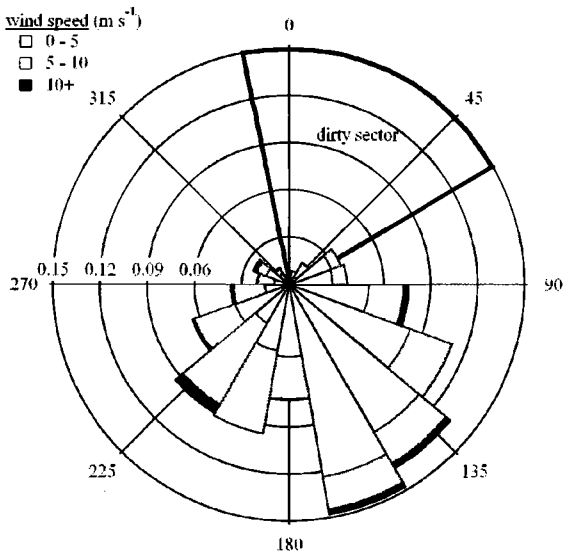

Figure V.1. Wind speed as a function of wind direction for the full sampling campaign at Summit during summer 2007. The fraction of samples of a given wind speed range is plotted on the radial axis, and wind directions are as follows: 0°=North, 90°=East, 180°=South, and 270°=West.

equipment and gasoline-powered snowmobiles causes local releases of gas- and aerosol-phase pollution. To alleviate local influence and provide pristine research environments, a 'clean-air sector' has been implemented where only foot-traffic is permitted; all atmospheric sampling is performed within this sector.

All atmospheric data presented here have been filtered to remove samples potentially contaminated by camp emissions using a method similar to that used by Hagler et al. (2008). Data recorded during periods of low wind speed (<0.5 m s^{-1}) and northerly wind direction (the 'dirty sector', between 350° and 60°) were discarded. The wind direction distribution for the 2007 sampling campaign is presented in Figure V.1. Only 5.5% of the aerosol data were removed due to potential camp influence, of which 84% were discarded due to wind direction from the dirty sector (outlined in black in Figure V.1) and 16% were discarded due to stagnant winds.

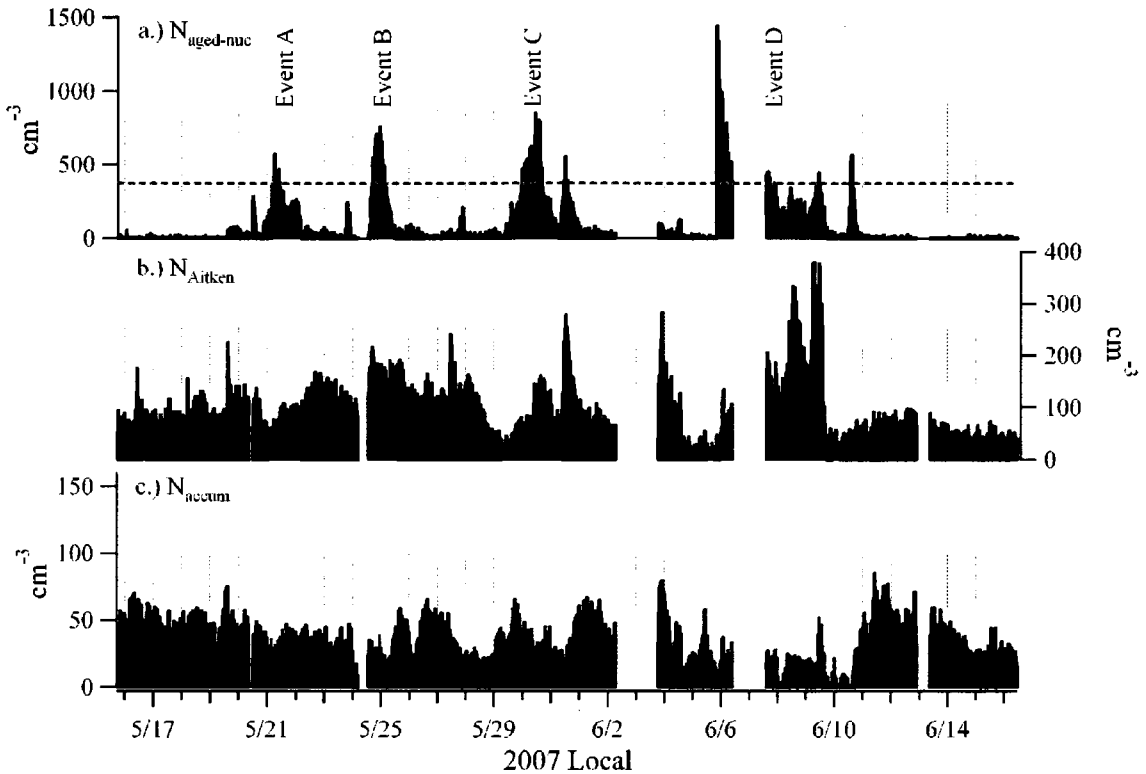

Figure V.2. $N_{aged-nuc}$ (a.), N_{Aitken} (b.), and N_{accum} (c.) at Summit. N_{nuc} is not plotted due to zero concentration throughout the campaign during summer 2007. Events are denoted by gray areas, and the 95th-percentile $N_{aged-nuc}$ is shown as a dotted line in panel a.). Note the different y-axis scales for each panel.

Analysis: Event Selection and Criteria

Integrated particle number concentrations were determined for the full-scanned size range of the SMPS (N_{SMPS}, 5.52 – 195 nm) and for four size classes to determine the variability of the aerosol distribution: nucleation mode of particle diameter < 9 nm (N_{nuc}); aged-nucleation mode from 9 to 30 nm particle diameter ($N_{aged-nuc}$); Aitken mode from 30 to 110 nm particle diameter (N_{Aitken}); and accumulation mode particles with diameter > 110 nm (N_{accum}). This scheme is identical to that used in Birmili et al. (2001). Number concentrations in each class were calculated by summing the particle number concentration of each size channel of the SMPS within that class. Because no nucleation-mode aerosol was detected during the campaign, four events were identified based on

concentrations greater than the 95th percentile value for the aged-nucleation-class for longer than 1 hour consecutively. These events are clearly shown in Figure V.2. Concentrations greater than the 95th percentile observed on 31 May and 10 June were not segregated as events due to their short durations.

Analysis: Calculation of Growth Rate

Geometric mean diameter (GMD) is a useful metric for describing a particle size distribution. Due to very low total particle number concentrations at Summit that resulted in significantly noisy size distributions, raw size distribution data (at 5-min time resolution) were averaged to 1 hour. GMD was calculated for each one-hour size distribution observed during the four events by manually fitting the data to a lognormal distribution according to Mäkelä et al. (2000). The maximum of the fitted lognormal curve is interpreted as the GMD of the distribution. Typically, an observed size distribution was characterized visually by more than one mode over the measured diameter size range of 5.5 to 195 nm, in which case only the mode at smaller aerosol diameter was considered. Aerosol of larger diameter was excluded from this analysis due to much lower N_{Aitken} and N_{accum} compared to $N_{aged\text{-}nuc}$ during events (Figure V.2) making mathematical fitting nearly impossible in the Aitken and accumulation modes. Thus, GMD calculations at larger aerosol size would have resulted in meaningless values. An example of this fitting procedure is shown in Figure V.3 with respect to the average number-size distribution for the full campaign, resulting in a calculated GMD of 26.2 nm.

The evolution of a size distribution over time was explored by calculation of an instantaneous, observed particle growth rate (GR_{obs}). Typically, a linear increase in

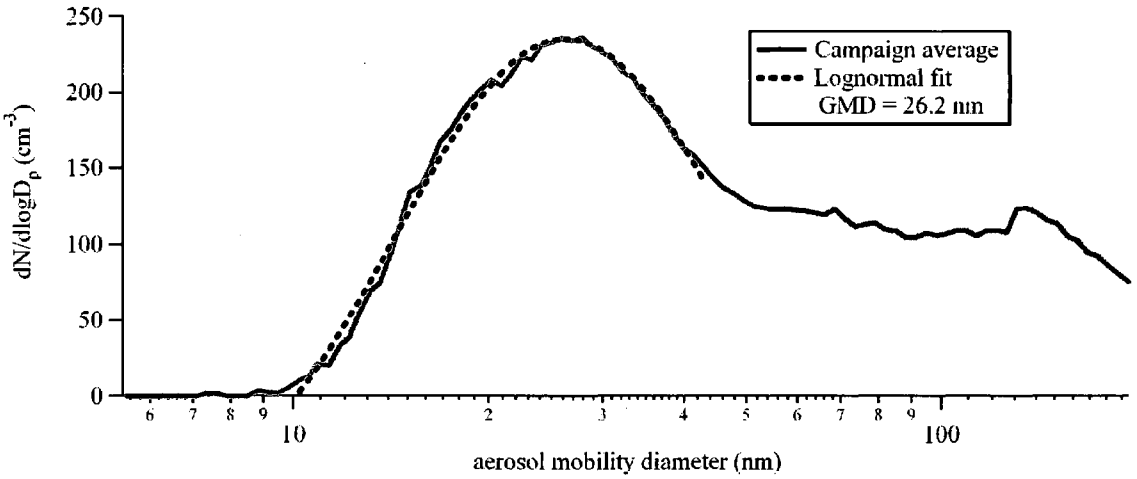

Figure V.3. Campaign-average aerosol number size distribution at Summit during summer 2007. A lognormal fit of the average distribution is shown to illustrate the manual fitting procedure for GMD determination.

GMD is observed if particle growth is due solely to gas-to-particle conversion, assuming gas-phase concentrations are constant. Because of this, GR_{obs} was determined from the calculated slope of a linear regression of GMD versus time. GR_{obs} was calculated for each event, and for each 4-hour period during events, starting every hour. Only positive GR_{obs} values with $r^2 > 0.5$ were used for the correlation analysis that is detailed below.

Relationships between measured variables were explored using regression analysis to identify potential conditions amenable to particle growth at Summit. Pearson correlation coefficients were calculated between GR_{obs} and surface temperature, temperature gradient (the difference between temperature measured at 10-m and 2-m above the surface, where a positive value denotes a more stable atmosphere), wind speed, relative humidity (RH), pre-existing aerosol surface area ($SA_{pre\text{-}exist}$), NO, O_3, and H_2SO_4. Correlations in which the calculated r-value was statistically different from zero (with a 95% confidence level) are referred to as 'significant'.

To assess the contribution to the GR_{obs} from condensation of H_2SO_4, a theoretical GR (GR_{H2SO4}, nm hr^{-1}) was calculated based on Held et al. (2004) and Kulmala et al. (2001) as:

$$GR_{H2SO4} = \frac{M_{H2SO4}\beta_M D_{H2SO4} c_{H2SO4}}{D_P \rho} \cdot 3.6x10^{12} \quad (1)$$

$$\beta_M = \frac{Kn + 1}{0.377Kn + 1 + \frac{4}{3}\alpha^{-1}Kn^2 + \frac{4}{3}\alpha^{-1}Kn} \quad (2)$$

$$Kn = \frac{2\lambda}{D_P} \quad (3)$$

where M_{H2SO4} is the molecular weight of H_2SO_4 (98.1 g mol^{-1}), β_M is the dimensionless mass transfer correction factor, D_{H2SO4} is the molecular diffusivity of H_2SO_4 (m^2 s^{-1}), c_{H2SO4} is the ambient concentration of H_2SO_4 (mol m^{-3}), D_P is the aerosol diameter (m), ρ is the aerosol density (assumed to be $1.2x10^6$ g m^{-3}), Kn is the dimensionless Knudsen number, and α is the sticking coefficient (assumed here to be unity). D_{H2SO4} was calculated as a function of ambient temperature and pressure from $D_{H2SO4,STP} = 8.89x10^{-6}$ m^2 s^{-1} (at standard temperature and pressure) (Massman, 1998).

Results

A total of 8,673 5-min size distributions were obtained over the 33-day measurement campaign. The occasional missing data (approximately 9% of the campaign) were attributed to instrument calibration, maintenance, and blank measurements. Blank samples were determined for both instruments simultaneously by sampling through a HEPA filter installed upstream of the inlet manifold. Average values for blank N_{CPC} and N_{SMPS} were 0.0010 ± 0.0018 (value ± standard deviation) cm^{-3} and 3.1

± 6.4 cm^{-3}, respectively, for 72 1-min CPC samples and 42 SMPS size distributions. Blank concentrations were not subtracted from ambient data but are reported to verify the performance of the sampling instrumentation. Campaign-average N_{CPC} and N_{SMPS} were 285 ± 245 (value ± standard deviation) cm^{-3} and 182 ± 249 cm^{-3}, respectively. A linear regression analysis between N_{CPC} (y-axis) and N_{SMPS} (x-axis) yielded a correlation coefficient (r^2) of 0.87 and a slope of 1.24. The discrepancy between the two is discussed in Section 4.

The average aerosol size distribution was dominated by small particles, with a peak in $dN/dlogD_p$ at 26 nm (Figure V.3). A secondary mode was also observed at D_p > 80 nm. N_{SMPS} was dominated by small particles, with average values for $N_{aged\text{-}nuc}$, N_{Aitken}, and N_{accum} of 71.9, 76.7, and 26.0 cm^{-3}, respectively. The size distribution was nearly void of nucleation-mode particles, with a N_{nuc} value of 0.10 cm^{-3}. Visually, there was little coincidence between the variation in $N_{aged\text{-}nuc}$, N_{aitken}, and N_{accum}. For example, the $N_{aged\text{-}nuc}$-events outlined in Figure V.2 generally occurred independently of increases in N_{Aitken} and N_{accum}. Similarly, instances of increased N_{accum} (on 27 May, 1 June, and 11 June, for example) showed no correlation with $N_{aged\text{-}nuc}$ or N_{Aitken}. Linear regression analysis confirms the lack of correlation between binned number concentrations, as no statistically significant relationships were obtained. The correlation coefficient for $N_{aged\text{-}nuc}/N_{aitken}$ was 0.25, that for $N_{aged\text{-}nuc}/N_{accum}$ was -0.27, and that for N_{aitken}/N_{accum} was -0.03.

While average values for $N_{aged\text{-}nuc}$ and N_{Aitken} were similar in magnitude, much larger variability was observed in $N_{aged\text{-}nuc}$. $N_{aged\text{-}nuc}$ is characterized by a smaller 5th-percentile value (0.0 cm^{-3} compared to 15 cm^{-3} for N_{Aitken}), a larger 95th-percentile value (372 cm^{-3} compared to 168 cm^{-3} for N_{Aitken}), and a larger standard deviation by nearly a

factor of 3 (145 cm^{-3} compared to 51 cm^{-3} for N_{Aitken}). Very little variation (smallest standard deviation) was observed in N_{accum} (15 cm^{-3}). Over 48% of samples had a $N_{aged-nuc}$ = 0.0, while 0.37% and 4.9% of samples had N_{Aitken}, and N_{accum} = 0.0. The large variation and magnitude of $N_{aged-nuc}$, shown clearly in Figure V.2, is the impetus for exploration of event-driven $N_{aged-nuc}$.

Event A

The first observed event occurred on 21 May. Statistics for events are presented in Table V.1. $N_{aged-nuc}$ initially increased from near zero to a maximum of 569 cm^{-3} at 0630 local time (Figure V.4a). $N_{aged-nuc}$ was elevated (above 100 cm^{-3}) for most of the day before returning to zero cm^{-3} at 0400 on 22 May. Negligible increases in N_{Aitken} and N_{accum} were observed. An event-average temperature of -24.6°C and a nearly constant wind direction were observed during the event (Table V.1). The event-average O_3 concentration was 52.8 ppbv (slightly below the campaign average) and did not vary by more than 1 ppbv throughout the event. The event-average NO concentration was 9.36 pptv, with a midday peak at 15.0 pptv. Similarly, the event-average RH was below campaign-average at 79.7%, and varied diurnally from 78.1 to 83.0%.

Very little change in aerosol GMD was observed during the event, 1.3 nm, resulting in a GR_{obs} of 0.089 nm hr^{-1} (Figure V.4a). This value is statistically greater than zero based on twice the standard deviation of the slope calculation. An event-average H_2SO_4 concentration of 1.67×10^6 molec cm^{-3} was observed, 26% larger than the campaign average. The average calculated GR_{H2SO4} during the event was 0.074 nm hr^{-1}, and constituted 83% of the observed GR_{obs}. Linear regression analysis between GR_{obs} and GR_{H2SO4} yielded an r-value of 0.72.

Table V.1. Statistics for growth events observed during 2007 campaign

	Event A	Event B	Event C	Event D	Campaign
Local start time[a]	5/21/07 0400	5/24/07 1500	5/29/07 1000	6/5/07 0800	NA
Local stop time[b]	5/22/07 0300	5/25/07 1200	5/31/07 0700	6/10/07 0200	NA
Ave. temp. (°C)	-24.6	-24.6	-21.4	-14.9	-19.8
Mode wind direction[c]	110° (71°-126°)[e]	120° (71°-143°)	220° (153°-237°)	240° (193°-330°)	Figure V.1[d]
Ave. wind speed (m s^{-1})	5.64	4.66	6.86	5.38	5.58
Ave. SA, $SA_{pre\text{-}exist}$ (μm^2 cm^{-3})	2.89, 2.58	3.32, 2.67	3.00, 2.53	1.80, 0.982	2.87, NA
Ave. O_3 (ppbv)	52.8 (51.7–53.4)[e]	51.9 (50.0–53.7)	55.8 (51.1–62.6)	49.1 (44.6–55.3)	55.6 (38.2–78.0)
Ave. NO (pptv)	9.36	12.0	8.51	10.9	10.9
Ave. RH (%)	79.7	82.3	81.6	88.8	83.3
Ave. H_2SO_4 (molec cm^{-3})	1.67×10^6	1.14×10^6	1.15×10^6	1.39×10^6	1.32×10^6
GR_{H2SO4} (nm hr^{-1})	0.074	0.047	0.051	0.043	NA
GR_{obs} (nm hr^{-1})	0.089 (0.020)[f]	0.297 (0.031)	0.265 (0.013)	0.183 (0.008)	NA
Δ GMD (nm)	1.3 (19.9–21.2)[e]	7.4 (21.4–28.8)	21.5 (13.5–35.0)	21.1 (13.7–35.8)	NA

[a]determined from start of increase of $N_{aged\text{-}nuc}$
[b]determined from the end of the GMD increase
[c]determined from wind rose analysis
[d]see Figure V.1 for wind direction distribution from wind rose analysis
[e]range of values inside parentheses
[f]twice the standard deviation value inside parentheses
NA: not applicable

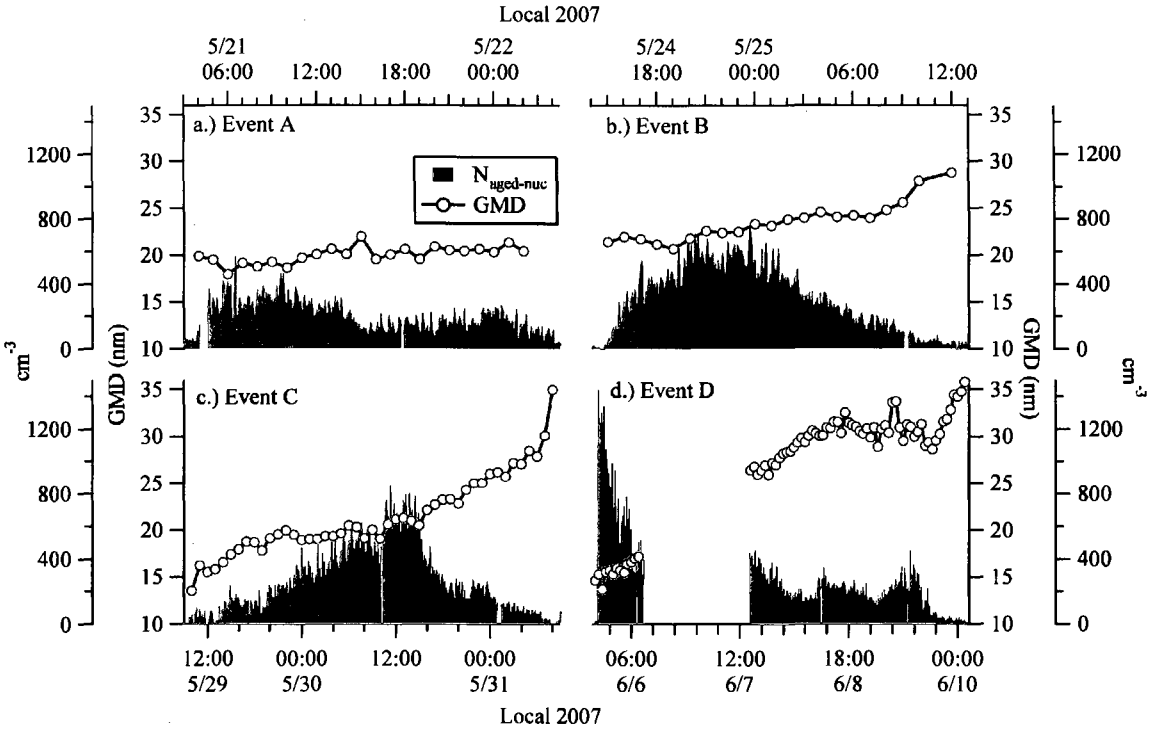

Figure V.4. $N_{aged\text{-}nuc}$ and GMD during event A (a.), event B (b.), event C (c.), and event D (d.). Note that the time scales for each panel are different.

Event B

Event B occurred on 24 May. $N_{aged\text{-}nuc}$ initially increased from near zero to a maximum of 759 cm^{-3} near midnight local time (Figure V.4b), making event B primarily a nighttime event. Again, no correlated increases in N_{Aitken} or N_{accum} were observed (Figure V.2). The temperature and wind direction profiles were nearly identical to those observed during event A. Wind direction drifted slowly from east to southeast during the event, only varying 72° (Table V.1) throughout. The event-average O_3 concentration (51.9 ppbv) was below the campaign average, and the mixing ratio decreased by 3 ppbv over the course of the event. Event-average NO concentrations were larger than the campaign average and followed the temperature trend during the evening/night hours (a minimum at 0300 LT).

While the event lasted a relatively short time (less than 24-hours), GMD monotonically increased throughout from 21.4 to 28.8 nm (GR_{obs} = 0.297 nm hr^{-1}, Figure V.4b). With a decreased average H_2SO_4 concentration (1.14×10^6 molec cm^{-3}) relative to the campaign average, the calculated average GR_{H2SO4} during the event was 0.047 nm hr^{-1}. This value is a small fraction (16%) of GR_{obs} during the event, and no correlation (r = -0.06) between GR_{obs} and GR_{H2SO4} was observed. Regression analysis between GR_{obs} and meteorological and gas-phase variables (Figure V.5) yielded several significant relationships. Positive correlations were found between GR_{obs} and temperature (r=0.78), RH (r=0.57), $SA_{pre\text{-}exist}$ (r=0.71), and O_3 (r=0.85). A negative correlation was found between GR_{obs} and temperature gradient. GR_{obs} and H_2SO_4 were not well correlated (r=0.29).

Event C

Event C occurred on 29 May and was sustained for almost 24 hours. Aged-nucleation mode aerosol was first observed at 1000 LT at a GMD of 13.5 nm (Figure V.4c). $N_{aged\text{-}nuc}$ reached a maximum at 1200 LT on 30 May at a GMD of 21 nm, at which time $N_{aged\text{-}nuc}$ started to decrease to near zero cm^{-3} by 0700 LT on 31 May. GMD at this time reaches a maximum of 35 nm. Contrary to the previously discussed events, event C is longer-lasting, and GMD does not increase linearly throughout, with an apparent slowing of growth from 0000 LT until 1100 LT on 30 May. Calculated 4-hr GR_{obs} values ranged from 0.878 nm hr^{-1} at 1700 LT on 30 May to -0.335 nm hr^{-1} at 2300 LT on 29 May (Figure V.4c). It is clear that growth occurs both at night (31 May) and during the daytime (1200 LT to 1800 LT on 29 May). An average GR_{obs} of 0.265 nm hr^{-1} and a total change in GMD of 21.5 nm were observed (Table V.1 and Figure V.4c).

Wind direction is much more variable during this period compared to events A and B (Table V.1). The highly variable wind direction for nearly 24 hours starting after 1000 LT on 30 May had little effect on the linear increase in GMD during that time. Wind speed was also variable and consistently greater than 3 m s^{-1} during the event. Event-average temperature (-21.4°C, Table V.1) was warmer than during previous events but still below the campaign average. Event-average O_3 and NO concentrations were at and below the campaign average, respectively.

Like during event B, decreased average H_2SO_4 concentration (1.15×10^6 molec cm^{-3}) relative to the campaign average resulted in a calculated GR_{H2SO4} (0.051 nm hr^{-1}) that was well below GR_{obs} (Table V.1). Contrary to results from event B, a statistically significant positive correlation (r = 0.53) between GR_{obs} and GR_{H2SO4} was observed. Regression analysis between GR_{obs} and meteorological and gas-phase variables (Figure V.5) yielded significant positive correlations between GR_{obs} and temperature (r=0.42), j_{NO2} (r=0.41), and NO (r=0.61) and negative correlations between GR_{obs} and temperature gradient (r=-0.61) and O_3 (r=-0.65). GR_{obs} and H_2SO_4 were again not well correlated (r=0.24).

Event D

Event D occurred on 5 June and was the longest-lasting event during the campaign. The maximum $N_{aged\text{-}nuc}$ during the event (nearly 1500 cm^{-3} at 2000 LT on 5 June) was the largest of the campaign (Figures V.2 and V.4d) and occurred coincident with the smallest GMD during the event (13.7 nm). GMD increased from this time until 1800 LT on 8 June at a GMD of 33 nm, at which point a period of stagnant growth was observed when GMD decreased to 29 nm at 1800 LT on 9 June (Figure V.4d). GMD

increased very quickly for 8 hrs following this period, from 29 to 36 nm. An average GR_{obs} of 0.183 nm hr^{-1} and a total change in GMD of 21.1 nm were observed (Table V.1 and Figure V.4d), although, clearly there was great variability in GR_{obs} values during the event. The largest 4-hr GR_{obs} during event D was 0.963 nm hr^{-1} at 1900 LT on 9 June and the smallest was -0.482 nm hr^{-1} at 1900 LT on 8 June (Figure V.4d).

Wind direction during event D was fairly constant except during a prolonged period of polluted, camp air from the northerly direction (0900 LT on 6 June through 1500 LT on 7 June). As discussed in Section 2.3.1, potentially contaminated data during this period were discarded. The wind direction for non-dirty-sector data varied from 200° to 350° during the event. Wind speeds were slow and reasonably constant, between 3 and 10 m s^{-1} during the event. The event-average temperature (-14.9°C, Table V.1) was much warmer than that in previous events, with maximum daytime temperature on 8 June and 9 June reaching -11°C and -9°C, respectively. The event-average O_3 concentration was considerably smaller than the campaign average, although the event-average NO concentration was identical to the campaign average. Event-average RH was distinctly higher than the campaign average, while $SA_{pre\text{-}exist}$ was distinctly smaller than during all other events (Table V.1).

The average H_2SO_4 concentration during event D (1.39×10^6 molec cm^{-3}, Table V.1) was similar to that in events B and C and the campaign average, and like during the previous two events, the average calculated GR_{H2SO4} (0.043 nm hr^{-1}) was much smaller than the average GR_{obs} (0.183 nm hr^{-1}). No correlation (r = 0.13) between GR_{obs} and GR_{H2SO4} was observed. Regression analysis between GR_{obs} and meteorological and gas-

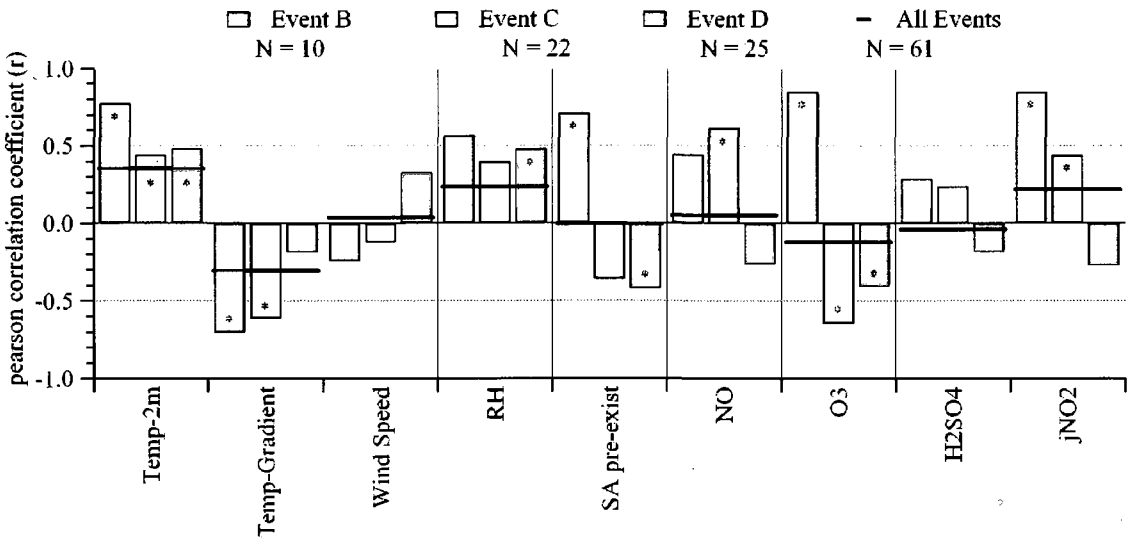

Figure V.5. Pearson correlation coefficients from linear regression analysis of 4-hr GR_{obs} and observed variables. Only data associated with both a positive value for GR_{obs} and GR_{obs} resulting from a linear regression (between GMD and time) with an r-value greater than 0.5 were used. The number of datapoints (N) used in each analysis is noted. No analysis was done for event A due to limited data (N=4). The r-values statistically different from zero (confidence level > 0.95) are marked with an asterisk. For all event data, only the GR_{obs} correlations with temperature and temperature gradient were significantly different from zero.

phase variables (Figure V.5) yielded significant positive correlations with temperature (r=0.48) and RH (r=0.48) similar to previous events. Less significant negative correlations were found between GR_{obs} and O_3 (r=-0.41) and $SA_{pre\text{-}exist}$ (r=-0.42). Again, GR_{obs} and H_2SO_4 were not well correlated (r=-0.19).

Discussion

The average number-based size distribution observed at Summit was dominated by aged-nucleation- and Aitken-mode particles, primarily with $D_p < 50$ nm (Figure V.3). While the good correlation between aerosol number concentrations measured using independent instrumentation (N_{CPC} and N_{SMPS}) indicates acceptable instrument

performance, the difference between average N_{CPC} and N_{SMPS} of 103 cm^{-3} and the truncated size distribution in Figure V.3 suggest that aerosol larger than D_p=198 nm is also important at Summit.

There was no evidence for local new particle formation at Summit during the campaign since N_{nuc} was zero throughout. Of the four instances presented here that were marked by enhanced $N_{aged\text{-}nuc}$, three (events B, C, and D) showed evidence of significant particle growth. In the case of events C and D, this growth was long-lasting, was initiated at $D_p < 15$ nm, and continued until particles were nearly 40 nm in diameter. The long duration of events C and D coupled with non-zero wind speeds (Table V.1) suggest that these events likely span a very large geographic area. For example, using an average wind speed of 5 m s^{-1}, a parcel of air could travel approximately 400 and 2000 km in 1 and 5 days, respectively, which represents an upper-limit approximation of the spatial extent of the observed growth events. The true spatial extent of growth events is likely smaller due to non-straight-line air mass trajectories and due to a possible dependence on air-snow interaction.

Very few previous studies have documented aerosol growth from extremely remote locations. One aerosol growth event has been documented at the South Pole (Park et al., 2004), a similarly remote site. A growth rate of 0.13 nm hr^{-1} was observed at South Pole, similar in magnitude to the growth events described here, although that event involved much smaller aerosol (approximately 3-nm diameter) and was observed for a much shorter duration (several hours). Not unexpectedly, the GR_{obs} values from Summit (on the order of 0.2 nm hr^{-1}) are smaller than those observed at mid-latitude sites, with a range of 1-20 nm hr^{-1} (Kulmala et al., 2004), a difference presumably due to site

proximity to sources of condensable species. Compared to mid-latitude sites, the colder temperatures found at Summit may help to offset the lack of condensable gases due to the inverse relationship between temperature and vapor pressure.

The size distribution observed at Summit and the prevalence of a strong aged-nucleation/Aitken mode in the Arctic are not unprecedented. Ström et al. (2003) reported a similar summertime number-size distribution from one month of observations at Zeppelin Station on Svalbard. This site is a similar remote, Arctic site that is considerably lower in elevation (474 m asl) than Summit. Long-term observations at Zeppelin Station from Engvall et al. (2008) confirm the prevalence of the small-particle mode, along with the distinct presence of an Aitken mode, a distribution qualitatively similar to that observed at Summit.

The source of the small particles in the Arctic summer is presently not well understood. The oxidation of dimethylsulfide (DMS), which is emitted from open ocean surfaces or released after being trapped under sea-ice, has long been used to explain Aitken-mode aerosol in the Arctic. DMS is oxidized to H_2SO_4 which partitions to the aerosol phase through nucleation and condensation (Bates et al., 1998; Ferek et al., 1995). Summertime new particle formation from H_2SO_4 is facilitated by decreased accumulation-mode aerosol (and thus $SA_{pre\text{-}exist}$) and increased oxidation rates. Direct emission of biologically derived aerosol in the form of fragmented microorganisms and bacteria (Leck and Bigg, 2005a; Leck and Bigg, 2005b) or of organic surfactants associated with sea spray (Martensson et al., 2003) also has been proposed as a source of sub-100-nm aerosol in the Arctic summer. Recent modeling suggests that H_2SO_4 is the more likely source based on an unrealistically high flux of sea-borne aerosol necessary to

support observed Aitken-mode particle concentrations at Zeppelin Station (Korhonen et al., 2008). The observations presented here do not directly support or refute any of the previously discussed source hypotheses, and the source of aged-nucleation mode aerosol at Summit is unknown.

The particle growth measured at ground level at Summit suggests that the snowpack may play a role in aerosol dynamics. The regression analysis discussed above (Figure V.5) provides no evidence for particle growth due to H_2SO_4 condensation since GR_{obs} shows no correlation with measured H_2SO_4 concentrations. Additionally, calculated GR_{H2SO4} values are significantly smaller than GR_{obs} during 3 of the 4 growth events observed, making the possibility that H_2SO_4 is the major condensing species very unlikely. Only during event A did H_2SO_4 likely contribute a large fraction of the condensable mass, and this event was marked by a much smaller GR_{obs} compared to all other events.

Particle growth events occurred during days of above- (event D) and below-average (events A, B, and C) temperature, although correlation analysis yielded a positive relationship between GR_{obs} and surface temperature for all events. This suggests that a mechanism more complicated than simple temperature-dependent condensation, which would conceivably yield a negative correlation between GR_{obs} and temperature, was important during events. The overall colder temperatures found at Summit compared to lower-latitude sites may still influence semi-volatile partitioning, but this analysis implies that temperature was not a limiting factor for condensation of precursor compounds. Similarly, events were observed during days of above- (event D) and below-average (events A, B, and C) RH, and GR_{obs} was also positively correlated with RH for all events.

Wind direction was not consistent during all events (Table V.1). Particle growth occurred on days of below- (event D) and above-average (events A, B, and C) aerosol surface area (SA) and both positive (event B) and negative (events C and D) relationships with GR_{obs} were observed.

The positive correlation between GR_{obs} and NO during events B and C (Table V.1) suggests the predominance of a local, photochemical source of condensable species during these events. NO is produced at Summit from the photolysis of nitric acid (HNO_3) in the snowpack (Honrath et al., 1999). Although NO is not likely a participant in particle growth, it can be thought of as a surrogate for other compounds, potentially including organics, that are photochemically produced at or beneath the snow surface. FLEXPART (Stohl, 2006) emission footprints (interpreted as backward trajectories) initiated at the end of events B and C support the potential snowpack source, as these air parcels reside over Greenland for greater than 2 and 3 days, respectively. These residence times are similar to the duration of events B and C, and thus the air mass arriving at Summit at the end of events B and C could have been interacting with the snowpack during all of the observed particle growth. Conversely, the lack of a significant correlation between GR_{obs} and NO suggests that snowpack emissions may be less important during event D. The residence time over Greenland based on FLEXPART emission footprints initiated at the end of event D was approximately one-day, meaning that snowpack emissions alone could not explain continuous growth during Event D.

Significant concentrations of organic compounds have been measured in the snowpack at Summit. Snow-pit sampling of water-soluble organic carbon (WSOC) (Hagler et al., 2007b), irradiation experiments (Grannas et al., 2004), and gradient

measurements of WSOC (Anderson et al., 2008) and monocarboxylic acids (Dibb and Arsenault, 2002) all suggest that the organic compounds originally deposited to the snow are subject to post-depositional processing. For example, Anderson et al. (2008) report gas-phase WSOC concentrations in the firn that are more than a factor of ten larger than concentrations above the snowpack, suggesting that the snow surface was a source of gas-phase WSOC to the atmosphere. By concurrently measuring WSOC in the gas- and aerosol-phases, Anderson et al. (2008) show that temperature-driven, gas-to-particle conversion occurred on several occasions at Summit. This, coupled with GR_{obs}/NO correlations and FLEXPART residence times, suggests that organic compounds are emitted from the snowpack and may contribute to particle growth during events B and C, and partially during event D.

The organic compounds deposited to the snowpack likely are transported great distances to Summit. Vascular-plant-derived compounds identified by Grannas et al. (2004) implicate long-range transport from mid-latitude locations as the source of at least a fraction of the organic compounds in Summit snow. Transported biomass burning emissions are also a likely important source (Dibb et al., 1996) of snow-phase organic compounds.

Average or below-average O_3 concentrations in Table V.1 suggest that particle growth events are not due to direct transport from the upper atmosphere. Helmig et al. (2007) showed that O_3 enhancements (> 60 ppbv) observed in the summer of 2002 were more likely due to down-mixing from the upper troposphere/lower stratosphere and less likely due to influence of continental pollution sources. The negative correlation between GR_{obs} and O_3 during events C and D suggests that the source of condensable species

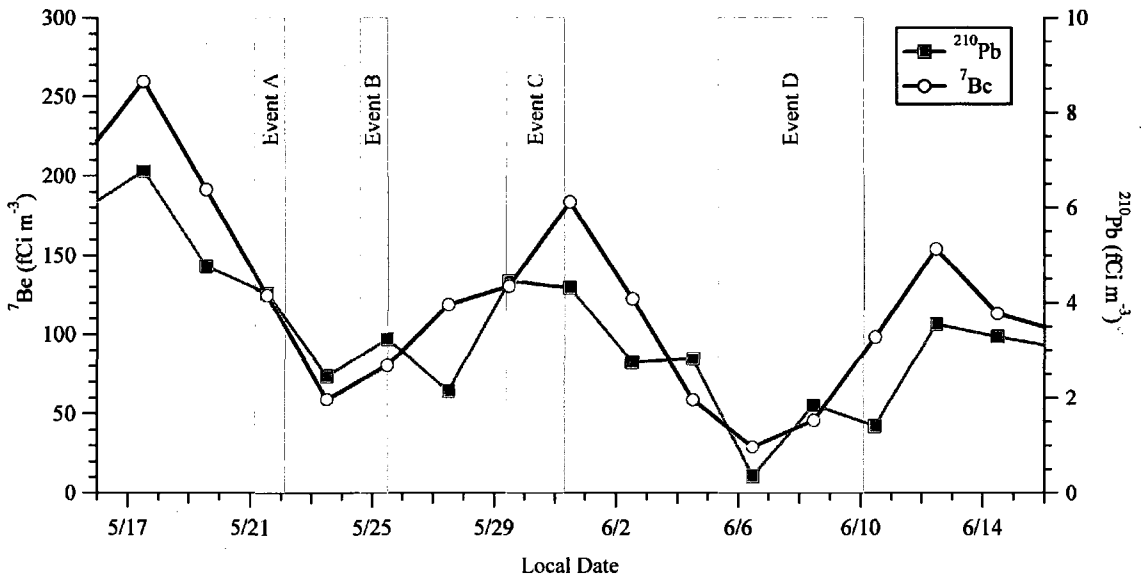

Figure V.6. ^{7}Be and ^{210}Pb activity from bulk filter aerosol sampling in summer 2007. Events are denoted by gray areas

during growth events is not vertical transport. However, the consistent negative correlation between observed GR_{obs} and temperature gradient (Figure V.5) suggests that some atmospheric mixing is important during events. If snowpack emissions were involved in particle growth, some daytime mixing would be necessary for surface ventilation (Cohen et al., 2007).

Aerosol-phase ^{7}Be and ^{210}Pb activities presented in Figure V.6 suggest that growth events are observed during periods of enhanced and depressed vertical mixing. Despite the fact that ^{7}Be and ^{210}Pb have different sources, in the stratosphere and in the continental boundary layer, respectively, both show similar trends on short-timescales. This coincident behavior is clear in Figure V.6, is highly characteristic of the Summit atmosphere, and is controlled by boundary layer dynamics, where increased vertical mixing enhances both ^{7}Be and ^{210}Pb activities near the surface (Dibb, 2007). Conversely, stable surface conditions promote depositional loss and decreased ^{7}Be and ^{210}Pb

activities. Event D is most distinctly associated with depleted ^{7}Be and ^{210}Pb (Figure V.6) and thus depressed mixing from aloft. This is consistent with the negative correlation with O_3 during the event and poor correlation of GR_{obs} and temperature gradient. The relative maximum in ^{7}Be and ^{210}Pb activity that occurred on 31 May during event C suggests that during this event vertical mixing was more prevalent. The significant negative correlation between GR_{obs} and temperature gradient also suggests that vertical mixing is important during event C. It is important to note that because ^{7}Be and ^{210}Pb activities are derived from 48-hour-integrated filter sampling (compared to variations in GMD at one-hour time resolution) the results shown here are only qualitatively suggestive of the mixing state of the Summit boundary layer.

Conclusions

Particle growth observed during events B, C, and D, those that could not be explained by H_2SO_4 condensation, was likely due to condensation of organic material. The source of condensing organic compounds is not clear, although snowpack emission following long-range transport and surface deposition seems viable. The snowpack is a currently an unexplored source of secondary organic aerosol mass.

Unfortunately, the extremely low mass concentrations of aged-nucleation-mode aerosol at Summit make obtaining chemical information difficult, and more sensitive, high-time-resolution observations are needed in the future. Identification of the chemical composition of ultrafine aerosol during growth events would not only aid in understanding the source of condensable mass, but also the source of 10-20 nm particles prior to growth. The role of vertical transport is also unclear, as correlation analysis and

activities of ^{7}Be and ^{210}Pb suggest that growth events are observed during both suppression and enhancement of vertical mixing. An anti-correlation between GR_{obs} and temperature gradient indicates that some surface mixing, at least up to the 10-m height of temperature measurement, is necessary to promote particle growth. Summit, and presumably other remote Arctic sites, may be unique in this regard compared to the Antarctic. Reduced daytime surface heating at South Pole (compared to Summit) results in less efficient surface ventilation (Cohen et al., 2007). Based on results presented here, this scenario may retard the potential for surface-mediated particle growth. New particle formation has been observed at South Pole based on observation of nucleation-mode aerosol (Park et al., 2004), but no such nucleation was observed at Summit. Thus, while the conditions at Summit seem more conducive to growth of ultrafine aerosol than at South Pole, transport of newly formed particles prior to interaction with the Summit snowpack is a necessary precursor to growth.

The climate effects of particle growth events described here are unknown although the increases in GMD undoubtedly increase the potential for CCN activation. The highly-water-soluble composition of Summit aerosol (Hagler et al., 2007b) likely increases CCN activity. Thus, whether particles actually affect cloud droplet formation still depends on updraft velocity and water supersaturation. The particle growth events reported here may provide a link between long-range transport of pollutants, deposition to the snowpack, and climate feedbacks in remote, pristine environments. This system may be of global significance given the large spatial extent of snow-coverage on Earth.

References

Alam, A., Shi, J.P., and Harrison, R.M., 2003. Observations of new particle formation in urban air. Journal of Geophysical Research 108, doi:10.1029/2001JD001417.

Anderson, C.H., Dibb, J.E., Griffin, R.J., Hagler, G.S.W., and Bergin, M.H., 2008. Atmospheric water-soluble organic carbon measurements at Summit, Greenland. Atmospheric Environment 42, 5612-5621.

Bates, T.S., Kapustin, V.N., Quinn, P.K., Covert, D.S., Coffman, D.J., Mari, C., Durkee, P.A., De Bruyn, W.J., and Saltzmann, E.S., 1998. Processes controlling the distribution of aerosol particles in the lower marine boundary layer during the first Aerosol Characterization Experiment (ACE 1). Journal of Geophysical Research 103, 16369-16383.

Birmili, W., Wiedensohler, A., Heintzenberg, J., and Lehmann, K., 2001. Atmospheric particle number size distribution in central Europe: Statistical relations to air masses and meteorology. Journal of Geophysical Research 23, 32005-32018.

Cohen, L., Helmig, D., Neff, W.D., Grachev, A.A., and Fairall, C.W., 2007. Boundary-layer dynamics and its influence on atmospheric chemistry at Summit, Greenland. Atmospheric Environment 41, 5044-5060.

Curry, J. A., 1995. Interactions among aerosols, clouds, and climate of the Arctic Ocean. The Science of the Total Environment 160/161, 777-791.

Dibb, J.E., 2007. Vertical mixing above Summit, Greenland: Insights into seasonal and high frequency variability from the radionuclide tracers Be-7 and Pb-210. Atmospheric Environment 24, 5020-5030.

Dibb, J.E. and Arsenault, M., 2002. Shouldn't the snowpacks be a sources of □onocarboxylic acids? Atmospheric Environment 36, 2513-2522.

Dibb, J.E., Talbot, R.W., Whitlow, S.I., Shipham, M.C., Winterle, J., McConnell, J., and Bales, R., 1996. Biomass burning signatures in the atmosphere and snow at Summit, Greenland: An event on 5 August 1994. Atmospheric Environment 30, 533-561.

Dusek, U., Frank, G.P., Hildebrandt, L., Curtius, J., Schneider, J., Walter, S., Chand, D., Drewnick, F., Hings, S., Borrmann, S., and Andreae, M.O., 2006. Size matters more than chemistry for cloud-nucleating ability of aerosol particles. Science, 312, 1375-1378.

Engvall, A.-C., Krejci, R., Treffeisen, R., Scheele, R., Hermansen, O., and Paatero, J., 2008. Changes in aerosol properties during spring-summer period in the Arctic troposphere. Atmospheric Chemistry and Physics 8, 445-462.

Ferek, R.J., Hobbs, P.V., Radke, L.F., Herring, J.A., Sturges, W.T., and Cota, G.F., 1995. Dimthyl sulfide in the Arctic atmosphere. Journal of Geophysical Research 100, 26093-26104.

Garrett, T.J., Zhao, C., Dong, X., Mace, G.G., and Hobbs, P.V., 2004. Effects of varying aerosol regimes on low-level Arctic stratus. Geophysical Research Letters 31, doi:10.1029/2004GL019928.

Grannas, A.M., Shepson, P.B., and Filley, T.R., 2004. Photochemistry and nature of organic matter in Arctic and Antarctic snow. Global Biogeochemical Cycles 18, doi:10.1029/2003GB002133.

Hagler, G.S.W., Bergin, M.H., Smith, E.A., and Dibb, J.E., 2007a. A summer time series of particulate carbon in the air and snow at Summit, Greenland. Journal of Geophysical Research 112, doi:10.1029/2007JD008993.

Hagler, G.S.W., Bergin, M.H., Smith, E.A., Dibb, J.E., Anderson, C., and Steig, E.J., 2007b. Particulate and water-soluble carbon measured in recent snow at Summit, Greenland. Geophysical Research Letters 34, doi:10.1029/2007GL030110.

Hagler, G.S.W., Bergin, M.H., Smith, E.A., Town, M., and Dibb, J.E., 2008. Local anthropogenic impact on particulate elemental carbon concentrations at Summit, Greenland. Atmospheric Chemistry and Physics 8, 2485-2491.

Held, A., Nowak, A., Birmili, W., Wiedensohler, A., Forkel, R., and Klemm, O., 2004. Observations of particle formation and growth in a mountainous forest region in central Europe. Journal of Geophysical Research 109, doi:10.1029/2004JD005346.

Helmig, D., Oltmans, S.J., Morse, T.O., and Dibb, J.E., 2007. What is causing high ozone at Summit, Greenland? Atmospheric Environment 41, 5031-5043.

Honrath, R.E., Peterson, M.C., Guo, S., Dibb, J.E., Shepson, P.B., and Campbell, B., 1999. Evidence of NO_X production within or upon ice particles in the Greenland snowpack. Geophysical Research Letters 26, 695-698.

Kerminen, V.M., Lihavainen, H., Komppula, M., Viisanen, Y., and Kulmala, M., 2005. Direct observational evidence linking atmospheric aerosol formation and cloud droplet activation. Geophysical Research Letters 32, doi:10.1029/2005GL023130.

Korhonen, H., Carslaw, K.S., Spracklen, D.V., Ridley, D.A., and Ström, J., 2008. A global model study of processes controlling aerosol size distributions in the Arctic spring and summer. Journal of Geophysical Research 113, doi:10.1029/2007JD009114.

Kulmala, M., Dal Maso, M., Makela, J.M., Pirjola, L., Vakeva, M., Aalto, P., Miikkulainen, P., Hameri, K., and O'Dowd, C.D., 2001. On the formation, growth, and composition of nucleation mode particles. Tellus 53B, 479-490.

Kulmala, M., Vehkamäki, H., Petäjä, T., Dal Maso, M., Lauri, A., Kerminen, V.M., Birmili, W., and McMurry, P.H., 2004. Formation and growth rates of ultrafine atmospheric particles: a review of observations. Journal of Aerosol Science 35, 143-176.

Leck, C. and Bigg, E.K., 2005a. Source and evolution of the marine aerosol – A new perspective. Geophysical Research Letters 32, doi:10.1029/2005GL023651.

Leck, C. and Bigg, E.K., 2005b. Biogenic particles in the surface microlayer and overlaying atmosphere in the central Arctic Ocean during summer. Tellus 57B, 305-316.

Mäkelä, J.M., Koponen, I.K., Aalto, P., and Kulmala, M., 2000. One-year data of submicron size modes of tropospheric background aerosol in southern Finland. Journal of Aerosol Science 31, 595-611.

Martensson, E.M., Nilsson, E.D., de Leeuw, G., Cohen, L.H., and Hansson, H.-C., 2003. Laboratory simulations and parameterization of the primary marine aerosol production. Journal of Geophysical Research 108, doi:10.1029/2002JD002263.

Massman, W.J.. 1998. A review of the molecular diffusivities of H_2O, CO_2, CH_4, CO, O_3, SO_2, NH_3, N_2O, NO, and NO_2 in air, O_2 and N_2 near STP. Atmospheric Environment, 32, 1111-1127.

Oberdörster, G., 2000. Toxicology of ultrafine particles: in vivo studies. Philosphical Transactions of the Royal Society of London 358, 2719-2740.

O'Dowd, C.D., Jimenez, J.L., Bahreini, R., Flagan, R.C., Seinfeld, J.H., Hameri, K., Pirjola, L., Kulmala, M., Jennings, S.G., and Hoffmann, T., 2002. Marine aerosol formation from biogenic iodine emissions. Nature 417, 632-636.

Park, J., Sakurai, H., Vollmers, K., and McMurry, P.H., 2004. Aerosol size distributions measured at the South Pole during ISCAT. Atmospheric Environment 38, 5493-5500.

Quinn, P.K., Shaw, G., Andrews, E., Dutton, E.G., Ruoho-Airola, T., and Gong, S.L., 2007. Arctic haze: current trends and knowledge gaps. Tellus 59B, 99-114.

Sjostedt, S.J., Huey, L.G., Tanner, D.J., Peischl, J., Chen, G., Dibb, J.E., Lefer, B., Hutterli, M.A., Beyersdorf, A.J., Blake, N.J., Blake, D.R., Sueper, D., Ryerson, T., Burkhart, J., and Stohl, A., 2007. Observations of hydroxyl and sum of

peroxy radicals at Summit, Greenland during summer 2003. Atmospheric Environment 24, 5122-5137.

Stohl, A., 2006. Characteristics of atmospheric transport into the Arctic troposphere. Journal of Geophysical Research 111, doi:10.1029/2005JD006888.

Ström, J., Umegard, J., Tørseth, K., Tunved, P., Hansson, H.-C., Holmén, K., Wismann, V., Herber, A., and König-Langlo, G., 2003. One year of particle size distributions and aerosol chemical composition measurements at the Zeppelin Station, Svalbard, March 2000-2001. Physics and Chemistry of the Earth 28, 1181-1190.

Vehkamäki, H., Dal Maso, M., Hussein, T., Flagagan, R., Hyvarinen, A., Lauros, J., Merikanto, J., Monkkonen, P., Pihlatie, M., Salminen, K., Sogacheva, L., Thurm, T., Ruuskanen, T.M., Keronen, P., Aalto, P.P., Hari, P., Lehtinen, K.E.J., Rannik, U., and Kulmala, M., 2004. Atmospheric particle formation events at Varrio measurement station in Finnish Lapland 1998-2002. Atmospheric Chemistry and Physics 4, 2015-2023.

Weber, R.J., Orsini, D., Wang, B., Scheuer, E., Talbot, R.W., Dibb, J.E., Seid, G.K., DeBell, L., Mauldin, R.L., Kosciuch, C., Cantrell, C., and Eisele, F., 2003. New particle formation in anthropogenic plumes advecting from Asia observed during TRACE-P. Journal of Geophysical Research 108, doi:10.1029/2002JD003112.

Winklmayr, W., Reischl, G. P., Lindner, A. O., and Berner, A., 1991. A new electromobility spectrometer for the measurement of aerosol size distributions in the size range from 1 to 1000 nm. Journal of Aerosol Science 22, 289-296.

Young, L.-H., Benson, D.R., Montanaro, W.M., Lee, S.-H., Pan, L.L., Rogers, D.C., Jensen, J., Stith, J.L., Davis, C.A., Campos, T.L., Bowman, K.P., Cooper, W.A., and Lait, L.R., 2007 Enhanced new particle formation observed in the northern midlatitude tropopause region. Journal of Geophysical Research 112, doi:10.1029/2006JD008109.

CHAPTER VI

CONCLUDING REMARKS

Conclusions

Organic aerosols constitute a large fraction of ambient aerosol mass. The size distribution and chemical composition of OA varies with location and is indicative of formation processes and suggestive of climate and human health effects. In Chapter II of this work, which focuses on ambient measurements in a suburban, forested atmosphere, mass spectral analysis revealed the importance of both regionally- and locally-produced sub-micron OA, with a minor influence from combustion processes. Direct SOA formation was observed at this site as manifested by observation of aerosol geometric growth and coincident increases in OA mass.

Further chemical analysis of OA is presented in Chapter III at coastal sites in New England. Organic mass occurred in accumulation, droplet, and coarse aerosol size modes and a significant fraction of that mass was water-soluble. Oxalic acid was a major component of WSOC and was likely produced mainly by aqueous reactions in cloud and fog droplets. Limited HNMR results suggested that all accumulation- and droplet-mode WSOC resembled SOA. At IOS, coarse-mode WSOC also resembled SOA suggesting that the WSOC thought to be emitted from the ocean in sea-salt aerosol likely undergoes some atmospheric processing. The coarse-mode WSOC at TF on the other hand had a distinct HNMR fingerprint suggesting the prevalence an additional aerosol source. Coupling the limited speciation and HNMR analyses, a large fraction of WSOC,

concentrated in the droplet mode but occurring in all sub-10-micron aerosol, was unresolved and had characteristics of atmospheric HULIS.

Chapter IV presents mass-spectral measurements in the highly polluted Houston, TX, atmosphere showing that OA was responsible for large increases in aerosol SA during several early mornings, due mainly to mobile source emissions. During these events, significant depletion of gas-phase HNO_3 was observed coincident with increases in gas-phase HONO. Linear regression and mole-balance analysis suggested that the dominant HONO source was HNO_3, not previously identified reaction mechanisms. Correlations with SA coupled with changes in OA mass spectra suggest that POA, and likely specific PAH compounds, contribute to HNO_3-to-HONO conversion through a heterogeneous mechanism.

Lastly, Chapter V presents several events of clear particle growth due to evolution of aerosol GMD. While no aerosol chemical composition information is available, calculations using measured mixing ratios suggested that only a small fraction of observed growth could only be attributed H_2SO_4. Growth was likely due to condensation of organic compounds, the origin of which is unknown. Linear regression analysis showed that surface mixing likely played a role in the observation of growth events and that snowpack emissions were also important.

Recommendations for Future Research

Recommendations for future research are summarized below and are presented with respect to each independent chapter.

Chapter II

Understanding the mixing state of ambient aerosol is important in understanding aerosol growth processes and heterogeneous chemistry. By evaluating the chemically-resolved evolution of GMD coupled with changes in size-resolved aerosol mass concentrations, a clear picture of aerosol condensational growth is revealed. This is a unique analysis and should be applied to other AMS datasets, especially when deployed in environments with mixed pollution influence. Additionally, environments with significantly larger OA mass loadings could provide improved signal-to-noise to facilitate calculation of GMD for important m/z fragments of OA, such as m/z = 44, 43, 57, etc., and attribution of condensational growth to OOAI, OOAII, and HOA, rather than simply to OA as concluded above. From an instrumental point-of-view, collocation of an SMPS to measure number-size distributions would be necessary to confirm the calculated GMD and calculated GR determined from Q-AMS measurements. Additionally, an SMPS would confirm or refute the hypothesized new particle formation that presumably occurred prior to each of the reported events.

Chapter III

The supposition that HULIS contributes a majority of $[H\text{-}C\text{-}C{=}O]_{unresolved}$ mass due to discrepancies between IC and HNMR analysis is not quantitative but is only an indication that a large fraction of WSOC is chemically unknown and has a source similar to that of LMWCA. A more quantitative determination of HULIS may have been possible had an internal standard been employed for HNMR analysis. This is necessary for future analysis, but would likely only confirm a large discrepancy between LMWCA and the [H-C-C=O] fraction. Additional analyses have been employed on bulk aerosol to

identify HULIS, and these could be used on size-segregated samples to understand source pathways. To determine if the coarse-mode WSOC at IOS is SOA or aged POA associated with sea salt, HNMR analysis of seawater, or of pure sea salt aerosol, is necessary to establish a fingerprint for primary marine emissions. Overall, analyses for this work were limited by mass and by sample number. Thus, sampling for longer durations and accumulating more samples will only help to establish the particle size dependence of HNMR fingerprints and of oxalate and its precursors in order to better understand sources.

Chapter IV

Laboratory work is necessary to confirm the hypothesized heterogenous HONO formation pathway. The observation of HNO_3 depletion and HONO formation on POA surrogate surfaces would confirm the mechanism. However a lack of HONO formation would not necessarily refute the proposed pathway as the POA observed in Houston, TX was likely a highly complex mixture of organic constituents with chemical characteristics that surrogate species may not be able to mimic. In-situ mixing of HNO_3 with ambient POA aerosol may be necessary to replicate accurately atmospheric conditions and confirm the heterogenous HONO formation described here. If confirmed, reaction yields as a function of ambient conditions and aerosol chemical composition are needed to represent correctly HONO formation in models.

Chapter V

Many questions are yet to be answered regarding the growth events reported at Summit, not the least of which is the source of aged-nucleation-mode aerosol. The sub-40-nm D_P and extremely low associated mass precludes AMS measurements from

identifying the chemical composition of aerosol during growth. Microscopy and atomic analysis techniques have been used previously to identify bacterial and viral fragments and elemental constituents in single particles, and these techniques could be used at Summit to identify the source of aged-nucleation-mode aerosol. Detailed meteorological measurements, especially extending vertically, would facilitate a better understanding of potential transport of precursor particles from aloft and potential precursor gases from the snowpack. Measurements of particle number size distributions and potential precursor gases (speciated carboxylic acids or total gas-phase WSOC).at the snow surface and above it may elucidate the source of growth events.

CHPATER VII

COMPLETE LIST OF REFERENCES

Aggarwal, S.G. and Kawamura, K., 2008. Molecular distributions and stable carbon isotope compositions of dicarboxylic acids and related compounds in aerosols from Sapporo, Japan: Implications for photochemical aging during long-range transport. Journal of Geophysical Research 113, doi:10.1029/2007JD009365.

Alam, A., Shi, J.P., and Harrison, R.M., 2003. Observations of new particle formation in urban air. Journal of Geophysical Research 108, doi:10.1029/2001JD001417.

Alfarra, M.R., et al., 2004. Characterization of urban and rural organic particulate in the Lower Fraser Valley using two Aerodyne aerosol mass spectrometers. Atmospheric Environment 38 (34), 5745-5758.

Alicke, B., Geyer, A., Hofzumahaus, A., Holland, F., Konrad, S., Patz, H.W., Schafer, J., Stutz, J., Voltz-Thomas, A., and Platt, U., 2003. OH formation by HONO photolysis during the Berlioz experiment. Journal of Geophysical Research-Atmospheres 108, doi:10.1029/2001JD000579.

Allan, J.D., Alfarra, M.R., Bower, K.N., Coe, H., Jayne, J.T., Worsnop, D.R., Aalto, P.P., Kulmala, M., Hyötyläinen, T., Cavalli, F., and Laaksonen, A., 2006. Size and composition measurements of background aerosol and new particle growth in a Finnish forest during QUEST 2 using an Aerodyne Aerosol Mass Spectrometer. Atmospheric Chemistry and Physics 6, 315-327.

Allan, J.D., Delia, A.E., Coe, H., Bower, K.N., Alfarra, M.R., Jimenez, J.L., Middlebrook, A.M., Drewnick, F., Onasch, T.B., Canagaratna, M.R., Jayne, J.T., and Worsnop, D.R., 2004. A generalized method for the extraction of chemically resolved mass spectra from Aerodyne aerosol mass spectrometer data. Journal of Aerosol Science 35, 909-922.

Allan, J. D., Jimenez, J.L., Williams, P.I., Alfarra, M.R., Bower, K.N., Jayne, J.T., Coe, H., and Worsnop, D.R., 2003. Quantitative sampling using an Aerodyne aerosol mass spectrometer – 1. Techniques of data interpretation and error analysis. Journal of Geophysical Research 108, doi:10.1029/2002JD002358.

Ammann, M., Kalberer, M., Jost, D.T., Tobler, L., Rossler, E., Piguet, D., Gaggeler, H.W., Baltensperger, U., 1998. Heterogeneous production of nitrous acid on soot in polluted air masses. Nature 395 (6698), 157-160.

Ammann, M., Rossler, E., Strekowski, R., George, C., 2005. Nitrogen dioxide multiphase chemistry: Uptake kinetics on aqueous solutions containing phenolic compounds. Physical Chemistry Chemical Physics 7 (12), 2513-2518.

Anderson, C.H., Dibb, J.E., Griffin, R.J., Hagler, G.S.W., and Bergin, M.H., 2008. Atmospheric water-soluble organic carbon measurements at Summit, Greenland. Atmospheric Environment 42, 5612-5621.

Arens, F., Gutzwiller, L., Baltensperger, U., Gäggeler, H.W., and Ammann, M., 2001. Heterogeneous reaction of NO2 on diesel soot particles. Environmental Science and Technology 35 (11), 2191-2199.

Bae, M.S., Schwab, J.J., Zhang, Q., Hogrefe, O., Demerjian, K.L., Weimer, S., Rhoads, K., Orsini, D., Venkatachari, P., and Hopke, P.K., 2007. Interference of organic signals in highly time resolved nitrate measurements by low mass resolution aerosol mass spectrometry. Journal of Geophysical Research-Atmospheres 112 (D22), doi:10.1029/2007JD008614.

Bahreini, R., Keywood, M.D., Ng, N.L., Varutbangkul, V., Gao, S., Flagan, R.C., Seinfeld, J.H., Worsnop, D.R., and Jimenez, J.L., 2005. Measurements of secondary organic aerosol from oxidation of cycloalkenes, terpenes, and m-xylene using an Aerodyne aerosol mass spectrometer. Environmental Science and Technology 15, 5674-5688.

Bates, T.S., Kapustin, V.N., Quinn, P.K., Covert, D.S., Coffman, D.J., Mari, C., Durkee, P.A., De Bruyn, W.J., and Saltzmann, E.S., 1998. Processes controlling the distribution of aerosol particles in the lower marine boundary layer during the first Aerosol Characterization Experiment (ACE 1). Journal of Geophysical Research 103, 16369-16383.

Birch, M.E. and Cary, R.A., 1996. Elemental carbon-based method for monitoring occupational exposures to particulate diesel exhaust, Aerosol Science and Technology 25, 221-241.

Birmili, W., and Wiedensohler, A., 2000. New particle formation in the continental boundary layer: Meteorological and gas phase parameter influence. Geophysical Research Letters 27, 3325-3328.

Birmili, W., Wiedensohler, A., Heintzenberg, J., and Lehmann, K., 2001. Atmospheric particle number size distribution in central Europe: Statistical relations to air masses and meteorology. Journal of Geophysical Research 23, 32005-32018.

Boy, M., Karl, T., Turnipseed, A., Mauldin, R.L., Kosciuch, E., Greenberg, J., Rathbone, J., Smith, J., Held, A., Barsanti, K., Wehner, B., Bauer, S., Wiedensolhler, A., Bonn, B., Kulmala, M., and Guenther, A., 2008. New particle formation in the Front Range of the Colorado Rocky Mountains. Atmospheric Chemistry and Physics 8, 1577-1590.

Burkholder, J.B., Baynard, T., Ravishankara, A.R., and Lovejoy, E.R., 2007. Particle nucleation following the O3 and OH initiated oxidation of alpha-pinene and beta-pinene between 278 and 320 K. Journal of Geophysical Research 112, doi:10.1029/JD007783.

Cahill, T.M., Seaman, V.Y., Charles, M.J., Holzinger, R., and Goldstein, A.H., 2006. Secondary organic aerosols fromed from oxidation of biogenic volatile organic compounds in the Sierra Nevada Mountains of California. Journal of Geophysical Research 111, doi:10.1029/2006JD007178.

Canagaratna, M.R., Jayne, J.T., Ghertner, D.A., Herndon, S., Shi, Q., Jimenez, J.L., Silva, P.J., Williams, P., Lanni, T., Drewnick, F., Demerjian, K.L., Kolb, C.E., and Worsnop, D.R., 2004. Chase studies of particulate emissions from in-use New York City vehicles. Aerosol Science and Technology 38 (6), 555-573.

Canagaratna, M., Jayne, J., Jimenez, J.L., Allan, J.A., Alfarra, R., Zhang, Q., Onasch, T., Drewnick, F., Coe, H., Middlebrook, A., Delia, A., Williams, L., Trimborn, A., Northway, M., DeCarlo, P., Kolb, C., Davidovits, P., and Worsnop, D., 2007. Chemical and microphysical characterization of ambient aerosols with the Aerodyne aerosol mass spectrometer. Mass Spectrometry Reviews 26, doi:10.1002/mas.20115.

Carlton, A.G., Turpin, B.J., Lim, H.-J., Altieri, K.E., and Seitzinger, S., 2006. Geophysical Research Letters 33, doi:10.1029/2005GL025374.

Charlson, R.J., Schwartz, S.E., Hales, J.M., Cess, R.D., Coakley, J.A., Hansen, J.E., and Hofmann, D.J., 1992. Climate forcing by anthropogenic aerosols. Science 255, 423-430.

Claeys, M., Wang, W., Ion, A.C., Kourtchev, I., Gelencser, A., and Maenhaut, W., 2004. Formation of secondary organic aerosols from isoprene and its gas-phase oxidation products through reaction with hydrogen peroxide. Atmospheric Environment 38, 4093-4098.

Clarke, A.D., Eisele, F., Kapustin, V.N., Moore, K., Tanner, D., Mauldin, L., Litchy, M., Lienert, B., Carroll, M.A., and Albercook, G., 1999. Nucleation in the equatorial free troposphere: Favorable environments during PEM-Tropics. Journal of Geophysical Research 104, 5735-5744.

Clemitshaw, K.C., 2006. Coupling between the tropospheric photochemistry of nitrous acid (HONO) and nitric acid (HNO3). Environmental Chemistry 3 (1), 31-34.

Cohen, L., Helmig, D., Neff, W.D., Grachev, A.A., and Fairall, C.W., 2007. Boundary-layer dynamics and its influence on atmospheric chemistry at Summit, Greenland. Atmospheric Environment 41, 5044-5060.

Cottrell, L.D., Griffin, R.J., Jimenez, J.L., Zhang, Q., Ulbich, I., Ziemba, L.D., Beckman, P.J., Sive, B.C., and Talbot, R.W., 2008. Submicron particles at Thompson Farm during ICARTT measured using aerosol mass spectrometry. Journal of Geophysical Research 113, doi:10.1029/2007JD009192.

Crahan, K.K., Hegg, D., Covert, D.S., and Jonsson, H., 2004. An exploration of aqueous oxalic acid production in the coastal marine atmosphere. Atmospheric Environment 38, 3757-3764.

Curry, J. A., 1995. Interactions among aerosols, clouds, and climate of the Arctic Ocean. The Science of the Total Environment 160/161, 777-791.

Cwiertny, D.M., Young, M.A., and Grassian, V.H., 2008. Chemistry and photochemistry of mineral dust aerosol. Annual Review of Physical Chemistry 59, 27-51.

Dal Maso, M., Kulmala, M., Riipinen, I., Wagner, R., Hussein, T., Aalto, P.P., and Lehtinen, K.E.J., 2005. Formation and growth of fresh atmospheric aerosols: Eight years of aerosol size distribution data from SMEAR II, Hyytiala, Finland. Boreal Environmental Research 10, 323-336.

de Gouw, J.A., Middlebrook, A.M., Warneke, C., Goldan, P.D., Kuster, W.C., Roberts, J.M., Fehsenfeld, F.C., Worsnop, D.R., Canagaratna, M.R., Pszenny, AAP., Keene, W.C., Marchewka, M., Bertman, S.B., and Bates, T.S., 2005. Budget of organic carbon in a polluted atmosphere: Results from the New England Air Quality Study in 2002. Journal of Geophysical Research 110, doi:10.1029/2004JD005623.

DeBell, L.J., Vozzella, M., Talbot, R.W., and Dibb, J.E., 2004. Asian dust storm events of spring 2001 and associated pollutants observed in New England by the Atmospheric Investigation, Regional Modeling, Analysis, and Prediction (AIRMAP) monitoring network. Journal of Geophysical Research 109, doi:10.1029/2003JD003733.

Decesari, S., Facchini, M.C., Fuzzi, S., and Tagliavini, E., 2000. Characterization of water-soluble organic compounds in atmospheric aerosol: A new approach. Journal of Geophysical Research 105, 1481-1489.

Decesari, S., Fuzzi, S., Facchini, C., Mircea, M., Emblico, L., Cavalli, F., Maenhaut, W., Chi, X., Schkolnik, G., Falkovich, A., Rudich, Y., Claeys, M., Pashynska, V., Vas, G., Kourtchev, I., Vermeylen, R., Hoffer, A., Andreae, M.O., Tagliavini, E., Moretti, F., and Artaxo, P., 2006. Characterization of the organic composition of aerosols from Rondonia, Brazil, during the LBA-SMOCC 2002 experiment and its representation through model compounds. Atmospheric Chemistry and Physics 6, 375-402.

Decesari, S., Mircea, M., Cavalli,, F., Fuzzi, S., Moretti, F., Tagliavini, E., and Facchini, M.C., 2007. Source attribution of water-soluble organic aerosol by nuclear magnetic resonance spectroscopy. Environmental Science and Technology 41,

2479-2484.

Dibb, J.E., 2007. Vertical mixing above Summit, Greenland: Insights into seasonal and high frequency variability from the radionuclide tracers Be-7 and Pb-210. Atmospheric Environment 24, 5020-5030.

Dibb, J.E. and Arsenault, M., 2002. Shouldn't the snowpacks be a sources of onocarboxylic acids? Atmospheric Environment 36, 2513-2522.

Dibb, J.E., Scheuer, E., Whitlow, S.I., Vozella, M., Williams, E., Lerner, B.M., 2004. Ship-based nitric acid measurements in the gulf of Maine during New England Air Quality Study 2002. Journal of Geophysical Research-Atmospheres 109 (D20), doi:10.1029/2004JD004843.

Dibb, J.E., Talbot, R.W., Whitlow, S.I., Shipham, M.C., Winterle, J., McConnell, J., and Bales, R., 1996. Biomass burning signatures in the atmosphere and snow at Summit, Greenland: An event on 5 August 1994. Atmospheric Environment 30, 533-561.

Draxler, R.R. and Rolph, G.D., 2003. HYSPLIT (HYbrid Single-Particle Lagrangian Integrated Trajectory) Model access via NOAA ARL READY Website (http://www.arl.noaa.gov/ready/hysplit4.html). NOAA Air Resources Laboratory, Silver Spring, MD.

Drewnick, F., Jayne, J.T., Canagaratna, M., Worsnop, D.R., and Demerjian, K.L., 2004. Measurement of ambient aerosol composition during PMTACS-NY 2001 using an aerosol mass spectrometer. Part II: Chemically speciated mass distributions. Aerosol Science and Technology 38, 104-117.

Dusek, U., Frank, G.P., Hildebrandt, L., Curtius, J., Schneider, J., Walter, S., Chand, D., Drewnick, F., Hings, S., Borrmann, S., and Andreae, M.O., 2006. Size matters more than chemistry for cloud-nucleating ability of aerosol particles. Science, 312, 1375-1378.

Dzepina, K., Arey, J., Marr, L.C., Worsnop, D.R., Salcedo, D., Zhang, Q., Onasch, T.B., Molina, L.T., Molina, M.J., and Jimenez, J.L., 2007. Detection of particle-phase polycyclic aromatic hydrocarbons in Mexico City using an aerosol mass spectrometer. International Journal of Mass Spectrometry 263, 152-170.

Engvall, A.-C., Krejci, R., Treffeisen, R., Scheele, R., Hermansen, O., and Paatero, J., 2008. Changes in aerosol properties during spring-summer period in the Arctic troposphere. Atmospheric Chemistry and Physics 8, 445-462.

Ervens, B., Feingold, G., Frost, G.J., and Kreidenweis, S.M., 2004. A modeling study of aqueous production of dicarboxylic acids: Chemical pathways and speciated organic mass production. Journal of Geophysical Research 109, doi:1029/2003JD004387.

Feingold, G. and Chuang, P.Y., 2002. Analysis of the influence of film-forming compounds on droplet growth: Implications for cloud microphysical processes and climate. Journal of Atmospheric Sciences 59, 2006-2018.

Ferek, R.J., Hobbs, P.V., Radke, L.F., Herring, J.A., Sturges, W.T., and Cota, G.F., 1995. Dimthyl sulfide in the Arctic atmosphere. Journal of Geophysical Research 100, 26093-26104.

Finlayson-Pitts, B.J., Wingen, L.M., Sumner, A.L., Syomin, D., Ramazan, K.A., 2003. The heterogeneous hydrolysis of NO2 in laboratory systems and in outdoor and indoor atmospheres: An integrated mechanism. Physical Chemistry Chemical Physics 5 (2), 223-242.

Fisseha, R., Dommen, J., Gaeggeler, K., Weingartner, E., Samburova, V., Kalberer, M., and Baltensperger, U., 2006. Online gas and aerosols measurements of water soluble carboxylic acids in Zurich. Journal of Geophysical Research 111, doi:10.1029/2005JD006782.

Forstner, H.J.L., Flagan, R.C., and Seinfeld, J.H., 1997. Secondary organic aerosol from the photooxidation of aromatic hydrocarbons: Molecular composition. Environmental Science and Technology 31, 1345-1358.

Fry, B., Peltzer, E.T., Hopkinson Jr., C.S., Nolin, A., and Redmond, L., 1996. Analysis of marine DOC using a dry combustion method. Marine Chemistry 54, 191-201.

Garrett, T.J., Zhao, C., Dong, X., Mace, G.G., and Hobbs, P.V., 2004. Effects of varying aerosol regimes on low-level Arctic stratus. Geophysical Research Letters 31, doi:10.1029/2004GL019928.

George, C., Strekowski, R.S., Kleffmann, J., Stemmler, K., and Ammann, M., 2005. Photoenhanced uptake of gaseous NO2 on solid organic compounds: a photochemical source of HONO. Faraday Discussions 130, 195-210.

Gilardoni, S., Russell, L.M., Sorooshian, A., Flagan, R.C., Seinfeld, J.H., Bates, T.S., Quinn, P.K., Allan, J.D., Williams, B., Goldstein, A.H., Onasch, T.B., and Worsnop, D.R., 2007. Regional variation of organic functional groups in aerosol particles on four U.S. east coast platforms during the ICARTT 2004 campaign. Journal of Geophysical Research 112, doi:10.1029/2006JD007737.

Graber, E.R. and Rudich, Y., 2006. Atmospheric HULIS: How humic-like are they? A comprehensive and critical review. Atmospheric Chemistry and Physics 6, 729-753.

Graham, B., Guyon, P., Taylor, P.E., Artaxo, P., Maenhaut, W., Glovsky, M.M., Flagan, R.C., and Andreae, M.O., 2003. Organic compounds present in the natural Amazonian aerosol: Characterization by gas chromatography – mass spectrometry. Journal of Geophysical Research 108, doi:10.1029/2003JD003990.

Grannas, A.M., Shepson, P.B., and Filley, T.R., 2004. Photochemistry and nature of organic matter in Arctic and Antarctic snow. Global Biogeochemical Cycles 18, doi:10.1029/2003GB002133.

Guenther, A., Hewitt, C.N., ,Erickson, D., Fall, R., Geron, C., Graedel, T., Harley, P., Klinger, L., Lerdau, M., Mckay, W.A., Pierce, T., Scholes, B., Steinbrecher, R., Tallamraju, R., Taylor, J., and Zimmerman, P., 1995. A global-model of natural volatile organic-compound emissions. Journal of Geophysical Research 100, 8873-8892.

Gutzwiller, L., Arens, F., Baltensperger, U., Gaggeler, H.W., Ammann, M., 2002. Significance of semivolatile diesel exhaust organics for secondary HONO formation. Environmental Science & Technology 36 (4), 677-682.

Hagler, G.S.W., Bergin, M.H., Smith, E.A., and Dibb, J.E., 2007a. A summer time series of particulate carbon in the air and snow at Summit, Greenland. Journal of Geophysical Research 112, doi:10.1029/2007JD008993.

Hagler, G.S.W., Bergin, M.H., Smith, E.A., Dibb, J.E., Anderson, C., and Steig, E.J., 2007b. Particulate and water-soluble carbon measured in recent snow at Summit, Greenland. Geophysical Research Letters 34, doi:10.1029/2007GL030110.

Hagler, G.S.W., Bergin, M.H., Smith, E.A., Town, M., and Dibb, J.E., 2008. Local anthropogenic impact on particulate elemental carbon concentrations at Summit, Greenland. Atmospheric Chemistry and Physics 8, 2485-2491.

Handley, S.R., Clifford, D., Donaldson, D.J., 2007. Photochemical loss of nitric acid on organic films: A possible recycling mechanism for NOX. Environmental Science & Technology 41 (11), 3898-3903.

Hari, P., Raivonen, M., Vesala, T., Munger, J.W., Pilegaard, K., and Kulmala, M., 2003. Atmospheric science – Ultraviolet light and leaf emission of NOx. Nature 422, 134.

Harley, R.A., Hannigan, M.P., Cass, G.R., 1992. Respeciation of organic gas emissions and the detection of excess unburned gasoline in the atmosphere. Environmental Science & Technology 26 (12), 2395-2408.

Harrison, R.M., Grenfell, J.L., Savage, N., Allen, A., Clemitshaw, K.C., Penkett, S., Hewitt, C.N., and Davison, B., 2000. Observations of new particle formation in the atmosphere of a moderately polluted site in eastern England. Journal of Geophysical Research 105, 17819-17832.

Harrison, R.M., Peak, J.D., Collins, G.M., 1996. Tropospheric cycle of nitrous acid. Journal of Geophysical Research-Atmospheres 101 (D9), 14429-14439.

Heald, C.L., Jacob, D.J., Park, R.J., Russell, L.M., Huebert, B.J., Seinfeld, J.H., Liao, H., and Weber, R.J., 2005. A large organic aerosol source in the free troposphere

missing from current models. Geophysical Research Letters 32, doi:10.1029/2005GL02381.

Held, A., Nowak, A., Birmili, W., Wiedensohler, A., Forkel, R., and Klemm, O., 2004. Observations of particle formation and growth in a mountainous forest region in central Europe. Journal of Geophysical Research 109, doi:10.1029/2004JD005346.

Helmig, D., Oltmans, S.J., Morse, T.O., and Dibb, J.E., 2007. What is causing high ozone at Summit, Greenland? Atmospheric Environment 41, 5031-5043.

Herndon, S.C., Onasch, T.B., Wood, E.C., Kroll, J.H., Canagaratna, M.R., Jayne, J.T., Zavala, M.A., Knighton, W.B., Mazzoleni, C., Dubey, M.K., Ulbich, I.M., Jimenez, J.L., Seila, R., de Gouw, J.A., de Foy, B., Fast, J., Molina, L.T., Kolb, C.E., and Worsnop, D.R., 2008. Correlation of secondary organic aerosol with odd oxygen in Mexico City. Geophysical Research Letters 35, doi:10.1029/2008GL034058.

Hock, B.N., Schneider, J., Borrmann, S., Rompp, A., Moortgat, G., Franze, T., Schauer, C., Poschl, U., Plass-Dulmer, C., and Berresheim, H., 2008. Rural continental aerosol properties and processes observed during the Hohenpeissenberg Aerosol Characterization Experiment (HAZE2002), Atmospheric Chemistry and Physics 8, 603-623.

Hoffmann, T., Odum, J.R., Bowman, F., Collins, D., Klockow, D., Flagan, R.C., and Seinfeld, J.H., 1997. Formation of organic aerosols from the oxidation of biogenic hydrocarbons. Journal of Atmospheric Chemistry 26, 189-222.

Honrath, R.E., Peterson, M.C., Guo, S., Dibb, J.E., Shepson, P.B., and Campbell, B., 1999. Evidence of NOX production within or upon ice particles in the Greenland snowpack. Geophysical Research Letters 26, 695-698.

Hsieh, L.-Y., Kuo, S.-C., Chen, C.-L., and Tsai, Y.I., 2007. Origin of low-molecular-weight dicarboxylic acids and their concentration and size distribution variation in suburban aerosol. Atmospheric Environment 41, 6648-6661.

Huang, X.-F. and Yu, J.Z., 2007. Is vehicle exhaust a significant primary source of oxalic acid in ambient aerosols? Geophysical Research Letters 34, doi:10.1029/2006GL028457.

Huang, X.-F., Yu, J.Z., He, L.-Y., and Yuan, Z., 2006. Water-soluble organic carbon and oxalate in aerosols at a coastal urban site in China: Size distribution characteristics, sources, and formation mechanisms. Journal of Geophysical Research 111, doi:10.1029/2006JD007408.

Jaffrezo, J.L., Aymoz, G., Delaval, C., and Cozie, J., 2005. Seasonal variation of the water soluble organic carbon mass fraction of aerosol in two valleys of the French Alps. Atmospheric Chemistry and Physics 5, 2809-2821.

Jaffrezo, J.L., Calas, N., and Bouchet M., 1998. Carboxylic acids measurements with ion chromatography, Atmospheric Environment 32, 2705-2708.

Jaffrezo, J.L., Davidson, C.I., Kuhns, H.D., Bergin, M.H., Hillamo, R., Maenhaut, W., Kahl, J.W., and Harris, J.M., 1998. Biomass burning signatures in the atmosphere of central Greenland, Journal of Geophysical Research 103, 31067-31078.

Jayne, J.T., Leard, D.C., Zhang, X.F., Davidovits, P., Smith, K.A., Kolb, C.E., Worsnop, D.R., 2000. Development of an aerosol mass spectrometer for size and composition analysis of submicron particles. Aerosol Science and Technology 33, 49-70.

Jimenez, J.L., Jayne, J.T., Shi, Q., Kolb, C.E., Worsnop, D.R., Yourshaw, I., Seinfeld, J.H., Flagan, R.C., Zhang, X.F., Smith, K.A., Morris, J.W., and Davidovits, P., 2003. Ambient aerosol sampling using the aerodyne aerosol mass spectrometer. Journal of Geophysical Research-Atmospheres 108, doi:10.1029/2001JD001213.

Jordan, C.E. and Talbot, R.W., 2000. Direct atmospheric deposition of water-soluble nitrogen to the Gulf of Maine. Global Biogeochemical Cycles 14, 1315-1329.

Kalberer, M., Ammann, M., Arens, F., Gaggeler, H.W., Baltensperger, U., 1999. Heterogeneous formation of nitrous acid (HONO) on soot aerosol particles. Journal of Geophysical Research-Atmospheres 104 (D11), 13825-13832.

Kalberer, M., Yu, J., Cocker, D.R., Flagan, R.C., and Seinfeld, J.H., 2000. Aerosol formation in the cyclohexene-ozone system. Environmental Science and Technology 34, 4894-4901.

Kanikidou, M. et al., 2005. Organic aerosol and global climate modeling: a review. Atmospheric Chemistry and Physics 5, 1053-1123.

Kawamura, K. and Ikushima, K., 1993. Seasonal changes in the distribution of dicarboxylic acids in the urban atmosphere. Environmental Science and Technology 27, 2227-2235.

Kawamura, K., and Kaplan, I.R., 1987. Motor exhaust emissions as a primary source for dicarboxylic acids in Los Angeles ambient air. Environmental Science and Technology 21, 105-110.

Keene, W.C., Maring, H., Maben, J.R., Kieber, D.J., Pszenny, A.A.P., Dahl, E.E., Izaguirre, M.A., Davis, A.J., Long, M.S., Zhou, X., Smoydzin, L., and Sander, R., 2007. Chemical and physical characteristics of nascent aerosols produced by bursting bubbles at a model air-sea interface. Journal of Geophysical Research 112, doi:10.1029/2007JD008464.

Kerminen, V.-M., and Wexler, A.S., 1995. Growth laws for atmospheric aerosol particles: An examination of the bimodality of the accumulation mode. Atmospheric Environment 29, 3263-3275.

Kerminen, V.M., Lihavainen, H., Komppula, M., Viisanen, Y., and Kulmala, M., 2005. Direct observational evidence linking atmospheric aerosol formation and cloud droplet activation. Geophysical Research Letters 32, doi:10.1029/2005GL023130.

Kerminen, V.-M., Teinilä, K., Hillamo, R., and Mäkelä, T., 1999. Size-segregated chemistry of particulate dicarboxylic acids in the Arctic atmosphere, Atmospheric Environment 33, 2089-2100.

Kiendler-Scharr, A., Zhang, Q., Hohaus, T., Kleist, E., Mensah, A., Mentel, T., Spindler, C., Tillmann, R., and Wildt, J., 2009. Aerosol Mass Spectrometric Features of Biogenic SOA: Observations from a Plant Chamber and in Rural Atmospheric Environments, Atmospheric Chemistry and Physics, in preparation.

Kirchstetter, T.W., Harley, R.A., Littlejohn, D., 1996. Measurement of nitrous acid in motor vehicle exhaust. Environmental Science & Technology 30 (9), 2843-2849.

Kleffmann, J., Becker, K.H., Lackhoff, M., Wiesen, P., 1999. Heterogeneous conversion of NO2 on carbonaceous surfaces. Physical Chemistry Chemical Physics 1 (24), 5443-5450.

Knipping, E.M., Dabdub, D., 2002. Modeling surface-mediated renoxification of the atmosphere via reaction of gaseous nitric oxide with deposited nitric acid. Atmospheric Environment 36 (36-37), 5741-5748.

Korhonen, H., Carslaw, K.S., Spracklen, D.V., Ridley, D.A., and Ström, J., 2008. A global model study of processes controlling aerosol size distributions in the Arctic spring and summer. Journal of Geophysical Research 113, doi:10.1029/2007JD009114.

Krivácsy, Z., Kiss, G., Varga, B., Galambos, I., Sárvári, Z., Gelencsér, A., Molnár, Á., Fuzzi, S., Facchini, M.C., Zappoli, S., Andracchio, A., Alsberg, T., Hansson, H.C., and Persson, L., 2000. Study of humic-like substances in fog and interstitial aerosol by size-exclusion chromatography and capillary electrophoresis. Atmospheric Environment 34, 4273-4281.

Kroll, J.H., Ng, N.L., Murphy, S.M., Flagan, R.C., and Seinfeld, J.H., 2006. Secondary organic aerosol formation from isoprene photooxidation. Environmental Science and Technology 40, 1869-1877.

Kulmala, M., 2003. How particles nucleate and grow. Science 302, 1000-1001.

Kulmala, M., Dal Maso, M., Makela, J.M., Pirjola, L., Vakeva, M., Aalto, P., Miikkulainen, P., Hameri, K., and O'Dowd, C.D., 2001. On the formation, growth, and composition of nucleation mode particles. Tellus 53B, 479-490.

Kulmala, M., Pirjola, U., and Makela, J.M., 2000. Stable sulphate clusters as a source of new atmospheric particles, Nature 404, 66-69.

Kulmala, M., Vehkamäki, H., Petäjä, T., Dal Maso, M., Lauri, A., Kerminen, V.M., Birmili, W., and McMurry, P.H., 2004. Formation and growth rates of ultrafine atmospheric particles: a review of observations. Journal of Aerosol Science 35, 143-176.

Kurtenbach, R., Becker, K.H., Gomes, J.A.G., Kleffmann, J., Lorzer, J.C., Spittler, M., Wiesen, P., Ackermann, R., Geyer, A., and Platt, U., 2001. Investigations of emissions and heterogeneous formation of HONO in a road traffic tunnel. Atmospheric Environment 35 (20), 3385-3394.

Lanz, V.A., Alfarra, M.R., Baltensperger, U., Buchmann, B., Hüglin, C., and Prévôt, A.S.H., 2007. Source apportionment of submicron organic aerosols at an urban site by factor analytical modelling of aerosol mass spectra, Atmospheric Chemistry and Physics 7, 1503-1522, 2007.

Leck, C. and Bigg, E.K., 2005a. Source and evolution of the marine aerosol – A new perspective. Geophysical Research Letters 32, doi:10.1029/2005GL023651.

Leck, C. and Bigg, E.K., 2005b. Biogenic particles in the surface microlayer and overlaying atmosphere in the central Arctic Ocean during summer. Tellus 57B, 305-316.

Lightly, J.S., Veranth, J.M., and Sarofim, A.F., 2000. Combustion aerosols: Factors governing their size and composition and implications to human health, Journal of Air and Waste Management Association 50, 1565-1618.

Lim, H.J., Carlton, A.G., and Turpin, B.J., 2005. Isoprene forms secondary organic aerosol through cloud processing: Model simulations. Environmental Science and Technology 39, 4441-4446.

Liu, P., Ziemann, P.J., Kittelson, D.B., and McMurry, P.H., 1995. Generating particle beams of controlled dimensions and divergence. 2. Experimental evaluation of particle motion in aerodynamic lenses and nozzle expansions. Aerosol Science and Technology 22, 314-324.

Lohmann, U. and Feichter, J., 2005. Global indirect aerosol effects: A review. Atmospheric Chemistry and Physics 5, 715-737.

Ludwig, J., Meixner, F.X., Vogel, B., and Forstner, J., 2001. Soil-air exchange of nitric oxide: An overview of processes, environmental factors, and modeling studies. Biogeochemistry 52, 225-257.

Lunden, M.M., Black, D.R., Mckay, M., Revzan, K.L., Goldstein, A.H., and Brown, N.J., 2006. Characteristics of fine particle growth events observed above a forested ecosystem in the Sierra Nevada Mountains of California. Aerosol Science and Technology 40, 373-388.

Mäkelä, J.M., Aalto, P., Jokinen, V., Pohja, T., Nissinen, A., Plamroth, S., Markkanen, T., Seitsonen, K., Lihavainen, H., Kulmala, M., 1997. Observations of ultrafine aerosol particle formation and growth in a boreal forest. Geophysical Research Letters 24, 1219-1222.

Mäkelä, J.M., Koponen, I.K., Aalto, P., and Kulmala, M., 2000. One-year data of submicron size modes of tropospheric background aerosol in southern Finland. Journal of Aerosol Science 31, 595-611.

Malm, W.C., Schichtel, B.A., Pitchford, M.L., Ashbaugh, L.L., and Eldred, R.A., 2004. Spatial trends in speciated fine aerosol concentration in the United States, Journal of Geophysical Research 109, doi:10.1029/2003JD003739.

Mao, H.T., Talbot, R.W., Troop, D., Johnson, R., Businger, S., and Thomposon, A.M., 2006. Smart balloon observations over the North Atlantic: O3 data analysis and modeling. Journal of Geophysical Research 111, doi:10.1029/2005JD006507.

Marquez, C., Castro, T., Muhlia, A., Moya, M., Martinez-Arroyo, A., and Baez, A., 2005. Measurement of aerosol particles, gases and flux radiation in the Pico de Orizaba National Park, and its relationship to air pollution transport. Atmospheric Environment 39, 3877-3890.

Marr, L.C., Dzepina, K., Jimenez, J.L., Reisen, F., Bethel, H.L., Arey, J., Gaffney, J.S., Marley, N.A., Molina, L.T., and Molina, M.J., 2006. Sources and transformations of particle-bound polycyclic aromatic hydrocarbons in Mexico City. Atmospheric Chemistry and Physics 6, 1733-1745.

Martensson, E.M., Nilsson, E.D., de Leeuw, G., Cohen, L.H., and Hansson, H.-C., 2003. Laboratory simulations and parameterization of the primary marine aerosol production. Journal of Geophysical Research 108, doi:10.1029/2002JD002263.

Massman, W.J.. 1998. A review of the molecular diffusivities of H2O, CO2, CH4, CO, O3, SO2, NH3, N2O, NO, and NO2 in air, O2 and N2 near STP. Atmospheric Environment, 32, 1111-1127.

McGaughey, G.R., Desai, N.R., Allen, D.T., Seila, R.L., Lonneman, W.A., Fraser, M.P., Harley, R.A., Pollack, A.K., Ivy, J.M., and Price, J.H., 2004. Analysis of motor vehicle emissions in a Houston tunnel during the Texas Air Quality Study 2000. Atmospheric Environment 38 (20), 3363-3372.

McLafferty, F.W., and Turecek, F., 1993. Interpretation of mass spectra. University Science Books 4th edition.

McMurry, P.H., Fink, M., Sakurai, H., Stolzenburg, M.R., Mauldin, R.L., Smith, J., Eisele, F., Moore, K., Sjostedt, S., Tanner, D., Huey, L.G., Nowak, J.B., Edgerton, E., and Voisin, D., 2005. A criterion for new particle formation in the sulfur-rich Atlanta atmosphere. Journal of Geophysical Research 110, doi:10.1029/2005JD005901.

Meng, Z., and Seinfeld, J.H., 1994. On the source of the submicrometer droplet mode of urban and regional aerosols. Aerosol Science and Technology 20, 253-265.

Menon, S., Hansen, J., Nazarenko, L., and Luo, Y.F.,2002. Climate effects of black carbon aerosols in China and India. Science 297, 2250-2253.

Mochida, M., Umemoto, N., Kawamura, K., Lim, H.-J., and Turpin, B.J., 2007. Bimodal size distributions of various organic acids and fatty acids in the marine atmosphere: Influence of anthropogenic aerosols, Asian dusts, and sea spray off the coast of East Asia. Journal of Geophysical Research 112, doi:10.1029/2006JD007773.

Mochida, M., Umemoto, N., Kawamura, K., Uematsu, M., 2003. Bimodal size distribution of C2-C4 dicarboxylic acids in the marine aerosols. Geophysical Research Letters 30, doi:10.1029/2003GL017451.

Moretti, F., Tagliavini, E., Decesari, S., Facchini, M.C., Rinaldi, M., and Fuzzi, S., 2008. NMR determination of total carbonyls and carboxyls: A tool for tracing the evolution of atmospheric oxidized organic aerosols. Environmental Science and Technology 42, 4844-4849.

Moussiopoulos, N., Papalexiou, S., Lammel, G., Arvanitis, T., 2000. Simulation of nitrous acid formation taking into account heterogeneous pathways: Application to the Milan metropolitan area. Environmental Modeling & Software 15 (6-7), 629-637.

Mozurkewich, M., Chan, T.W., Aklilu, Y.A., and Verheggen, B., 2004. Aerosol particle size distributions in the lower Fraser Valley: evidence for particle nucleation and growth. Atmospheric Chemistry and Physics 4, 1047-1062.

Naik V., Delire, C., and Wuebbles, D.J., 2004. Sensitivity of global biogenic isoprenoid emissions to climate variability and atmospheric CO2. Journal of Geophysical Research 109, D06301, doi:10.1029/2003JD004236.

O'Dowd, C.D., Jimenez, J.L., Bahreini, R., Flagan, R.C., Seinfeld, J.H., Hameri, K., Pirjola, L., Kulmala, M., Jennings, S.G., and Hoffmann, T., 2002. Marine aerosol formation from biogenic iodine emissions. Nature 417, 632-636.

Oberdörster, G., 2000. Toxicology of ultrafine particles: in vivo studies. Philosphical Transactions of the Royal Society of London 358, 2719-2740.

Odum, J.R., Jungkamp, T.P.W., Griffin, R.J., Forstner, H.J.L., Flagan, R.C., and Seinfeld, J.H., 1997. Aromatics, reformulated gasoline, and atmospheric organic aerosol formation. Environmental Science and Technology 31, 1890-1897.

Park, J., Sakurai, H., Vollmers, K., and McMurry, P.H., 2004. Aerosol size distributions measured at the South Pole during ISCAT. Atmospheric Environment 38, 5493-5500.

Peltier, R.E., Weber, R.J., and Sullivan, A.P., 2007. Investigating a liquid-based method for online organic carbon detection in atmospheric particles, Aerosol Science and Technology 12, 1117-1127.

Penner, J.E., Chuang, C.C., and Grant, K., 1998. Climate forcing by carbonaceous and sulfate aerosols. Climate Dynamics 14, 839-851.

Phillips, M.A., Savage, T.J., and Croteau, R., 1999. Monoterpene synthases of loblolly pine (Pinus taeda) produce pinene isomers and enatniomers. Archives of Biochemistry and Biophysics 372, 197-204.

Presto, A.A., Hartz, K.E.H., and Donahue, N.M., 2005. Secondary organic aerosol production from terpene ozonolysis. 2. Effect of NOx concentration. Environmental Science and Technology 39, 7046-7054.

Qian, S., Sakurai, H., and McMurry, P.H., 2007. Characteristics of regional nucleation events in urban East St. Louis. Atmospheric Environment 41, 4119-4127.

Quinn, P.K., Shaw, G., Andrews, E., Dutton, E.G., Ruoho-Airola, T., and Gong, S.L., 2007. Arctic haze: current trends and knowledge gaps. Tellus 59B, 99-114.

Ramanathan, V., Li, F., Ramana, M.V., Praveen, P.S., Kim, D., Corrigan, C.E., Nguyen, H., Stone, E.A., Schauer, J.J., Carmichael, G.R., Adhikary, B., and Yoon, S.C., 2007. Atmospheric brown clouds: Hemispheric and regional variations in long-range transport, absorption, and radiative forcing. Journal of Geophysical Research 112, doi:10.1029/2006JD008124.

Rivera-Figueroa, A.M., Sumner, A.L., Finlayson-Pitts, B.J., 2003. Laboratory studies of potential mechanisms of renoxification of tropospheric nitric acid. Environmental Science & Technology 37 (3), 548-554.

Sage, A.M., Weitkamp, E.A., Robinson, A.L., Donahue, N.M., 2008. Evolving mass spectra of the oxidized component of organic aerosol: Results from aerosol mass spectrometer analyses of aged diesel emissions. Atmospheric Chemistry and Physics 8 (5), 1139-1152.

Sarwar, G., Roselle, S.J., Mathur, R., Appel, W., Dennis, R.L., Vogel, B., 2008. A comparison of CMAQ HONO predictions with observations from the Northeast Oxidant and Particle Study. Atmospheric Environment 42 (23), 5760-5770.

Schauer, J.J., Rogge, W.F., Hildemann, L.M., Mazurek, M.A., and Cass, G.R., 1996. Source apportionment of airborne particulate matter using organic compounds as tracers. Atmospheric Environment 30, 3837-3855.

Scheuer, E., Talbot, R.W., Dibb, J.E., Seid, G.K., DeBell, L., Lefer, B., 2003. Seasonal distributions of fine aerosol sulfate in the North American Arctic basin during TOPSE. Journal of Geophysical Research-Atmospheres 108 (D4), doi:10.1029/2001JD001364.

Schichtel, B.A., Husar, R.B., Falke, S.R., and Wilson, W.E., 2001. Haze trends over the United States, 1980-1995. Atmospheric Environment 35, 5205-5210.

Schwartz, J., Dockery, D.W., and Neas, L.M., 1996. Is daily mortality associated specifically with fine particles? Journal of Air and Waste Management Association 46, 927-939.

Seinfeld, J.H., and Pankow, J.F., 2003. Organic atmospheric particulate material. Annual Review of Physical Chemistry 54, 121-140.

Sive, B.C., Zhou, Y., Troop, D., Wang, Y.L., Little, W.C., Wingenter, O.W., Russo, R.S., Varner, R.K., and Talbot, R.W., 2005. Development of a cryogen-free concentration system for measurements of volatile organic compounds. Analytical Chemistry 77, 6989-6998.

Sjostedt, S.J., Huey, L.G., Tanner, D.J., Peischl, J., Chen, G., Dibb, J.E., Lefer, B., Hutterli, M.A., Beyersdorf, A.J., Blake, N.J., Blake, D.R., Sueper, D., Ryerson, T., Burkhart, J., and Stohl, A., 2007. Observations of hydroxyl and sum of peroxy radicals at Summit, Greenland during summer 2003. Atmospheric Environment 24, 5122-5137.

Smith, J.N., Dunn, M.J., VanReken, T.M., Iida, K., Stolzenburg, M.R., McMurry, P.H., and Huey, L.G., 2008. Chemical composition of atmospheric nanoparticles formed from nucleation in Tecamac, Mexico: Evidence for an important role of organic species in nanoparticle growth. Geophysical Research Letters 35, doi:10.1029/2007GL032523.

Song, C., Na, K.S., and Cocker, D.R., 2005. Impact of the hydrocarbon to NOx ratio on secondary organic aerosol formation. Environmental Science and Technology 39, 3143-3149.

Sorooshian, A., Lu, M.-L., Brechtel, F.J., Jonsson, H., Feingold, G., Flagan, R.C., and Seinfeld, J.H., 2007a. On the source of organic acid aerosol layers above clouds. Environmental Science and Technology 41, 4647-4654.

Sorooshian, A., Ng, N.L., Chan, A.W.H., Feingold, G., Flagan, R.C., and Seinfeld, J.H., 2007b. Particulate organic acids and overall water-soluble aerosol composition measurements from the 2006 Gulf of Mexico Atmospheric Composition and Climate Study (GoMACCS). Journal of Geophysical Research 112, doi:10.1029/2007JD008537.

Sorooshian, A., Varutbangkul, V., Brechtel, F.J., Ervens, B., Feingold, G., Bahreini, R., Murphy, S.M., Holloway, J.S., Atlas, E.L., Buzorius, G., Jonsson, H., Flagan, R.C., and Seinfeld, J.H., 2006. Oxalic acid in clear and cloudy atmospheres: Analysis of data from ICARTT 2004. Journal of Geophysical Research 111, doi:10.1029/2005JD006880.

Stanier, C.O., Khlystov, A.Y., and Pandis, S.N., 2004. Ambient aerosol size distributions and number concentrations measured during PAQS. Atmospheric Environment 38, 3275-3284.

Stemmler, K., Ammann, M., Donders, C., Kleffmann, J., George, C., 2006. Photosensitized reduction of nitrogen dioxide on humic acid as a source of nitrous acid. Nature 440 (7081), 195-198.

Stohl, A., 2006. Characteristics of atmospheric transport into the Arctic troposphere. Journal of Geophysical Research 111, doi:10.1029/2005JD006888.

Ström, J., Umegard, J., Tørseth, K., Tunved, P., Hansson, H.-C., Holmén, K., Wismann, V., Herber, A., and König-Langlo, G., 2003. One year of particle size distributions and aerosol chemical composition measurements at the Zeppelin Station, Svalbard, March 2000-2001. Physics and Chemistry of the Earth 28, 1181-1190.

Stroud, C.A., Nenes, A., Jimenez, J.L., DeCarlo, P.F., Huffman, J.A., Bruintjes, R., Nemitz, E., Delia, A.E., Toohey, D.W., Guenther, A.B., Nandi, S., 2007. Cloud activating properties of aerosol observed during CELTIC. Journal of Atmospheric Sciences 64, 441-459.

Tagliavini, E., Moretti, F., Decesari, S., Facchini, M.C., Fuzzi, S., and Maenhaut, W., 2005. Functional group analysis by H NMR/chemical derivatization for the characterization of organic aerosol from the SMOCC field campaign. Atmospheric Chemistry and Physics 6, 1003-1019.

Tedetti, M., Kawamura, K., Charrière, B., Chevalier, N., and Sempéré, R., 2006. Determination of low molecular weight dicarboxylic and ketocarboxylic acids in seawater samples. Analytical Chemistry 78, 6012-6018.

Tsigaridis, K., and Kanakidou, M., 2007. Secondary organic aerosol importance in the future atmosphere. Atmospheric Environment 41, 4682-4692.

Ulbrich , I.M., Canagaratna, M.R., Zhang, Q., Worsnop, D.R., and Jimenez, J.L., 2008. Interpretation of organic components from positive matrix factorization of aerosol mass spectrometric data. Atmospheric Chemistry and Physics Discussions, 8, 6729-6791.

VanReken, T.M., Greenberg, J.P., Harley, P.C., Guenther, A.B., and Smith, J.N., 2006. Direct measurement of particle formation and growth from the oxidation of biogenic emissions. Atmospheric Chemistry and Physics 6, 4403-4413.

Vehkamäki, H., Dal Maso, M., Hussein, T., Flagagan, R., Hyvarinen, A., Lauros, J., Merikanto, J., Monkkonen, P., Pihlatie, M., Salminen, K., Sogacheva, L., Thurm, T., Ruuskanen, T.M., Keronen, P., Aalto, P.P., Hari, P., Lehtinen, K.E.J., Rannik, U., and Kulmala, M., 2004. Atmospheric particle formation events at Varrio

measurement station in Finnish Lapland 1998-2002. Atmospheric Chemistry and Physics 4, 2015-2023.

Venkataraman, C., Lyons, J.M., and Friedlander, S.K., 1994. Size distributions of polycyclic aromatic hydrocarbons and elemental carbon. 1. Sampling, measurement methods, and source characterization, Environmental Science and Technology 28, 555-562.

Vogel, B., Vogel, H., Kleffmann, J., Kurtenbach, R., 2003. Measured and simulated vertical profiles of nitrous acid - part II. Model simulations and indications for a photolytic source. Atmospheric Environment 37 (21), 2957-2966.

von Glasow, R., and Crutzen, P.J., 2004. Model study of multiphase DMS oxidation with a focus on halogens. Atmospheric Chemistry and Physics 4, 589-608.

Weber, R.J., McMurry, P.H., Eisele, F.L., and Tanner, D.J., 1995. Measurement of expect nucleation precursor species and 3-500-nm diameter particles at Mauna-Loa-Observatory, Hawaii. Journal of the Atmospheric Sciences 52, 2242-2257.

Weber, R.J., Orsini, D., Wang, B., Scheuer, E., Talbot, R.W., Dibb, J.E., Seid, G.K., DeBell, L., Mauldin, R.L., Kosciuch, C., Cantrell, C., and Eisele, F., 2003. New particle formation in anthropogenic plumes advecting from Asia observed during TRACE-P. Journal of Geophysical Research 108, doi:10.1029/2002JD003112.

White, M. L., Russo, R.S., Zhou, Y., Ambrose, J.L., Haase, K., Frinak, E.K., Varner, R.K., Wingenter, O.W., Mao, H., Talbot, R., and Sive, B.C., 2009. Are biogenic emissions a significant source of summertime atmospheric toluene in the rural Northeastern United States? Atmospheric Chemistry and Physics 9, 81-92.

Winklmayr, W., Reischl, G. P., Lindner, A. O., and Berner, A., 1991. A new electromobility spectrometer for the measurement of aerosol size distributions in the size range from 1 to 1000 nm. Journal of Aerosol Science 22, 289-296.

Yao, X., Fang, M., and Chan, C.K., 2002. Size distributions and formation of dicarboxylic acids in atmospheric particles. Atmospheric Environment 36, 2099-2107.

Young, L.-H., Benson, D.R., Montanaro, W.M., Lee, S.-H., Pan, L.L., Rogers, D.C., Jensen, J., Stith, J.L., Davis, C.A., Campos, T.L., Bowman, K.P., Cooper, W.A., and Lait, L.R., 2007 Enhanced new particle formation observed in the northern midlatitude tropopause region. Journal of Geophysical Research 112, doi:10.1029/2006JD008109.

Yttri, K.E., Dye, C., and Kiss. G., 2007. Ambient aerosol concentrations of sugars and sugar-alcohols at for different sites in Norway. Atmospheric Chemistry and Physics 7, 4267-4279.

Yu, S., 2000. Role of organic acids (formic, acetic, pyruvic, and oxalic) in the formation of cloud condensation nuclei (CCN): A review. Atmospheric Research 53, 185-217.

Yu, J.Z., Hong, Y., Zhang, H., and Lau, A.K.H., 2004. Size distributions of water-soluble organic carbon in ambient aerosols and its size-resolved thermal characteristics. Atmospheric Environment 38, 1061-1071.

Yu, J.Z., Huang, X.-F., Xu, J., and Hu, M., 2005. When aerosol sulfate goes up, so does oxalate: Implications for the formation mechanisms of oxalate. Environmental Science and Technology 39, 128-133.

Zhang, Q. et al., 2007. Ubiquity and dominance of oxygenated species in organic aerosols in anthropogenically-influenced Northern Hemispheric midlatitudes. Geophysical Research Letters 34, doi:10.1029/2007GL029979.

Zhang, Q., Alfarra, M.R., Worsnop, D.R., Allan, J.D., Coe, H., Canagaratna, M.R., Jimenez, J.L., 2005a. Deconvolution and quantification of hydrocarbon-like and oxygenated organic aerosols based on aerosol mass spectrometry. Environmental Science & Technology 39 (13), 4938-4952.

Zhang, Q., Stanier, C.O., Canagaratna, M.R., Jayne, J.T., Worsnop, D.R., Pandis, S.N., and Jimenez, J.L., 2004. Insights into the chemistry of new particle formation and growth events in Pittsburgh based on Aerosol Mass Spectrometry. Environmental Science and Technology, 38, 4797-4809.

Zhang, Q., Worsnop, D.R., Canagaratna, M.R., and Jimenez, J.L., 2005. Hydrocarbon-like and oxygenated organic aerosols in Pittsburg: insights into sources and processes of organic aerosols. Atmospheric Chemistry and Physics 5, 3289-3311.

Zhou, X.L., Gao, H.L., He, Y., Huang, G., Bertman, S.B., Civerolo, K., Schwab, J., 2003. Nitric acid photolysis on surfaces in low-NOX environments: Significant atmospheric implications. Geophysical Research Letters 30 (23), doi:10.1029/2003GL018620.

Zielinska, B, Sagebiel, J., McDonald, J.D., Whitney, K., and Lawson, D.R., 2004. Emission rates and comparative chemical composition from selected in-use diesel and gasoline-fueled vehicles. Journal of Air and Waste Management 54, 1138-1150.